



# Review of Iberia-Eurasia plate-boundary basins: Role of sedimentary burial and salt tectonics during rifting and continental breakup

Nicolas Saspiturry, Philippe Razin, Thierry Baudin, Riccardo Asti, Yves Lagabrielle, Cécile Allanic, Olivier Serrano, Thibault Duretz

## ► To cite this version:

Nicolas Saspiturry, Philippe Razin, Thierry Baudin, Riccardo Asti, Yves Lagabrielle, et al.. Review of Iberia-Eurasia plate-boundary basins: Role of sedimentary burial and salt tectonics during rifting and continental breakup. *Basin Research*, 2021, 33 (2), pp.1626-1661. 10.1111/bre.12529 . insu-03046985

**HAL Id: insu-03046985**

**<https://insu.hal.science/insu-03046985>**

Submitted on 8 Dec 2020

**HAL** is a multi-disciplinary open access archive for the deposit and dissemination of scientific research documents, whether they are published or not. The documents may come from teaching and research institutions in France or abroad, or from public or private research centers.

L'archive ouverte pluridisciplinaire **HAL**, est destinée au dépôt et à la diffusion de documents scientifiques de niveau recherche, publiés ou non, émanant des établissements d'enseignement et de recherche français ou étrangers, des laboratoires publics ou privés.

# **Review of Iberia-Eurasia plate-boundary basins: Role of sedimentary burial and salt tectonics during rifting and continental breakup**

Nicolas Saspiturry<sup>1\*</sup>, Benoit Issautier<sup>2</sup>, Philippe Razin<sup>1</sup>, Thierry Baudin<sup>2</sup>, Riccardo Asti<sup>3</sup>, Yves Lagabrielle<sup>3</sup>, Cécile Allanic<sup>2</sup>, Olivier Serrano<sup>2</sup> and Thibault Duretz<sup>2</sup>

<sup>1</sup> Université Bordeaux Montaigne / EA 4592 Géoressources & Environnement, 1 allée Fernand Daguin, 33607 Pessac cedex, France

<sup>2</sup> Université Rennes, CNRS, Géosciences Rennes - UMR 6118, F-35000, Rennes, France

<sup>3</sup> BRGM-French Geological Survey, 3 Avenue Claude Guillemin, 45100 Orléans, France

\*Corresponding author (e-mail: saspiturry.nicolas@gmail.com)

Data sharing is not applicable to this article as no new data were created or analysed in this study.

## **Acknowledgement**

This work is part of Saspiturry's Ph.D. research conducted as part of the OROGEN project, cofunded by Total S.A., Bureau de Recherches Géologiques et Minières (BRGM), and Institut National de Sciences de l'Univers (INSU). We thank OROGEN project managers Sylvain Calassou (Total), Emmanuel Masini (Total), Olivier Vidal (CNRS, Centre National de la Recherche Scientifique) and Isabelle Thinon (BRGM). We specially thank Basin Research's deputy editor Kerry Gallagher and the three reviewers, Tiago M. Alves, Per Terje Osmundsen and Nicholas Christie-Blick for their constructive comments, which significantly improved the initial manuscript.

## **Keywords**

Iberian-European boundary; Sedimentary burial; Salt tectonics; Depth-dependent thinning; Ductile regime; HT/LP metamorphism

## 25    **Abstract**

26    We document the role of sedimentary burial and salt tectonics in controlling the deformation  
27    style of continental crust during hyperextension. The Iberian-European boundary records a  
28    complex history of Cretaceous continental extension, which has led to the development of so-  
29    called smooth-slope type basins. Based on the review of the available geological constraints  
30    (crustal-balanced cross sections, sedimentary profile evolution, RSCM thermometer, low-  
31    temperature thermochronology) and geophysical data (Bouguer anomaly, Moho depth,  
32    seismic reflection profiles, and Vp/Vs velocity models) on the Tartas, Arzacq, Cameros,  
33    Parentis, Columbrets, Mauléon, Basque-Cantabrian and Internal Metamorphic Zone basins,  
34    we shed light on the main characteristics of this type of basin. This synthesis indicates that  
35    crustal thinning was influenced by two decoupling horizons: the middle crust and Triassic  
36    pre-rift salt, initially located between the basement and pre-rift sedimentary cover. These two  
37    horizons remained active throughout basin formation and were responsible for depth-  
38    dependent thinning of the crust and syn-rift salt tectonics. We therefore identify several  
39    successive deformation phases involving (1) pure shear dominated thinning, (2) simple shear  
40    dominated thinning and (3) continental breakup. In the first phase, distributed deformation  
41    resulted in the development of a symmetric basin. Field observations indicate that the middle  
42    and lower crust were under dominantly ductile conditions at this stage. In the second phase,  
43    deformation was localized along a crustal detachment rooted between the crust and the mantle  
44    and connecting upwards with Triassic pre-rift salt. During continental breakup, basin  
45    shoulders recorded the occurrence of brittle deformation while the hyperextended domain  
46    remained under predominantly ductile thinning. The formation of smooth-slope type  
47    extensional basins was intrinsically linked to the combined deposition of thick syn-rift and  
48    breakup sequences, and regional salt tectonics. They induced significant burial and allowed

the continental crust and the pre-rift sequence to deform under high temperature conditions from the rifting to continental breakup stages.

## **1 Introduction**

Recent models and concepts related to hyperextended continental margins have been defined on North Atlantic passive margins such as West Iberia/Newfoundland (Boillot et al., 1980, 1995; Reston et al., 1995; Whitmarsh et al., 2001; Péron-Pinvidic & Manatschal, 2009; Péron-Pinvidic et al., 2015), Norway/Greenland (Osmundsen et al., 2002; Osmundsen & Ebbing, 2008; Osmundsen & Péron-Pinvidic, 2018), and the Alps (Lemoine et al., 1987; Froitzheim & Manatschal, 1996; Manatschal & Nievergelt, 1997; Manatschal et al., 2006; Masini et al., 2011; Mohn et al., 2014). They describe the mechanisms responsible for continental crust thinning and subcontinental mantle exhumation at the ocean-continent transition, and have shown that the hyperextended domain of continental margins is characterized by (1) sediment starved conditions with very thin pre-rift and syn-rift sedimentary sequences, (2) asymmetric margins, and (3) coupled deformation between the basement and sedimentary cover resulting in the formation of extensional allochthons. The syn-rift and post-rift units have been respectively defined as strata deposited during (1) the last extension episode leading to continental breakup and (2) a period of relative tectonic quiescence above a regional breakup unconformity (Driscoll et al., 1995; Wilson et al., 2001). DSDP and ODP drilling expeditions along the West-Iberia margin have also contributed to a more complete understanding of how continental breakup is recorded in syn-rift to post-rift sedimentary sequences (Alves & Cunha, 2018), and how it evolves through time along the strike of continental margins (Alves et al., 2009). Indeed, such data allowed the identification of syn-rift, breakup and post-rift sequences as correlating with major phases of crustal thinning, mantle denudation and oceanic spreading (Alves et al., 2009; Soares et al., 2012; Soares, 2014; Alves & Cunha, 2018; Alves et al.,

2020). Continental breakup is thus defined as the deposits that are correlated with the phases of hyperextension and mantle denudation on magma-poor continental margins (Soares et al., 2012). Alves et al. (2020) have demonstrated that continental breakup is only possible along magma-poor Type I margins (sensu Huisman & Beaumont, 2003, 2008, 2011, 2014). Indeed, the upper lithosphere in Type I margins is much more coupled to the continental crust than in Type II margins (Alves et al., 2020). Thus, along Type II margins, the upper lithosphere is laterally subtracted and mantle denudation cannot occur. Syn-rift and breakup sequences are delimited by major unconformities corresponding (from bottom to top) to the base syn-rift unconformity (BSU; base of syn-rift sequence), the lithospheric breakup surface (LBS; base of the breakup sequence) and the base post-rift unconformity (BPU; base of the post-rift sequence) as defined by Soares et al. (2012) and Soares (2014). While Atlantic-type margins develop under conditions of high mantle heat flow, as the product of asthenosphere upwelling and subsequent denudation of subcontinental mantle (e.g., Huisman & Beaumont, 2003, 2008, 2011, 2014; Lavie & Manatschal, 2006; Brune et al., 2014, 2016), the North Pyrenean hyperextended rift system differs from the Atlantic type by the presence of high-temperature/low-pressure (HT/LP) metamorphism (Albarède & Michard-Vitrac, 1978a, 1978b; Golberg et al., 1986; Montigny et al., 1986; Golberg & Maluski, 1988; Golberg & Leyreloup, 1990; Thiébaud et al., 1992). The North Pyrenean rift basins were affected by a syn-rift stage throughout the Early Cretaceous that evolved to continental breakup and mantle denudation during the Latest Albian to Early Cenomanian (Debroas et al., 2010; Saspiturry et al., 2019a; Espurt et al., 2019; Labaume & Teixell, 2020). Thus, these margins can be defined as Type I margins as mantle denudation occurred during continental breakup (sensu Huisman & Beaumont, 2003, 2008, 2011, 2014). The hyperextended domain of these basins is interpreted to have stretched under high-temperature conditions under a predominantly ductile regime, resulting in the generation of large-scale boudins whose formation was controlled by

98 a strong thermal and structural inheritance (Clerc & Lagabriele, 2014; Clerc et al., 2015,  
99 2015b; Corre et al., 2016; de Saint Blanquat et al., 2016; Teixell et al., 2016; Lagabriele et  
100 al., 2016, 2019; Asti et al., 2019). The major difference between the hyperextended Atlantic-  
101 type and Pyrenean Cretaceous rift margins is the rare occurrence of tilted crustal blocks and  
102 related stepping fault scarps in the central parts of the basins, thus defining a dominantly  
103 symmetrical basement profile with smooth slopes (see Lagabriele et al., 2020 for a review).  
104 Several other rift basins apart from the North Pyrenean rift basins exist along the plate  
105 boundary separating Iberia from the Eurasia plate and share several features in common with  
106 the Pyrenean system. They include the Tartas, Arzacq, Columbrets, Cameros and Parentis  
107 syn-rift basins, which developed during Late Jurassic to Early Cretaceous rifting (more details  
108 in the review section). The development of these basins is time-equivalent to the Late  
109 Jurassic–Aptian rifting and Albian–Cenomanian breakup sequence of the V-shaped Bay of  
110 Biscay margin (Montadert et al., 1979; Barbier et al., 1986; Thinon, 1999; Vergés & García-  
111 Senz, 2001; Thinon et al., 2003; Tugend et al., 2014) and the NW-Iberia margin (Soares et al.,  
112 2012; Alves & Cunha, 2018; Alves et al., 2020). All of these basins share similarities that  
113 include (1) a small amount of brittle deformation affecting the upper crust, (2) a pre-rift cover  
114 that is efficiently decoupled from its substratum thanks to the thick layer of Late Triassic to  
115 earliest Jurassic evaporites, (3) hyperthinned continental crust resulting from a polyphase  
116 rifting history, (4) a thick pre-rift to syn-rift sedimentary pile and (5) HT/LP syn-rift  
117 metamorphism. This paper presents a structural and sedimentological review of these smooth-  
118 slope type basins that sheds light on the major role of sedimentary burial and decoupling  
119 levels in controlling the ductile crustal thinning of the Iberia-Eurasia plate boundary basins  
120 during the syn-rift and breakup stages. We also compare the processes responsible for  
121 continental crust thinning and discuss the timing of formation of the smooth-slope type basins

with respect to the evolution of the West Iberia and Bay of Biscay hyperextended continental margins.

## **2 Mesozoic basins of Iberia and Europe**

### **2.1 Aquitaine basin and the Tartas and Arzacq basins**

The Aquitaine basin started to develop during the Late Permian in an extensional context related to the breakup of Pangea (Burg et al., 1994). During the Triassic and earliest Jurassic (Hettangian), extension led to an aborted rift basin filled with clastic rocks, carbonates, and an evaporite sequence ~1–2 km thick (Curnelle et al., 1982; Curnelle, 1983; Curnelle & Dubois, 1986). The Jurassic was a tectonically stable period marked by the development of a widespread carbonate platform (Peybernès, 1976). At the end of the Jurassic, the entire platform was confined as suggested by the deposition of restricted dolomite and anhydrite facies (BRGM et al., 1974; Serrano et al., 2006). The Jurassic pre-rift carbonate platform was uplifted, weathered and partly eroded (Combes et al., 1998; James, 1998; Canérot et al., 1999) in response to asthenosphere upwelling that preceded Early Cretaceous rifting (Saspiturry et al., 2019a). The Early Cretaceous was a structurally active time in which the Aquitaine basin evolved into different syn-rift basins characterised by very rapid subsidence (up to 130 m/Myr; Désaglaux & Brunet, 1990; Brunet, 1991), including the symmetric Arzacq and Tartas basins. A ~1–3 km thick Early Cretaceous syn-rift sedimentary sequence unconformably overlies pre-rift deposits of Triassic and Jurassic age totalling 2–3 km in thickness (Serrano et al., 2006).

#### **2.1.1 Tartas basin**

The Tartas basin is located in the southern part of the Aquitaine domain (Fig. 1). It is bounded to the north by the Celtaquitaine Flexure (BRGM et al., 1974), which separates the Tartas Basin and the North Aquitaine Platform, and to the south by the Audignon-Pécorade-Antin

Maubourguet ridge. The Tartas basin is a relatively narrow (20 km) east-west elongated trough (Serrano et al., 2006) that lies on slightly thinned continental crust (20–25 km; Wang et al., 2016). It formed symmetrically during the Berriasian with the development of widespread shallow-water facies and continued this pattern throughout Early Cretaceous continental rifting. Sediments from this period range from marginal littoral facies (Berriasian to Barremian; e.g., Issautier et al., 2018) to inner-platform facies (Aptian and Albian; e.g., Delfaud, 1969; Arnaud-Vanneau et al., 1979; Bouroullec et al., 1979; Peybernès, 1979, 1982). Throughout the Early Cretaceous rifting, the balance between carbonate production and basin subsidence in the Tartas basin led to the aggradation of a shallow-marine carbonate succession 2500 m thick. The resulting palaeogeography was a homogeneous, flat-floored basin with no major brittle deformation recorded within the basin. High subsidence rates are consistent with ductile pure shear thinning of the lower/middle crust and formation of a symmetric syn-rift basin (Issautier et al., 2020). This regime was probably enhanced by the presence of a thick evaporite layer of Rhaetian-Hettangian age that favoured mechanical decoupling between the pre-rift sediments and the basement. This salt blanket may account for the lack of illustrated brittle structures in the syn-rift succession of the Tartas basin (Issautier et al., 2020).

### **2.1.2 Arzacq basin**

The Arzacq syn-rift basin lies to the south of the Tartas basin (Fig. 1). Similarly to the Tartas basin, it is 40 km wide, elongated in the N110° direction and overlies slightly thinned continental crust nearly 25 km thick (Wang et al., 2016). The Arzacq basin is bounded to the north by the Audignon-Pécorade-Antin Maubourguet ridge (Mauriaud, 1987; Mediavilla, 1987; Serrano et al., 2006) and to the south by the North Pyrenean Frontal Thrust (Choukroune & ECORS Team, 1989; Daignières et al., 1994; Bourrouilh et al., 1995). Its southern flank coincides with north-dipping normal faults on the south side of the Grand Rieu



171 ridge (Fig. 2) (e.g., Serrano et al., 2006; Masini et al., 2014; Gómez-Romeu et al., 2019;  
172 Saspiturry et al., 2019a). Early Mesozoic rifting (Triassic to Hettangian) was responsible for a  
173 high subsidence rate and the deposition of a thick anhydrite sequence (Curnelle, 1983). The  
174 basin's subsequent rifting history was characterised by two successive extensional regimes,  
175 the first one symmetric (Berriasian to Aptian) and the second one slightly asymmetric  
176 (Albian) (Issautier et al., 2020). The symmetric syn-rift stage, identical to that of the Tartas  
177 basin, was accommodated by ductile flow of the lower/middle continental crust. Again, no  
178 brittle structures are recorded, probably because deformation was decoupled by the thick salt  
179 blanket (Canérot et al., 2005; Duretz et al., 2019). From Berriasian to Barremian times, the  
180 palaeogeography was dominated by a shallow marginal carbonate platform (e.g., Bouroullec  
181 & Deloffre, 1970; Peybernès & Combes, 1994; Biteau et al., 2006; Biteau & Canérot, 2007).  
182 In late Aptian times, the basin differentiated with the growth of a median marl flanked by  
183 carbonate-reef and inner-platform deposits (Delfaud & Gautier, 1967; Delfaud & Villanova,  
184 1967). This second stage began during the Albian with a sudden change in both  
185 palaeogeography and basin geometry, when the depositional profile became asymmetric and  
186 salt tectonics affected its flanking ridges (Fig. 2; Issautier et al., 2020). Halokinesis consisted  
187 of gliding displacement of the Grand Rieu sedimentary cover on the southern side of the basin  
188 (Fig. 2), leading to the development of salt-detached ramp synclines as defined by Jackson  
189 and Hudec, (2005) and Pichel et al. (2018). Salt diapirism in the Audignon district in the  
190 northern side of the basin accompanied this stage (Mauriaud, 1987; Mediavilla, 1987;  
191 Issautier et al., 2020). As the syn-rift stage continued, the gliding of the sedimentary cover  
192 occurred. Motion resulted from simple shear strain localisation along an Albian detachment  
193 fault that followed ductile pure shear thinning of the lower/middle crust during the Barremian-  
194 Aptian interval (Issautier et al., 2020). The subsidence history of the Arzacq syn-rift basin  
195 also shows that the second stage coincided with an unusually steep geothermal gradient that

ended around the initiation of the Pyrenean compression (Angrand et al., 2018). The post-rift stage was marked by the deposition of Cenomanian shallow-water carbonates resting unconformably on Albian strata. Although this basin underwent simple shear thinning during the Albian, it did not reach the stage of continental breakup.

## **2.2 Cameros basin**

The Cameros basin, on the northwestern edge of the Iberian mountain chain (Fig. 1), is a WNW-ESE trending synclinorium 80 km wide and 120 km long resulting mostly from Early Cretaceous rifting (Guimerà et al., 1995) (Fig. 3). The basin infill has been thrust onto neighbouring Cenozoic basins, the Ebro basin to the north and the Duero basin to the south (Fig. 3E). It underwent separate rifting stages from Permian to Triassic (Alvaro et al., 1979) and Late Jurassic to Early Cretaceous times (Platt, 1990; Mas et al., 1993; Casas-Sainz & Gil-Imaz, 1998; Salas et al., 2001). The Late Jurassic to Early Cretaceous rifting stage was followed by Late Albian thermal subsidence recording the post-rift stage (Omodeo Salè et al., 2014; Omodeo-Salé et al., 2014, 2017). The associated Late Jurassic to Early Cretaceous syn-rift sequence ranges from 6.5 to 8 km in thickness (Fig. 3) (Casas-Sainz & Gil-Imaz, 1998; Mas et al., 2011; Omodeo-Salé et al., 2014; García-Lasanta et al., 2017).

The base of the Mesozoic sedimentary pile of the Cameros basin is a 500 m thick Late Triassic salt sequence (Fig. 3) (Casas Sainz, 1993; Casas-Sainz & Gil-Imaz, 1998). A pre-rift Jurassic sequence reaching 800 m in thickness, composed of shallow marine carbonate platform deposits, lies unconformably over both the Triassic salt and the Paleozoic basement (Valladares, 1980; Platt, 1990; Aurell & Meléndez, 1993; Aurell et al., 2003). The syn-rift sequence begins with 3–6 km of fluvial to lacustrine deposits and rare unconformable marine layers of Late Jurassic to Barremian age (Guiraud & Séguret, 1985; Platt, 1990; Alonso & Mas, 1993; Mas et al., 1993, 2011; Quijada et al., 2010; Suárez González et al., 2010). The late Barremian to early Aptian depositional profile is characterized by lithologies typical of

221 coastal wetlands with both freshwater and marine influences, grading laterally to alluvial and  
222 fluvio-lacustrine deposits (Platt, 1989, 1986). These syn-rift deposits show that the basin was  
223 continuously shallow. The syn-rift sequence thins gradually toward the basin's flanks, where  
224 it laps onto the pre-rift Jurassic sequence (Fig. 3). An apparent northward migration of the  
225 depocenter suggests a slight asymmetry in the basin (Casas-Sainz & Gil-Imaz, 1998; Guimerà  
226 et al., 1995; Mas et al., 1993; Omodeo-Salé et al., 2014, 2017). This northward migration of  
227 the depocenter likely indicates that simple shear deformation was concentrated along a  
228 detachment fault. This fault was reactivated as a reverse fault during the Pyrenean  
229 compression, inducing the northward thrusting of the Cameros basin onto the Ebro flexural  
230 basin (Fig. 3) (Omodeo-Salé et al., 2014).

231 The Cameros basin is characterised by (1) the perfect continuity of the pre-rift Jurassic  
232 sequence, that is not fragmented along the reactivated detachment (Fig. 3), (2) the absence of  
233 normal faulting affecting both basement and cover (Fig. 3) and (3) a lack of significant offset  
234 of the top of the basement (Casas-Sainz & Simón-Gómez, 1992; Casas Sainz, 1993; Casas-  
235 Sainz & Gil-Imaz, 1998; Casas et al., 2000, 2009; Omodeo-Salé et al., 2014). The basin has  
236 therefore been interpreted as an extensional ramp syncline, formed above a décollement in the  
237 Late Triassic evaporites rooting at depth on a blind south-dipping extensional ramp or crustal  
238 detachment (Mas et al., 1993, 2011; Guimerà et al., 1995; Casas-Sainz & Gil-Imaz, 1998;  
239 Casas et al., 2009; García-Lasanta et al., 2017; Omodeo-Salé et al., 2017). This interpretation  
240 explains the northward migration of the syn-rift depocenter and associated edgeward onlap  
241 onto the pre-rift deposits, and the development of a synformal rift basin (Fig. 3). The pre-rift  
242 Jurassic deposits were stretched by this fault movement, but remained continuous (Casas et  
243 al., 2009). The Triassic evaporite layer accommodated most of the shear strain during  
244 extension, leaving both cover and basement well preserved. The resulting basinward gliding

of the pre-rift cover was accompanied by thinning of the Triassic evaporites and by salt diapirism (Casas Sainz, 1993; Casas-Sainz & Gil-Imaz, 1998; Rat et al., 2019).

The Cameros syn-rift basin exhibits effects of HT/LP metamorphism in its deepest part, with temperatures that reached around 350–400°C (Fig. 3E) (Guiraud & Séguret, 1985; Golberg et al., 1988; Rat et al., 2019). The rifting stage developed under a high thermal gradient estimated at around 70°C/km, assuming a sediment thickness of 8 km (Mata et al., 2001; Del Río et al., 2009). Toward the basin's northern edge, the palaeogeothermal gradient decreases to 41.5°C/km, along with the intensity of the HT/LP metamorphism (Fig. 3F) (Omodeo-Salé et al., 2017). This lower thermal gradient is consistent with an estimated heat flow of approximately 60–65 mW/m<sup>2</sup> (Omodeo-Salé et al., 2017). The HT/LP metamorphism reached its peak temperature during the early post-rift stage and developed coevally with continental breakup in the North Pyrenean Zone basins (Golberg et al., 1988; Casquet et al., 1992; Casas-Sainz & Gil-Imaz, 1998; Mata et al., 2001).

### **2.3 Parentis Basin**

The E-W elongated Parentis basin lies between the Landes High (Ferrer et al., 2009) to the south and the Armorican Arc to the north (Lefort & Agarwal, 1999). This wedge-shaped basin opens westward to the eastern edge of the Bay of Biscay continental margin characterized by exhumed subcontinental mantle at the ocean-continent transition (Fig. 1) (Pinet et al., 1987; Bois & ECORS Scientific team, 1990; Bois & Gariel, 1994; Jammes, 2009; Tugend et al., 2014). The south edge of the basin is defined by the north-dipping Ibis fault (Fig. 4; Ferrer et al., 2008). The continental crust of the future Parentis basin underwent several extensional deformations during the Permian to Early Triassic period (Dardel & Rosset, 1971; Mathieu, 1986; Ferrer et al., 2009; Biteau et al., 2006). Extension was accompanied by the deposition of a 1–3 km thick sequence of Late Triassic to Early Jurassic evaporites (Fig. 4D; Curnelle,

1983; Ferrer et al., 2009). The basin was subsequently filled with a 10 km thick sequence of pre-rift Jurassic and Early Cretaceous syn-rift shallow platform carbonates and terrigenous sediments that rests upon the Late Triassic evaporites (Fig. 4D; Montadert & Winnock, 1971; Bourrouilh et al., 1995; Bois et al., 1997). Tectonic subsidence occurred in the Parentis basin during a latest Jurassic to Early Albian syn-rift stage, followed by post-rift thermal subsidence during a latest Albian to Late Cretaceous post-rift stage (Brunet, 1994; Ferrer et al., 2008).

The Parentis basin is characterised by a hyperextended continental crust with a Moho depth of about 10 km in the thinnest portion (Bois & ECORS Scientific team, 1990; Bois, 1992; Ferrer et al., 2008). The overall basin geometry shows gently dipping margins lacking major normal fault scarps (Fig. 4D). The lower continental crust appears to be absent or very thin in the hyperextended domain, while the proximal margins include both upper and lower crust (Fig. 4D; Pinet et al., 1987b; Marillier et al., 1988; Tomassino & Marillier, 1997; Ruiz, 2007). A positive Bouguer gravity anomaly coincides with the hyperextended domain of the Parentis rift basin (Pinet et al., 1987a), which originated during the latest Jurassic to Early Cretaceous rifting affecting the peri-Pyrenean realm (Jammes et al., 2009; Tugend et al., 2015).

The ECORS deep seismic profiling project documented the symmetrical synclinal shape of the Parentis basin and the paucity of normal faults in the stretched crust as well as in the proximal rift margins (Fig. 4D) (Pinet et al., 1987b; Bois et al., 1997; Bois & Courtillot, 1988). Once the syn-rift stage was well established, the Parentis basin sedimentary profile became slightly asymmetrical in response to simple shear localization along a crustal detachment during Albian time (Fig. 4D; Pinet et al., 1987a; Jammes, 2009). This evolution stage is comparable to the one identified in the Arzacq basin (Issautier et al., 2020). The southern and northern margins of the rift have been interpreted by various workers as parts of an asymmetric opening system (Jammes et al., 2010a, 2010b, 2010c; Masini et al., 2014; Tugend et al., 2014). However, Pinet et al. (1987b) argued that the location and the geometry

of the thinned zone make it difficult to apply a classical simple shear model to the Parentis basin. They proposed that mantle uplift induced stretching (i.e. active rifting) and ductile flow in the lower crust and consequently a decoupling between the upper and lower crust. This depth-dependent crustal thinning explains the discrepancy between the slight extension at the surface and the substantial thinning of the lower/middle crust (thinning ratio greater than 6) at depth (Fig. 4D). This interpretation implies that the crust beneath the Parentis basin reached the ductile strain regime and was thinned under high-temperature conditions, as was the case in the adjacent North Pyrenean Zone. Finally, according to various authors, the Parentis basin first developed as a latest Jurassic–Aptian symmetrical rift that became asymmetrical when thinning progressively occurred through simple shear concentrated along a ductile crustal shear zone during Albian time. This suggests that the processes responsible for the Parentis basin continental crust thinning bear similarities with the ones defined in the Arzacq and Cameros syn-rift basins.

Jammes et al. (2010c) highlighted the major role played by the thick pre-rift salt sequence in decoupling the deformation between the basement and the rest of the Mesozoic sedimentary cover. The southern margin of the Parentis basin underwent gravity-driven cover gliding followed by syn-rift thin-skinned extensional faulting along a décollement plane within the salt (Fig. 4D; Tugend et al., 2014). This process induced the development of syn-rift salt anticlines and welded diapirs affecting the Mesozoic sedimentary pile (Fig. 4D; Mathieu, 1986; Mediavilla, 1987; Ferrer et al., 2008). Moreover, Ferrer et al. (2012) reported that salt structures are mainly localised on basin flanks (Fig. 2).

## **2.4 Columbrets basin**

The Columbrets offshore basin is the southwestern part of the Valencia Trough between Spain and the Balearic Islands (Figs. 1 & 5A). This ENE-WSW trending basin represents a mildly

inverted and thus exceptionally preserved hyperextended rift of Late Jurassic to Early Cretaceous age (Fig. 5; e.g., Etheve et al., 2018). The pre-rift and syn-rift successions occupy a large-scale synclinal basin with thinned borders, shaped by displacement along extensional detachments (Figs. 5D-E). This domain underwent a polyphase rifting history that spanned three major rifting events. During the Late Permian to Early Triassic, distributed deformation formed an intracontinental rift basin filled by continental deposits (Arche & López-Gómez, 1996; Vargas et al., 2009). This first rifting stage was followed by a Late Triassic–Early Jurassic rifting event related to the opening of the Alpine-Ligurian Tethys (Jiménez-Munt et al., 2010; Frizon de Lamotte et al., 2011; Schettino & Turco, 2011). The climax of this rifting event was marked by the deposition of a thick layer of evaporites that became a major décollement during subsequent events (Ortí, 1974; Ortí et al., 2017). The Jurassic post-rift sequence is mainly composed of shallow-water limestone (e.g., Roca, 1996). Partial crustal thinning occurred during the first rifting stage (Salas et al., 2001; Nebot & Guimerà, 2016; Etheve, 2016; Etheve et al., 2018; Roma et al., 2018).

The main rifting stage leading to the hyperthinning of the continental crust in the Columbrets basin (Fig. 5D) occurred during the Late Jurassic to early Albian. The syn-rift succession consists of platform carbonate deposits, which grade basinward into deep-water marl and give way locally toward the basin's flanks to fluvial and deltaic deposits (Etheve et al., 2018 and references therein). The platform limestones preserve the record of post-rift thermal subsidence from the middle Albian to the Late Cretaceous (Salas et al., 2001; Nebot & Guimerà, 2016; Etheve et al., 2018).

The Moho depth is 25–30 km under the margins of the Columbrets basin and only 8–10 km under the central portion (Fig. 5A; Gallart et al., 1990; Banda & Santanach, 1992; Dañobeitia et al., 1992; Torné et al., 1996; Vidal et al., 1997; Ayala et al., 2003, 2015; Gomez-Ortiz et al., 2011; Etheve et al., 2018). The thickness of the continental crust reaches a minimum of

3.5 km in the hyperextended domain (Fig. 5D; Etheve et al., 2018), where it coincides with an unusually strong Bouguer gravity anomaly ranging in amplitude between 60 and 80 mGal (Fig. 5B; Ayala et al., 2015). Both features are consistent with the shallowing of the lithosphere-asthenosphere boundary (60–65 km depth) indicated by geoid modelling and 3-D gravity data consistent with extreme crustal thinning (Zeyen & Fernàndez, 1994; Ayala et al., 1996, 2003; Carballo et al., 2015).

The Columbrets basin has been interpreted as a salt-detached syn-rift ramp-syncline basin (Roma et al., 2018). The eastern side of the basin features an extensional detachment fault, rooting at depth in the continental crust beneath the hyperextended rift domain (Figs. 5D-E; Etheve et al., 2018) that coincides with the Triassic salt décollement. This detachment is responsible for the overall thin-skinned extensional deformation of the pre-rift sedimentary cover experiencing basinward halokinetic gliding (Etheve et al., 2018). Nevertheless, finite motion along the detachment imaged in seismic reflection profiles is not enough to account for the extreme crustal thinning identified in the basin core and the large discrepancy in thinning ratios between the lower and upper crust (Etheve et al., 2018). In fact, the reflective lower crust becomes thinner toward the axis of the Columbrets basin, where it appears to be either absent or no thicker than 1–2 km (Gallart et al., 1990, 1994; Dañobeitia et al., 1992; Torné et al., 1992; Sàbat et al., 1997; Vidal et al., 1997). These observations highlight the differences in the rheological response of the upper and lower crust to crustal stretching as deduced from the Parentis basin architecture. Etheve et al. (2018) suggested that the lower crust underwent large-scale ductile deformation/boudinage during the Late Jurassic to Early Cretaceous syn-rift stage followed by simple shear along a single crustal detachment at the end of the syn-rift stage. In summary, the evolution of the Columbrets rift system was controlled by shallow decoupling in the Triassic pre-rift evaporites and deep decoupling in the middle crust (Etheve et al., 2018). Thus, its syn-rift evolution shares similarities with the



behaviour of the Arzacq, Cameros and Parentis basins, which first experienced homogeneous ductile crustal thinning of the lower crustal levels passing to the activation of a shallower crustal detachment.

The present-day surface heat flow in the southwestern Valencia Trough is about 65 to 100 mW/m<sup>2</sup> (e.g., Ayala et al., 2015; Carballo et al., 2015). That area also displays the thinnest continental crust section (Banda & Santanach, 1992; Fernandez et al., 1995; Ayala et al., 2015), demonstrating that a stable high thermal regime was inherited from the Late Jurassic to Cretaceous rifting despite the fact that rifting ended in the Cenozoic.

## **2.5 North Pyrenean Zone basins**

In the Pyrenees, late Hercynian (Permian) post-orogenic extension led to the development of continental deposits in endorheic extensional basins (Bixel & Lucas, 1983, 1987; Bixel, 1984). At the same time, magmatic and granulitic rocks were exhumed all along the North Pyrenean Zone (de Saint Blanquat, 1993; Olivier et al., 2004; Cochelin, 2016; Cochelin et al., 2017; Saspiturry et al., 2019b). A consequence of the Hercynian collapse stage was major thinning of previously hot lithosphere, an important structural inheritance regarding the following Mesozoic stages. Recent studies have proposed that the continental crust was partly thinned before the onset of Early Cretaceous hyperextension. Restorations of Iberian-European crustal sections across the Mauléon basin (western Pyrenees) and the Ballongue basin (central Pyrenees) show that the Moho was already very shallow (~20 km depth) by the end of the Jurassic (Asti et al., 2019; Espurt et al., 2019; Saspiturry et al., 2020a). Thus, the latest Paleozoic thinning stage, as well as the Late Triassic regional extensional stage, should not be neglected when estimating the Cretaceous thinning in the North Pyrenean Zone.

The Triassic deposits of the Western Pyrenees are typical of the German-type succession, ending with a thick evaporite and ophite complex (Curnelle, 1983; Lucas, 1985; Rossi et al.,

2003). The salt unit has played a major role in the Pyrenees, acting as a décollement layer at the base of the Mesozoic sedimentary cover that controlled the deformational style during Early Cretaceous hyperextension (Canérot, 1988, 1989; Canérot & Lenoble, 1993; James & Canérot, 1999; Canérot et al., 2005; Jammes et al., 2010b; Lagabriele et al., 2010, 2020; Duretz et al., 2019). Unlike the previously described basins, the North Pyrenean Zone typically lacks Berriasian and Valanginian deposits (Combes et al., 1998; James, 1998; Canérot, 2008), a witness of the emersion of the area during the earliest Cretaceous. From Barremian to Aptian times, the Iberian and European margins of the North Pyrenean Zone basins were carbonate platforms grading to distal marls toward the basin axis. In summary, the North Pyrenean Zone hyperextended basins are characterised by sedimentary sequences consisting of (1) Late Triassic to Early Jurassic pre-rift evaporites 1–3 km thick (Curnelle, 1983), (2) Jurassic pre-rift carbonate platform rocks 0.5–2 km thick deposited in a relatively stable tectonic context (Delfaud & Henry, 1967; Lenoble, 1992; James, 1998), (3) Barremian to Aptian syn-rift carbonates and marls up to 1.6 km thick (Delfaud & Villanova, 1967, Arnaud-Vanneau et al., 1979), (4) syn-rift Albian flysch-like deposits (the Black Flysch or “Flysch Ardoisier”) 1–5 km thick (Debroas, 1978, 1987, 1990; Boirie, 1981; Boirie & Souquet, 1982; Fixari, 1984; Roux, 1983; Souquet et al., 1985; Debroas et al., 2010) and (5) post-rift turbidites 2–4 km thick (Casteras, 1971; Henry et al., 1987; Le Pochat et al., 1976; Razin, 1989).

In this section we discuss the reconstructed architecture of the Mauléon and Basque-Cantabrian basins, together with that of basins present within the Internal Metamorphic Zone. We show that similarly to the previously described basins, the North Pyrenean Zone basins is affected by a syn-rift stage characterised by pure shear ductile thinning of the lower middle crust. The North Pyrenean Zone basins are characterised by the presence of positive Bouguer gravity anomalies above their inverted hyperextended domain, as evidenced by the Basque-

Cantabrian, Mauléon and Saint-Gaudens anomalies (Fig. 6). These anomalies reflect the presence of subcontinental mantle at shallow depth that was exhumed during the climax of the Mesozoic extension. With the exception of the Columbrets basin, the North Pyrenean Zone rift basins record continental breakup and mantle exhumation from the latest Albian to Early Cenomanian (breakup sequence, sensu Soares et al., 2012).

### **2.5.1 Mauléon basin**

The Mauléon basin, located south of the Arzacq basin (Figs. 1 & 7), coincides with a strong positive gravity anomaly centred upon the basin axis (Figs. 6 & 7A; Gottis, 1972; Boillot et al., 1973). First interpreted as lower crustal material (Grandjean, 1994; Vacher & Souriau, 2001; Pedreira et al., 2007), the anomaly is currently attributed to the presence at shallow depth (~10 km) of a dome of subcontinental mantle (Fig. 7B; Casas et al., 1997; Jammes et al., 2010a). This interpretation has gained support from recent work documenting P-wave velocities of ~7.3 km/s in this deep material (Fig. 7B; Wang et al., 2016; Chevrot et al., 2018). Above the mantle dome, the thickness of the crust is assumed to be roughly 5 km (Fig. 7B). Mantle exhumation apparently occurred during Cretaceous hyperextension, when the Mauléon basin developed as a hyperextended rift (Jammes et al., 2009; Lagabrielle et al., 2010; Masini et al., 2014; Tugend et al., 2014; Corre et al., 2016; Teixell et al., 2016; Lagabrielle et al., 2019a; Labaume & Teixell, 2020). The basin was inverted during Eocene shortening and is a pop-up structure at present, bordered to the north and south by conjugate thrusts (Fig. 7B; Saspiturry et al., 2020a).

The Mauléon basin began as a symmetric syn-rift basin that subsided in response to pure shear ductile thinning of the lower/middle crust during the Early Cretaceous (Saspiturry et al., 2019a) (Fig. 7E). Its structural style changed from Albian to early Cenomanian time, leading to asymmetric basin morphology and sedimentary facies distribution. Gravity-flow conglomerates accumulated at the foot of the Iberian margin slope, forming the Mendibelza

fan conglomerates (Boirie, 1981; Fixari, 1984; Souquet et al., 1985), in response to activity on steep north-dipping normal faults (South Arbailles and North Arbailles faults; Saspiturry et al., 2019a). These rocks originated in fan deltas reworking freshly uplifted Paleozoic substratum. Restoration of syn-rift geometries indicates that the Iberian substratum was tilted 30° toward the north in Albian time (Saspiturry et al., 2019a). This implies a thickening of syn-rift deposits to the north toward the steep south-dipping Saint-Palais fault, where the conglomerates reach a maximum thickness of around 5 km (Fig. 7). This fault separated the marls of the central basin from the European proximal margin to the north, where a carbonate platform developed (Saspiturry et al., 2019a). The gentle southward slope of the European margin contrasts with the steep northward slope of the Iberian margin. This geometry points to the Saint-Palais fault as a major normal fault that was responsible for the change to asymmetric basin margins during Albian to early Cenomanian time. In this scheme, the steep north-dipping slope of the Iberian margin can be interpreted as a rollover structure in the hanging-wall of the Saint-Palais fault. The rollover structure is also accommodated by minor north-dipping normal faults that propagated toward the south.

Facies distribution significantly changed from the mid-Cenomanian to the late Santonian in the Mauléon basin as shallow carbonate platforms developed on the Iberian and European margins (Souquet, 1967; Alhamawi, 1992; Ternet et al., 2004; Serrano et al., 2006). On the European side, the transition from platform to basin coincided with the steep south-dipping South Grand Rieu fault (Fig. 7). The Iberian carbonate platform graded northward rather abruptly to deep-sea calcareous breccias at the site of the Lakhoura normal fault, which appears to have acted as a significant northward detachment during mid-Cenomanian times. This detachment, responsible for a southward tilt of the Iberian basement, crosscuts the lower part of the older Saint-Palais structure, which was inactive at that time. Thus, the Mauléon basin was affected by ductile pure shear thinning of the lower/middle crust from the

467 Barremian to the Aptian, followed by Albian simple shear concentrated along two major  
468 crustal detachments: (1) the south-verging Saint-Palais fault accommodating the thinning of  
469 the European margin and (2) the north-verging Lakhoura detachment crosscutting the Saint-  
470 Palais fault (Fig. 7C3). Along strike, the Mauléon basin was affected by continental breakup  
471 from the latest Albian to the Early Cenomanian (Fig. 7D) as evidenced by the presence of  
472 subcontinental mantle clasts into the latest Albian to Early Cenomanian Urdach breccias  
473 (Roux, 1983; Duée et al., 1984; Fortané et al., 1986; Debroas et al., 2010) as well as by the  
474 formation of ophicalcites at the surface of the denudated mantle (Jammes et al., 2009;  
475 Lagabrielle et al., 2010, 2019a; Debroas et al., 2010).

476 Rifting and continental breakup in the Mauléon basin developed, from the Early Cretaceous to  
477 the mid-Cenomanian (Fig. 7E), under a high geothermal gradient, as indicated by (1) Raman  
478 spectroscopy of carbon materials (RSCM) showing peak temperatures consistent with a  
479 gradient of 60–75°C/km (Corre, 2017; Saspiturry, 2019; Saspiturry et al., 2020b), (2) detrital  
480 zircon fission-track data indicating a 80°C/km gradient (Vacherat et al., 2014) and (3) (U-Th-  
481 Sm)/He thermochronology data indicating a 80–100°C/km gradient (Hart et al., 2017).  
482 Numerical thermal models suggest that the base of the hyperextended domain had a mantle  
483 heat flow of 100 mW/m<sup>2</sup> and a maximum temperature of 600°C during continental breakup  
484 (Saspiturry, 2019; Saspiturry et al., 2020b). Vitrinite reflectance values from the Mauléon  
485 basin also weigh in favour of HT/LP syn-rift metamorphism (Lescoutre, 2019; Lescoutre et  
486 al., 2019). It should be noted that the peak temperature was reached in the lower part of the  
487 basin during the post-rift period (Vacherat et al., 2014; Saspiturry, 2019), similar to the  
488 Cameros basin. Due to Pyrenean thrusting, a detached slice of mantle rock crops out in the  
489 eastern part of the basin (Urdach area). In that location, crustal material in contact with the  
490 Urdach lherzolites shows ductile shearing, suggesting that the upper/middle crust was  
491 extruded laterally from the basin axis at temperatures between 350°C and 450°C (Asti et al.,

2019). Hydrothermal fluid circulation sheds light on the ductile shearing of the Mauléon basin pre-rift cover during continental breakup at ~94 Ma (Incerpi et al., 2020). The thermal regime of the Mauléon basin from the end of the syn-rift stage (Albian, Fig. 7E) to the breakup sequence (latest Albian to Early Cenomanian; Fig. 7E) attests a ductilely stretched sedimentary cover and crystalline basement.

### **2.5.2 Basque-Cantabrian basin**

The Basque-Cantabrian basin records a similar Mesozoic history as the North Pyrenean Zone rift basins, although it developed to the eastern termination and south of the Pyrenean Axial Zone (AZ in Fig. 1). The rift axis is characterised by a succession of Upper Jurassic and Cretaceous sediments around 8–10 km thick with interlayered basic volcanic rocks of Aptian to Santonian age (Figs. 8A-B; Azambre & Rossy, 1976; Rat et al., 1983; Rat, 1988; García Mondéjar et al., 1996; Castañares et al., 1997; Castañares & Robles, 2004). The lithosphere is extremely thin in the western central part of the basin, as suggested by a positive Bouguer anomaly recorded in the Biscay Synclinorium (Fig. 6; Pedreira et al., 2007) that is interpreted as the consequence of lithospheric mantle exhumed at shallow depth (Figs. 8A-B; Pedrera et al., 2017, 2020; Garcia-Senz et al., 2019). Field observations and seismic interpretations indicate that the Basque-Cantabrian basin has an overall symmetric shape characterised by brittle deformation on its flanks and ductile deformation on its axis (DeFelipe et al., 2017; Pedrera et al., 2017; Ducoux et al., 2019).

The basin continental crust was stretched during the Early Cretaceous rifting stage. Locally, mantle denudation occurred during early Cenomanian continental breakup as revealed by the presence of a strongly weathered mantle fragment near the inverted Leiza major detachment fault (Mendia & Ibarguchi, 1991; DeFelipe et al., 2017; Ducoux, 2017; Ducoux et al., 2019). Hyperextension was also recorded by the development of Cretaceous HT/LP metamorphism (Golberg & Leyreloup, 1990; Cuevas & Tubia, 1999). Mineral assemblages and RSCM data

from the Nappes des Marbres, which represents the inverted eastern part of the Basque-Cantabrian basin, indicate that temperature in the pre-rift sedimentary cover locally reached 500–600°C during hyperextension (Figs. 8C-D; Lamare, 1936; Martínez-Torres, 1989; Mendia & Ibarguchi, 1991; Ducoux et al., 2019). Thus, the felsic crust and its sedimentary cover underwent ductile stretching during the Albian syn-rift stage and Cenomanian continental breakup. Interpretations of geophysical data have shown that decoupling between basement and cover rocks occurred in low-strength Triassic evaporites and mudstones and induced coeval formation of cover gliding, mini-basins, turtle salt anticlines, expulsion rollovers, and salt diapirs in the cover strata (Fig. 8; Pedrera et al., 2017, Ducoux et al., 2019; Cámara, 2020). The association of exhumed mantle along the Leiza fault with rift and post-rift structural geometries suggests that a major south-dipping ramp-flat-ramp extensional detachment was active from Albian to early Cenomanian time (Lagabriele et al., 2020).

### **2.5.3 Internal Metamorphic Zone basins**

The central and eastern portions of the North Pyrenean Zone include a narrow Internal Metamorphic Zone along their southern borders (Fig. 1). They consist of a east-west-trending stretched zone of Variscan basement and pre-rift to syn-rift metamorphic rocks (Casteras, 1933; Mattauer, 1968; Choukroune, 1974) with several outcrops of subcontinental mantle rocks (Monchoux, 1970; Choukroune & Mattauer, 1978; Fabriès et al., 1991, 1998; Lagabriele et al., 2010). Recent studies have shown that the Internal Metamorphic Zone is an inverted domain of continental crust that was hyperextended during Early Cretaceous rifting (Lagabriele & Bodinier, 2008; Lagabriele et al., 2010; Clerc & Lagabriele, 2014; Clerc et al., 2014, 2015; de Saint Blanquat et al., 2016; Teixell et al., 2018; Dielforder et al., 2019; Espurt et al., 2019; Garcia-Senz et al., 2019). In the central Pyrenees, the Internal Metamorphic Zone coincides with the Saint-Gaudens positive Bouguer anomaly (Fig. 9A) and corresponds to the inverted Early Cenomanian continental breakup domain (Figs. 9B-C).

542 It has been shown that the whole continental crust of the North Pyrenean Zone was affected  
543 by large-scale ductile boudinage during Early Cretaceous hyperextension, with E-W trending  
544 rift basins exhibiting a relatively symmetrical profile (Clerc et al., 2015; Lagabriele et al.,  
545 2020). The presence of a thick pre-rift salt layer led to basinward gliding of the overlying  
546 Jurassic cover during hyperextension (Lagabriele et al., 2010; Clerc & Lagabriele, 2014;  
547 Clerc et al., 2015; Duretz et al., 2019; Lagabriele et al., 2020).

548 Evidence of HT/LP metamorphism has been reported along the entire North Pyrenean Zone  
549 (Ravier, 1957; Albarède & Michard-Vitrac, 1978a, 1978b; Golberg et al., 1988; Golberg &  
550 Maluski, 1988; Golberg & Leyreloup, 1990; Clerc et al., 2015). This metamorphism resulted  
551 from Early Cretaceous continental-crust thinning and an associated increase in thermal  
552 gradient and burial (Choukroune & Mattauer, 1978; Vielzeuf & Kornprobst, 1984; Debroas,  
553 1990; Clerc et al., 2015). RSCM peak temperatures reached 400–600°C in the marbles of the  
554 Internal Metamorphic Zone, where some of the highest temperatures were recorded close to  
555 exhumed mantle outcrops (Fig. 9D; Clerc, 2012; Clerc et al., 2015; Boulvais, 2016; Chelalou  
556 et al., 2016; Lagabriele et al., 2016; Ducoux, 2017). During the Albian syn-rift stage and the  
557 Early Cenomanian breakup event, the crust was homogeneously and ductilely stretched in the  
558 hyperextended domain, while detachment faults at the transition between the mantle and the  
559 crust/sedimentary cover accommodated the thinning of the whole system (Lagabriele et al.,  
560 2019a). Likewise, mineral assemblages indicate that maximum temperatures of 550–650°C  
561 and pressures of 3–4 kbar were reached locally (Bernus-Maury, 1984; Golberg & Leyreloup,  
562 1990; Vauchez et al., 2013). Previous authors have established that this metamorphic event  
563 was linked to high syn-rift geothermal gradients (Dauteuil & Ricou, 1989; Golberg &  
564 Leyreloup, 1990; Clerc et al., 2015; Lagabriele et al., 2016). Finally, these data collectively  
565 indicate that the Jurassic to Early Cretaceous metacarbonate cover forming the current  
566 Internal Metamorphic Zone corresponds to pre-rift to basal syn-rift sediments located in the



deepest part of the former North Pyrenean Zone basin, which was also characterised by a thin continental crust.

The WNW-ESE trending Lourdes and Saint-Gaudens positive Bouguer anomalies coincide with the maximum thickness of the Albian syn-rift turbidites (Figs. 9A-B; Casas et al., 1997). Espurt et al. (2019) interpreted the Saint-Gaudens anomaly as a body of allochthonous mantle pushed northward onto the European margin on the North Pyrenean Frontal Thrust. It corresponds to an allochthonous body of subcontinental mantle that was previously exhumed during Early Cretaceous time (Fig. 9B).

## **3 Discussion: Tectono-sedimentary evolution of smooth-slope extensional basins**

### **3.1 Syn-rift**

#### **3.1.1. Pure-shear dominated thinning**

All the basins reviewed in this work are characterised by a strong heterogeneous structural pattern inherited from the Late Carboniferous to Triassic rifting events related to the collapse of the Variscan belt and the breakup of Pangea. These events ended with the deposition of ~1–3 km thick Late Triassic to Early Jurassic salt deposits. Thus, Mesozoic hyperextension initiated within a continental crust that was previously thinned to less than 30 km thick (Fig. 10A). Unfortunately, the precise thickness of the crust at the end of the Triassic remains undetermined. The Late Jurassic to Early Cretaceous syn-rift stage was driven by distributed deformation characterised by the lateral extraction of the lower/middle crust (Fig. 10B). During this stage, thinning of the lower/middle crust triggered progressive subsidence. Our review shows that homogeneous subsidence was partly balanced by the production of syn-rift carbonates in most of the studied basins. The result is a relatively smooth basin floor profile characterised by carbonate platform deposits with marls in a central trough. During this early

stage, the basin was symmetric and marked by edgeward onlap of the syn-rift deposits (Fig. 10B). The pre-rift cover was efficiently decoupled from its substratum thanks to the thick layer of Keuper evaporites at its base. This rheological layering and the progressive sinking of the central part of the rift system eventually led to the breakup of the pre-rift lid on the external margins of the basin. This resulted in a large-scale pre-rift cover which remained in the central part of the extensional system throughout the whole basin lifetime, while the continental crust was progressively thinned below it (Fig. 10B and C). In contrast to all other reviewed basins, the Tartas basin exemplifies this syn-rift stage since continental crust thinning was not followed by the activation of extensional detachments, allowing the basin floor profile to remain symmetric. During this first rift regime, the upper crust might have been affected by very minor brittle deformation beneath the salt décollement level that led to superficial salt diapirism affecting the pre-rift to syn-rift sedimentary cover (Fig. 10B), as evidenced in the Arzacq (Issautier et al., 2020), Parentis (Ferrer et al., 2012), Columbrets (Etheve et al., 2018), and Mauléon (Canérot et al., 2005) basins during Late Jurassic to Aptian time. However, during this syn-rift stage, continental crustal thinning was mainly accommodated by distributed ductile thinning within the lower/middle continental crust. This process was first suggested in the case of the Parentis basin (Pinet et al., 1987a). It was then put forward by Clerc and Lagabrielle (2014) in their interpretation of the architecture of the eastern North Pyrenean Zone basins and used by Corre et al. (2016) in the reconstruction of the eastern Mauléon basin border. It has more recently been applied to the central Mauléon basin (Saspiturry et al., 2019a; Asti et al., 2019), Arzacq basin (Issautier et al., 2020) and Columbrets basin (Etheve et al., 2018). It consists of a distributed thinning stage in which the lower/middle crust was homogeneously and symmetrically thinned without major brittle deformation of the upper crust. Interpretation of seismic profiles sheds light on the wide discrepancy in thinning ratios between the lower and upper crust in the Columbrets (Etheve et

al., 2018) and Parentis (Pinet et al., 1987a) basins as they were slightly inverted. Such a discrepancy in the amount of continental thinning has been numerically modelled and defined as depth-dependent continental crust thinning (Huismans & Beaumont, 2008, 2011, 2014). This pure shear dominated thinning stage is applicable to all the North Pyrenean Zone basins since (1) their sedimentary profile was symmetric throughout the Barremian to Aptian beginning of the syn-rift stage and (2) they do not record exhumation of the lower crust during Mesozoic hyperextension in their central part (see section 2.5 for more details).

### **3.1.2. Simple shear dominated thinning**

As thinning of the lower/middle crust continued, isostatic subsidence occurred in the centre of the basin. The early smooth synclinal-shape basin progressively deepened, triggering steepening of pre-to- syn-rift sequences. Deformation became localised and a simple shear regime initiated along a crustal detachment connecting upward to the Late Triassic pre-rift salt décollement. With the progression of extension, the pre-rift sequence was progressively dissected in several large-scale boudins and turtle structures separated by intervening salt diapirs (Fig. 10C and D). The top basement surface is steeper in the basin flanks than in the basin core, therefore portions of the pre-rift cover may undergone gravity-driven gliding leading to local syn-extensional thrusting (layer-parallel shortening). From a general point of view, gliding was controlled by thickness variations of the sedimentary pile that cause differential loading on the salt layer (Lundin, 1992; Liro & Coen, 1995; Rouby et al., 2002) and basinward tilting of the proximal margin (Cobbold & Szatmari, 1991; Demercian et al., 1993; Gaullier et al., 1993; Fort et al., 2004a, 2004b). The gravity gliding unroofed the basement of the proximal rift margin. As the pre-rift and syn-rift sequences glided along the décollement, salt was expelled both marginward and basinward as well as upward by buoyancy. Thus, in the reviewed basins, halokinesis led to (1) the development of salt-detachment synclines, salt rollovers or diapirs affecting and controlling syn-rift depocentres

and (2) the denudation of the proximal margin basement that was subsequently overlain by syn-rift sediments. This scenario is reported from most of the studied basins.

(1) In the Arzacq basin, the southern margin recorded northward cover gliding (Fig. 2; Issautier et al., 2020).

(2) In the Parentis basin, major diapirism (Pelican borehole, Fig. 4D; Ferrer et al., 2008, 2009, 2012) and denudation of its southern margin basement (Fig. 4D; Jammes, 2019) were documented.

(3) In the Columbrets basin, the SE margin basement was denudated (Etheve et al., 2018).

(4) In the Mauléon basin, the proximal margin basement was locally denudated on both edges of the rift (Fig. 7C3 & 7D; Teixell et al., 2016; Saspiturry et al., 2020a).

(5) In the Basque-Cantabrian basin, the prerift cover was removed from its proximal margins (Fig 8A; Pedrera et al., 2017).

(6) In the Internal Metamorphic Zone, the pre-rift allochthonous cover remained in its central part (Fig. 9C-D; Espurt et al., 2019).

Denudation of the basement proximal margin has also appeared in thermo-mechanical numerical models of lithospheric-scale extension that integrate recent data collected along the North Pyrenean Zone basins (Duretz et al., 2019). This process resulted in the formation of syn-gliding wedge-shaped sedimentary geometries and syn-rift sequence depocenter migration, as seen in (a) the Arzacq and Parentis basins, which display southward syn-rift depocenter migration (Fig. 2 and 4D; Jammes, 2009; Issautier et al., 2020), and (b) the Cameros, Columbrets and Mauléon basins which display northward, north-westward and northward syn-rift depocenter migration, respectively (Figs. 3F, 4D and 7C2-C3; Omodeo-Salé et al., 2014; Etheve et al., 2018; Saspiturry et al., 2020a). In the Mauléon basin, the

increasing northward slope-deepening of the Iberian margin is interpreted as a rollover effect linked to the Saint-Palais detachment. Increasing tilting of the Iberian margin led to cover gliding, immediately followed by the accumulation of deep basin gravity deposits. These latter consist of reworked sediment from rafts of the pre-rift sedimentary cover and the freshly exposed proximal margin basement (Teixell et al., 2016; Saspiturry et al., 2019a; Labaume & Teixell, 2020). A similar evolution cannot be clearly reconstructed for the Basque-Cantabrian and Internal Metamorphic Zone basins, which experienced severe inversion during the compressional stages of the Pyrenean orogeny (e.g. Pedrera et al., 2017, Fig. 8A; Espurt et al., 2019, Fig. 9C). In contrast to the Tartas basin, which did not reach the second syn-rift extensional stage, all the other basins became asymmetric, as evidenced by shifts of the basin depocenter.

Seismic profiles display clear images of crustal detachments in the Parentis (Fig. 4D; Jammes, 2009; Jammes et al., 2010c; Tugend et al., 2014) and Columbrets (Figs. 5D & 5E; Etheve et al., 2018) basins. Both basins exhibit an asymmetric outline associated with a very thin crust in their axial regions. This sheds light on the fact that important crustal thinning was partly accommodated by simple shear deformation along the imaged detachments (Fig. 2B; Issautier et al., 2020). In the Arzacq and Cameros basins, detachment faults have not been imaged but only inferred, although both basins evolved with cover gliding and depocenter migration during the syn-rift stage. For instance, the northern thrust edging the Cameros basin has been interpreted as a reactivated syn-rift southward deepening ramp-flat structure corresponding to an extensional detachment (Figs. 5E-F; Omodeo-Salé et al., 2014). Although the Arzacq, Cameros, Parentis and Columbrets basins did not record continental breakup like the North Pyrenean basins, crustal thinning was fairly advanced, developing under warm thermal conditions during the simple shear stage. Indeed, mature mantle exhumation is evidenced by a positive Bouguer anomaly and a current shallow Moho depth in the Parentis (Figs. 4A & 4D;

Jammes, 2009) and Columbrets basins (Figs. 5A-D; Ayala et al., 2015; Etheve et al., 2018). Due to progressive burial and continental crust thinning, the sedimentary cover in the centre of some smooth-slope basins experienced warm thermal regimes as typically shown by the HT/LP metamorphism of the North Pyrenean Basins (more than 400°C). This is also documented in the Cameros basin by mineralogical analysis, thermochronology and fluid inclusion studies (Fig. 3F; Rat et al., 2019), as well as in the Columbrets basin by an elevated mantle heat flow of around 100 mW/m<sup>2</sup> (Ayala et al., 2015; Carballo et al., 2015).

### **3.2 Breakup stage**

The North Pyrenean Basins first underwent significant pure shear ductile thinning of the lower/middle crust throughout the Barremian to Aptian, followed by simple shear localization on detachment faults during the Albian (Saspiturry et al., 2019a). In concept, continental breakup occurs once the sedimentary cover is removed from the proximal margins and the lower crust fully withdrawn from the basin centre (Fig. 10D). This results in the development of brittle deformation on the basin flanks and the formation of tilted basement blocks devoid of sedimentary cover, while the central hyperextended domain records dominantly ductile thinning and mantle exhumation (Fig. 10D). As previously shown by Soares et al. (2012), while the upper continental crust deforms in a brittle manner in the hyperextended domain during dominantly pure-shear thinning, the deformation regime switches during dominantly simple-shear thinning and subsequent mantle exhumation. As the lower and middle crust is removed from the basin centre during the syn-rift sequence, the isotherms rise under the most highly extended parts of the rift. The 300°C to 500°C isotherms can be traced above the top of the Variscan basement and overlying pre-rift and syn-rift sediments. This implies that large volumes of the basement and cover were in a ductile regime during this stage (Fig. 10D). Thus, during the breakup sequence, thinning of the crust is first controlled by the elevation of the thermal conditions in relation with mantle exhumation. An additional parameter triggering

temperature elevation is the progressive burial of the continental crust under a thick sedimentary cover that accumulates in the basin during the syn-rift stage. Both causes significantly increase the temperature at the base of the basin. This process has also been demonstrated by numerical modelling of the North Pyrenean Zone basins (Duretz et al., 2019). In the hyperextended domain, extension is localised along a ductile shear zone at the transition between mantle and continental crust/sedimentary cover.

Our review highlights important characteristics of the thinning processes in the most evolved basins. We confirm that the conditions of HT/LP metamorphism evident along the hyperextended domains of the North Pyrenean basins account for the ductile behaviour of the crust. The climax of this thermal metamorphism occurred during continental breakup (Albarède & Michard-Vitrac, 1978a; Montigny et al., 1986; Golberg et al., 1986; Golberg & Maluski, 1988; Thiébaud et al., 1992). The peak temperature reached in the Jurassic to Albian sedimentary cover varies between 500° and 600°C, as documented in various places: (1) the Mauléon basin (Figs. 7C4-D; Corre, 2017; Saspiturry, 2019), (2) the Nappes des Marbres in the Basque-Cantabrian basin (Fig. 8D; Lamare, 1936; Martínez-Torrez, 1989; Mendia & Ibarguchi, 1991; Ducoux, 2017; Ducoux et al., 2019) and (3) the Internal Metamorphic Zone basins in the central and eastern Pyrenees (Fig. 9D; Bernus-Maury, 1984; Golberg & Leyreloup, 1990; Azambre et al., 1992; Clerc, 2012; Vauchez et al., 2013; Clerc et al., 2015; Chelalou et al., 2016).

The Internal Metamorphic Zone and the Nappes des Marbres have been interpreted as the inverted base of the North Pyrenean hyperextended rift domain (Clerc, 2012; Clerc & Lagabrielle, 2014; Clerc et al., 2015; Lagabrielle et al., 2016; Ducoux, 2017). In these settings, continental crust thinning resulted in a high geothermal gradient estimated at around 60–100°C/km in the Mauléon basin (Vacherat et al., 2014; Corre, 2017; Hart et al., 2017; Saspiturry, 2019). The maximum temperature reached in the sedimentary cover increased

739 from the margins to the hyperextended domain. Thus, the thermal gradient increased together  
740 with the thickness of the sedimentary pile (Saspiturry, 2019). Numerical thermal modelling  
741 has shown that this thermal gradient was associated, in the Mauléon basin, with an elevated  
742 mantle heat flow of around  $100 \text{ mW/m}^2$  (Saspiturry, 2019). The basinward gliding of the pre-  
743 rift cover contributed significantly to the burial and thus to the peak temperature increase at  
744 the base of the hyperextended domain.

745 The coupled effects of heating by mantle exhumation and burial under the thick pre-rift (salt  
746 tectonic) to syn-rift sedimentary sequence prevented crustal normal faults from propagating  
747 into the hyperextended domain, as evidenced in the Nappes des Marbres (Fig. 8D; Ducoux et  
748 al., 2019) and the Internal Metamorphic Zone (Fig. 9D; Espurt et al., 2019). Thinning of both  
749 the Variscan basement and the allochthonous sedimentary pile occurred in the hyperextended  
750 domain within a thick zone of dominantly ductile shear (Lagabriele et al., 2019a). This  
751 process led to the formation of large-scale boudins and lenses of continental crust and  
752 strongly sheared metasedimentary rocks (Clerc & Lagabriele, 2014; Clerc et al., 2015b;  
753 Corre et al., 2016; Asti et al., 2019; Duretz et al., 2019; Lagabriele et al., 2019a). These  
754 mature basins then took the shape of typical pseudo-symmetric hyperextended rift basins;  
755 their margins were affected by brittle normal faulting and their centres were dominated by  
756 ductile stretching as observed along the most evolved smooth-slope basins of the North  
757 Pyrenean Zone. As shown by the presence of clasts of mantle rocks in the Cretaceous  
758 turbidite breakup sequence of the Urdach area, these basins underwent local denudation of  
759 subcontinental mantle thanks to motion along a major detachment during the Late Albian to  
760 Early Cenomanian continental breakup (Roux, 1983; Duée et al., 1984; Fortané et al., 1986;  
761 Jammes et al., 2009; Debroas et al., 2010; Lagabriele et al., 2010, 2019a, b). Although the  
762 Mauléon basin displays clasts of mantle rocks reworked in its breakup sequence sensu Soares  
763 et al. (2012), it underwent heterogeneous amounts of mantle denudation and seems to show a



less advanced stage of continental breakup than the Basque-Cantabrian and Internal Metamorphic Zone basins. According to Saspiturry et al. (2019a, 2020a), the amount of mantle denudation under the Mauléon basin varied along strike as a consequence of Permian inheritance along N20° transverse structures (Fig. 7C3; Saspiturry et al., 2019b). It was maximal in the eastern part (Urdach) but almost nonexistent in its western part (Fig. 7D; Teixell et al., 2016; Labaume & Teixell, 2020). In addition, the Internal Metamorphic Zone basin displayed a more advanced breakup sequence than the Basque-Cantabrian basin as evidenced by the widths of exhumed mantle along two restored crustal-balanced cross-sections, which are ~45 km (Fig. 9C; Espurt et al., 2019) and ~15 km (Fig. 8A; Pedrera et al., 2017) long, respectively. The Bilbao, Mauléon and Saint-Gaudens positive Bouguer anomalies (Fig. 6) represent the remains of continental breakup stages now buried at depth, as they correspond to major pieces of mantle exhumed during the latest Albian to Early Cenomanian breakup sequence and more recently inverted during the Pyrenean orogeny (Figs. 7A-B, 8A-B & 9A-B).

Based on the observations listed in this section, we may conclude that the reviewed smooth-slope extensional basins represent different degrees of hyperextension that occurred along the Iberia-Eurasia plate boundary during the Cretaceous drift of Iberia. We thus propose to rank these basins from least mature to most mature as follows: (1) Tartas, (2) Arzacq/Cameros, (3) Parentis/Columbrets, (4) Mauléon, (5) Basque-Cantabrian and (6) Internal Metamorphic Zone (Fig. 11). This ranking indicates that as the amount of extension increases in these basins, the intensity of various fundamental processes also increases. These processes are lower/middle crust lateral extraction, thermal gradient and heat flow, HT/LP metamorphism, ductile thinning of the crust and its sedimentary cover, relative gliding of the pre-rift cover and mantle exhumation.

788 A major consequence of all these processes is the formation of a succession of basins with  
789 smooth basement slopes, which differ significantly from rift basins controlled by dominantly  
790 normal faulting that affects both their borders and centres. These smooth-slope basins were  
791 the locus of gentle, homogeneous subsidence that led to the deposition of syn-rift flysch-like  
792 sediments a few kilometers thick. Therefore the response of the smooth-slope basins to  
793 extensional stress was the accumulation of sediments that in turn increased the thermal burial  
794 effect in the basin centres. Such burial appears to have been a key factor in the syn-rift  
795 evolution of smooth-slope basins, along with parameters that were critical earlier at the  
796 initiation of rifting, such as the Variscan-Triassic inheritance of thin crust (Asti et al., 2019)  
797 and the presence of a very thick (average 2 km) layer of evaporites and shale of the Keuper  
798 group that allowed the decoupling of the pre-rift cover and its stagnation within the centre of  
799 the studied basins (Lagabrielle et al., 2020). Syn-rift deposits of mature smooth-slope basins  
800 are well known in the North Pyrenean Zone as the “Flysch Noir” group (Souquet et al., 1985;  
801 Debroas et al., 1990). Pioneer authors such as Ravier (1959) have shown that this sequence  
802 locally experienced HT/LP metamorphism and deduced from microstructural analysis that a  
803 large part of this evolution was static and necessarily linked to passive burial in the Flysch  
804 Noir basins. These authors clearly showed that the thermal pulse did not affect the  
805 Cenomanian sediments, leading to the concept of a “phase ante-cénomaniennne” (e.g. Casteras,  
806 1933). In contrast, further studies pointed to the synkinematic character of some HT/LP  
807 mineral assemblages and claimed that Pyrenean metamorphism was linked to the orogenic  
808 evolution of the belt (e.g. Choukroune, 1976). Later detailed studies revisited the link between  
809 thermal metamorphism and the opening of the North Pyrenean basins (e.g. Golberg &  
810 Leyreloup, 1990). However, these studies did not consider the role of sedimentary burial.  
811 Therefore, in this review, we note the existence of pioneer works that despite the rudimentary

geological knowledge of the time deduced 60 years ago that sediment burial was a key factor in the thermal evolution of the basins at the Iberia-Eurasia plate boundary.

## **4 Comparison of smooth-slope type basins with Atlantic type margins: West Iberia and Bay of Biscay margins**

### **4.1. Review of the timing of the main Mesozoic events and unconformities**

In this section we address the timing of formation of the syn-rift, breakup, post-rift and drifting sequences in the reviewed basins as well as in the adjacent Northwest Iberia and Bay of Biscay margins (Fig. 12). As a reminder, the syn-rift, breakup, post-rift and drifting sedimentary sequences record respectively crustal thinning, mantle denudation, post-rift thermal cooling and oceanic spreading (e.g. Alves et al., 2009, 2020; Soares et al., 2012; Alves & Cunha, 2018). These sequences are delimited by major unconformities corresponding (from bottom to top) to the base syn-rift unconformity (BSU; base of syn-rift sequence), the lithospheric breakup surface (LBS; base of the breakup sequence) and the base post-rift unconformity (BPU; base of the post-rift sequence) as defined by Soares et al. (2012) and Alves and Cunha (2018).

All the reviewed basins as well as the West Iberia and Bay of Biscay margins are characterised by the onset of Mesozoic rifting between the Late Jurassic and earliest Cretaceous as they are all related to Iberia plate motion associated with the North Atlantic opening (e.g. Alves et al., 2009; Nirrengarten et al., 2017; Angrand et al., 2020). The beginning of rifting is slightly diachronous among these basins as evidenced by the timing of formation of their BSU (Fig. 12). Nearly all of the rifting sequences in the Tartas and Arzacq (Désaglaux & Brunet, 1990; Brunet, 1991; Serrano et al., 2006; Issautier et al., 2020), Parentis (Brunet, 1994; Ferrer et al., 2008; Jammes et al., 2009; Tugend et al., 2015) and Columbrets (Salas et al., 2001; Nebot & Guimerà, 2016; Etheve, 2016; Etheve et al., 2018; Roma et al.,

2018) basins end at the same time, in the Early or Middle Cenomanian (Fig. 12). The North Pyrenean Zone basins end their syn-rift sequence slightly earlier, as they are characterised by a breakup sequence developing between the latest Albian and the Early Cenomanian (Fig. 12; Masini et al., 2014; Teixell et al., 2016; Pedrera et al., 2017; Espurt et al., 2019; Labaume and Teixell, 2020). Thus, the North Pyrenean Zone basins are characterised by the development of a LBS surface (*sensu* Soares et al., 2012) separating the Early Cretaceous syn-rift sequence and the Latest Albian to Early Cenomanian breakup sequence. Hence the syn-rift sequence of the reviewed basins lasts around 35–45 Myr according to the timing of formation of the different basins whereas the breakup sequence of the North Pyrenean Zone basins lasts about 5 Myr (Fig. 12). In contrast to the reviewed basins, the West Iberia margins have a relatively short (~20 Myr) syn-rift sequence and a longer (~15 Myr) breakup sequence (Soares et al., 2012; Pereira & Alves, 2012; Alves & Cunha, 2018; Alves et al., 2020), and the Bay of Biscay margins have equally long syn-rift and breakup sequences (~20 Myr) (Fig. 12; Montardet et al., 1979; Brunet, 1994; Thinon, 1999; Thinon et al., 2001, 2003; Tugend et al., 2015). This is consistent with interpretations of the West Iberia margin as having a syn-rift sequence getting longer to the north and a continental breakup sequence becoming shorter to the north (Alves et al., 2002, 2006, 2009).

All the reviewed basins record a post-rift thermal cooling stage in which a post-rift sequence overlaps the syn-rift sequence in the Tartas, Arzacq, Cameros, Parentis and Columbrets basins and the breakup sequence in the North-Pyrenean Zone basins, where they record a more advanced Mesozoic extension. The post-rift unconformity is clearly visible in the reviewed basins as erosional truncation of the syn-rift/breakup sequences and onlap of the post-rift sequence, as seen in a seismic profile in the Arzacq (Fig. 2; Issautier et al., 2020), Parentis (Fig. 4D; Jammes, 2019), and Columbrets (Figs. 5C-E; Etheve et al., 2018) basins, and in field observations in the Cameros (Omodeo-Salé et al., 2014, 2017), Mauléon (e.g. Saspiturry

et al., 2019a), Basque-Cantabrian (Rat, 1988) and Internal Metamorphic Zone (Debroas, 1978, 1987, 1990) basins. Although the North Pyrenean Zone basins underwent continental breakup, it did not progress to oceanic spreading. It is conceivable that the Pyrenean compression may have obliterated the stratigraphic evidence for a drifting stage in the North Pyrenean Zone basins. However, (1) the entire mid-Cenomanian to Late Santonian post-rift sequence is fully preserved above the North Pyrenean Zone hyperextended domain and clearly records a post-rift thermal cooling stage, (2) there is no evidence of subducted oceanic crust in a passive seismic Vp/Vs model of the Mauléon basin (Fig. 7B, Wang et al., 2016) and Internal Metamorphic Zone basins (Fig. 9B, Chevrot et al., 2018) or in a crustal-scale 3D gravity inversion of the Basque-Cantabrian basin (Pedrera et al., 2017). In contrast to the North Pyrenean Zone basins, oceanic spreading occurred during mid-Cenomanian time in the eastern Bay of Biscay margins (Fig. 12; Montadert et al., 1979; Brunet 1994; Thinon, 1999; Thinon et al., 2001, 2003; Gong et al., 2008; Tugend et al., 2015) and at the Cenomanian-Turonian boundary in the Northwest Iberia margin and western Bay of Biscay margins (Fig. 12; Gong et al., 2008; Soares et al., 2012; Pereira & Alves, 2012; Alves & Cunha, 2018; Alves et al., 2020). Although the duration of the breakup sequence differs strongly between the North Pyrenean Zone basins and the Bay of Biscay and West Iberia margins, the breakup affected all of these regions simultaneously from the mid-Cenomanian to the earliest Turonian (Fig. 12).

## **4.2 Architectural contrasts and discrepancies in the modes of crustal thinning**

Atlantic-type margins such as West Iberia (Boillot et al., 1980, 1995; Reston et al., 1995; Whitmarsh et al., 2001; Péron-Pinvidic & Manatschal, 2009; Sutra et al. 2013; Péron-Pinvidic et al., 2015) or the Bay of Biscay margins (Jammes, 2009; Jammes et al., 2010a, 2010b, 2010c; Tugend et al., 2014) are characterized by five distinctive features: (1) deformation coupling that occurs when the ductile layer has been removed and deformation in the strong

and brittle upper crust couples with deformation in the strong lower crust/upper mantle, (2) detachment faults at the top of the basement that accommodate crustal extension through tilting of blocks of the basement and their pre-rift cover showing a coupled deformation, (3) formation of continental crust extensional allochthons, made up of upper crust and pre-rift cover, tectonically placed over exhumed lower crust or serpentinized mantle, (4) a wide domain of exposed subcontinental mantle at the ocean-continent transition and (5) large-scale serpentinization of the exhumed mantle that was still active at ambient seawater temperatures (Fig. 13A). Numerical models of such systems reproduce the palaeoarchitecture of the continental margins and the detachment faults responsible for crustal thinning (Lavrier & Manatschal, 2006; Huisman & Beaumont, 2011). Numerical studies have also shown that continental crust thinning develops under conditions of high heat flow from the mantle due to asthenospheric upwelling. In these sediment-starved Atlantic-type margins, only small volumes of syn-rift sedimentary cover can be found in the hyperextended domain (Masini et al., 2011, 2012; Péron-Pinvidic et al., 2015; Ribes et al., 2019) (Fig. 13A).

Palaeogeographic reconstructions (Ziegler, 1982; Dercourt et al., 1986; Ortí et al., 2017; Soto et al., 2017) show that the distribution of the Pyrenean and peri-Pyrenean smooth-slope extensional basins corresponds closely to the distribution of Late Triassic evaporites and claystones (Lagabrielle et al., 2020). Numerical modelling shows that these Triassic deposits played a major role at the onset of continental rifting as zones of decoupling between the Palaeozoic basement and the Jurassic to Albian sedimentary cover (Duretz et al., 2019). Thus Triassic salt does not allow the coupling of the basement and its sedimentary cover during crustal extension characteristic of Atlantic-type margins. Moreover, in smooth-slope basins, the lower/middle crust is not exhumed during the breakup sequence, unlike Atlantic-type margins, as it has been laterally extracted during initial rifting. In fact, the only lower crustal rocks cropping out along the Cretaceous North Pyrenean Rift axis are quite old, having been

previously exhumed during Permian time (de Saint-Blanquat, 1993; Olivier et al., 2004; Cochelin et al., 2018a, 2018b; Saspiturry et al., 2019b).

Finally, unlike Atlantic-type margins, the hyperextended domain of smooth-slope basins deforms under ductile conditions and HT/LP conditions due to (1) the displaced cover remaining preserved in the centre of the basin while the lower crust is thinned ductilely and (2) the continental crust being buried under a very thick pre-rift to syn-rift sedimentary cover. However, as in Atlantic-type margins, the proximal margins become subject to extensional brittle faulting as the crust acquires a normal thermal gradient of  $\sim 30^{\circ}\text{C}/\text{km}$  (Saspiturry, 2019) and the proximal sedimentary cover is thinned or removed (Fig. 13B). Thus in smooth-slope basin margins, the proximal margins undergo brittle deformation while the hyperextended domain undergoes ductile thinning due to a complex interaction between salt beds, sedimentary burial and changes in the syn-rift thermal gradient (Fig. 13B). This elevated thermal regime is associated with intense metasomatism and fluid circulation affecting both the continental basement and the sedimentary cover at temperatures of  $500\text{--}600^{\circ}\text{C}$  (Corre et al., 2016; Quesnel et al., 2019; Lagabrielle et al., 2019a, 2019b). The peak syn-rift temperature is mainly controlled by burial but can be locally influenced by fluid circulation. Indeed, adiabatic temperatures in the sedimentary cover have been interpreted as the presence of local fluid generation and convective cells in the Mauléon (Saspiturry, 2019) and Boucheville (Boulvais et al., 2016) basins.

An important difference between the two geological settings is the fact that Atlantic-type margin are sediment-starved (less than 2 km of burial) while smooth-slope basins are sediment-rich (syn-rift sequence is more than 5 km thick). In addition, in the reviewed basins, the pre-rift cover remaining in the central part of the basin, thanks to the Late Triassic salt décollement, contributes significantly to the increase in burial and thus the peak temperature at the base of the hyperextended domain by adding around 2–3 km of pre-rift sediments to

preexisting syn-rift and breakup sedimentary sequences that are nearly 5 km thick. Therefore, the thinned continental basement and the exhumed mantle may be buried under 7–10 km of pre-rift to syn-breakup sediments. This allows the crust to deform in a ductile way. Finally, the pre-rift salt, which is mostly absent along Atlantic-type margins, is also a major contributor to sedimentary burial. Thus, it participates in the ductile thinning of the continental crust and its sedimentary cover, as pointed out by Lagabriele et al. (2020).

The review of the sequence of the main tectono-stratigraphic events presented in section 4.1 (Fig. 12) also sheds light on another possible controlling factor. Indeed, the duration of syn-rift sequences in smooth-slope basins (~35–45 Myr) is significantly longer than those of the West Iberia and Bay of Biscay margins (~15–20 Myr). Thus, the long lifetime of smooth-slope extensional basins could favour the depth-dependent ductile thinning of the lower/middle crust by pure shear at the beginning of the rifting stage and may prevent brittle structures from forming within the upper crust.

## 5 Conclusions

We infer the evolution of smooth-slope type basins in the Iberian-Eurasian plate junction from the rifting to the breakup stage. At the beginning of the syn-rift stage, depth-dependent crustal thinning is dominantly controlled by distributed pure shear thinning within the lower/middle crust due to the presence of two decoupling levels: (1) the middle crust, which allows the lower crust to be extracted laterally without disturbing significantly the upper crust, and (2) within pre-rift Triassic salt beds, which act as a décollement between the upper crust and the overlying sedimentary cover. Then simple shear becomes localized along a crustal detachment connecting upward with the Late Triassic décollement layer, inducing shearing in the pre-rift salt. When continental breakup occurs, the basin flanks are affected by brittle deformation while the hyperextended domain undergoes dominantly ductile thinning. The rise



of the 300°C to 500°C isotherms in the hyperextended domain, from the syn-rift to the continental breakup stage, implies that the originally crystalline upper continental crust and the overlying pre-rift and syn-rift sedimentary pile are affected by depth-dependent ductile thinning. The deformation style during rifting and continental breakup is mainly controlled by burial that results from the complex interaction between the syn-rift sedimentary sequence and the pre-rift salt beds that indirectly contribute to the burial by preserving from disruption the pre-rift sequence in the basin core.

To summarize, hyperextension in Atlantic-type margins leads to a progressive embrittlement of the continental crust due to progressive extraction of the ductile middle crust (e.g. Pérez-Gussinyé et al., 2001; Reston, 2009; Sutra et al., 2013; Mohn et al., 2015). In margins with smooth-slope basins, in contrast, crustal thinning is mostly ductile. The latter is favoured by the lateral extraction of the deep crust and the occurrence of thick sedimentary cover (Asti et al., 2019; Duretz et al., 2019; Lagabrielle et al., 2020). This implies that in the distal domain of smooth-slope margins deformation coupling never occurs, thanks to progressive upward migration of the brittle/ductile transition during rifting. Finally, in the reviewed basins, sedimentary burial coupled to the presence of pre-rift salt and a long-lived rifting sequence allow the continental crust to stretch in a dominantly ductile regime from rifting until breakup.

## References

- Albarède, F., & Michard-Vitrac, A., 1978a. Datation du métamorphisme des terrains secondaires des Pyrénées par les méthodes  $^{39}\text{Ar}$ - $^{40}\text{Ar}$  et  $^{87}\text{Rb}$ - $^{87}\text{Sr}$ ; ses relations avec les peridotites associées. *Bull. Société Géologique Fr.* 7, 681–687.
- Albarède, Francis, & Michard-Vitrac, A., 1978b. Age and Significance of the North Pyrenean Metamorphism. *Earth Planet. Sci. Lett.* 327–332.
- Alhamawi, M., 1992. Sédimentologie, pétrographie sédimentaire et diagenèse des calcaires Crétacé supérieur de la marge ibérique, Vallées d'Ossau - Vallée d'Aspe, Haute Chaîne, Pyrénées Atlantiques. Université Bordeaux 1.
- Alonso, A., & Mas, J.R., 1993. Control tectónico e influencia del eustatismo en la sedimentación del Cretácico inferior de la cuenca de Los Cameros.

988 Alvaro, M., del Villar, R.C., & Vegas, R., 1979. Un modelo de evolución geotectónica para la  
989 Cadena Celtibérica. *Acta Geológica Hispánica* 14, 172–177.

990 Alves, T. M., R. L. Gawthorpe, D. H. Hunt, and J. H. Monteiro., 2002, Jurassic tectono-  
991 sedimentary evolution of the Northern Lusitanian Basin (offshore Portugal), *Mar. Pet.*  
992 *Geol.*, 19, 727–754, doi:10.1016/S0264-8172(02)00036-3.

993 Alves, T. M., C. Moita, F. Sandnes, T. Cunha, J. H. Monteiro, and L. M. Pinheiro (2006),  
994 Mesozoic – Cenozoic evolution of North Atlantic continental slope basins: The  
995 Peniche basin, western Iberian margin, *AAPG Bull.*, 90, 31 – 60,  
996 doi:10.1306/08110504138.

997 Alves, T.M., Moita, C., Cunha, T., Ullnaess, M., Myklebust, R., Monteiro, J.H., Manupella,  
998 G., 2009. Diachronous evolution of Late Jurassic–Cretaceous continental rifting in the  
999 northeast Atlantic (west Iberian margin). *Tectonics* 28.  
1000 <https://doi.org/10.1029/2008TC002337>.

1001 Alves, T.M., Cunha, T.A., 2018. A phase of transient subsidence, sediment bypass and  
1002 deposition of regressive–transgressive cycles during the breakup of Iberia and  
1003 Newfoundland. *Earth Planet Sci. Lett.* 484, 168–183.  
1004 <https://doi.org/10.1016/j.epsl.2017.11.054>.

1005 Alves, T.M., Fetter, M., Busby, C., Gontijo, R., Cunha, T., Mattos, N.H., 2020, A tectono-  
1006 stratigraphic review of continental breakup on intraplate continental margins and its  
1007 impact on resultant hydrocarbon systems. *Marine and Petroleum Geology*, 117.  
1008 <https://doi.org/10.1016/j.marpetgeo.2020.104341>

1009 Angrand, P., Ford, M., & Watts, A.B., 2018. Lateral Variations in Foreland Flexure of a  
1010 Rifted Continental Margin: The Aquitaine Basin (SW France): Flexure of the  
1011 Aquitaine Foreland Basin. *Tectonics* 37, 430–449.  
1012 <https://doi.org/10.1002/2017TC004670>

1013 Angrand, P., Mouthereau, F., Masini, E., Asti, R., 2020. A reconstruction of Iberia accounting  
1014 for W-Tethys/N-Atlantic kinematics since the late Permian-Triassic, *Solid Earth*.  
1015 10.5194/se-2020-24.

1016 Arche, A., & López-Gómez, J., 1996. Origin of the Permian-Triassic Iberian Basin, central-  
1017 eastern Spain. *Tectonophysics* 266, 443–464. [https://doi.org/10.1016/S0040-](https://doi.org/10.1016/S0040-1951(96)00202-8)  
1018 [1951\(96\)00202-8](https://doi.org/10.1016/S0040-1951(96)00202-8)

1019 Arnaud-Vanneau, A., Arnaud, H., Charollais, J., Conrad, M.-A., Cotillon, P., Ferry, S.,  
1020 Masse, J.-P., & Peybernès, B., 1979. Paléogéographie des calcaires urgoniens du sud  
1021 de la France. *Géobios* 3, 363–383.

1022 Asti, R., Lagabrielle, Y., Fourcade, S., Corre, B., & Monié, P., 2019. How Do Continents  
1023 Deform During Mantle Exhumation? Insights From the Northern Iberia Inverted  
1024 Paleopassive Margin, Western Pyrenees (France). *Tectonics* 2018TC005428.  
1025 <https://doi.org/10.1029/2018TC005428>

1026 Aurell, M., & Meléndez, A., 1993. Sedimentary evolution and sequence stratigraphy of the  
1027 Upper Jurassic in the central Iberian Chain, northeast Spain. *Spec. Publ. Int. Ass.*  
1028 *Sediment.*

1029 Aurell, M., Robles, S., Bádenas, B., Rosales, I., Quesada, S., Meléndez, G., & García-Ramos,  
1030 J., 2003. Transgressive–regressive cycles and Jurassic palaeogeography of northeast  
1031 Iberia. *Sediment. Geol.* 162, 239–271. [https://doi.org/10.1016/S0037-0738\(03\)00154-](https://doi.org/10.1016/S0037-0738(03)00154-4)  
1032 [4](https://doi.org/10.1016/S0037-0738(03)00154-4)

1033 Ayala, C., Pous, J., & Torné, M., 1996. The lithosphere–asthenosphere boundary of the  
1034 Valencia Trough (western Mediterranean) deduced from 2D Geoid and Gravity  
1035 Modelling. *Geophys. Res. Lett.* 23, 3131–3134. <https://doi.org/10.1029/96GL03005>

1036 Ayala, C., Torne, M., & Pous, J., 2003. The lithosphere–asthenosphere boundary in the  
1037 western Mediterranean from 3D joint gravity and geoid modeling: tectonic

1038 implications. *Earth Planet. Sci. Lett.* 209, 275–290. <https://doi.org/10.1016/S0012->  
 1039 821X(03)00093-1  
 1040 Ayala, C., Torne, M., & Roca, R., 2015. A review of the current knowledge of the crustal and  
 1041 lithospheric structure of the Valencia Trough Basin. *Bol. Geológico Min.* 126, 533–  
 1042 552.  
 1043 Azambre, B., & Rossy, M., 1976. Le magmatisme alcalin d'âge crétacé, dans les Pyrénées  
 1044 occidentales et l'Arc basque; ses relations avec le métamorphisme et la tectonique.  
 1045 *Bull. Société Géologique Fr.* 7, 1725–1728.  
 1046 Banda, E., & Santanach, P., 1992. The Valencia trough (western Mediterranean): An  
 1047 overview. *Tectonophysics* 208, 183–202. <https://doi.org/10.1016/0040->  
 1048 1951(92)90344-6  
 1049 Barbier, F., Duvergé, J., & Le Pichon, X., 1986. Structure profonde de la marge Nord  
 1050 Gascogne. Implications sur le mécanisme de rifting et de formation de la marge  
 1051 continentale. *Bull. Cent. Rech. Explor. Prod. Elf Aquitaine* 10, 105–121.  
 1052 Bernus-Maury, C., 1984. Etude des paragéneses caractéristiques du métamorphisme  
 1053 mésozoïque dans la partie orientale des Pyrénées. Pierre et Marie Curie, Paris.  
 1054 Biteau, J., & Canérot, J., 2007. La Chaîne des Pyrénées et ses avant-pays d'Aquitaine et de  
 1055 l'Ebre: caractéristiques structurales, évolution géodynamique et tectono-sédimentaire.  
 1056 *Geol.-PARIS-* 155, 16.  
 1057 Biteau, J.-J., Le Marrec, A., Le Vot, M., & Masset, J.-M., 2006. The Aquitaine Basin. *Pet.*  
 1058 *Geosci.* 12, 247–273.  
 1059 Bixel, F., 1984. Le volcanisme stéphano-permien des Pyrénées. Université Paul Sabatier de  
 1060 Toulouse (Sciences).  
 1061 Bixel, F., & Lucas, C.L., 1983. Magmatisme, tectonique et sédimentation dans les fossés  
 1062 stéphano-permiens des Pyrénées occidentales. *Rev. Géologie Dyn. Géographie Phys.*  
 1063 24, 329–342.  
 1064 Bixel, F., & Lucas, C., 1987. Approche Géodynamique du Permien et du Trias des Pyrénées  
 1065 dans le cadre du sud-ouest européen. *Cuad. Geol. Ibérica* 11, 57–81.  
 1066 Boillot, G., Beslier, M.O., Krawczyk, C.M., Rappin, D., & Reston, T.J., 1995. The formation  
 1067 of passive margins: constraints from the crustal structure and segmentation of the deep  
 1068 Galicia margin, Spain. *Geol. Soc. Lond. Spec. Publ.* 90, 71–91.  
 1069 Boillot, G., Capdevilla, R., Hennequin-Marchand, I., Lamboy, M., & Lepretre, J.P., 1973. La  
 1070 zone nord-pyrénéenne, ses prolongements sur la marge continentale nord-espagnole et  
 1071 sa signification structurale. *Comptes Rendus Acad. Sci. Paris* 227, 2629–2632.  
 1072 Boillot, G., Féraud, G., Recq, M., & Girardeau, J., 1989. Undercrusting by serpentinite  
 1073 beneath rifted margins: the example of the west Galicia margin (Spain). *Nature* 341,  
 1074 523–525.  
 1075 Boillot, G., Grimaud, S., Mauffret, A., Mougénot, D., Kornprobst, J., Mergoill-Daniel, J., &  
 1076 Torrent, G., 1980. Ocean-continent boundary of the Iberian margin: a serpentinite  
 1077 diapir west of the Galicia Bank. *Earth Planet. Sci. Lett.* 48, 23–34.  
 1078 Boillot, G., Recq, M., Winterer, E.L., Meyer, A.W., Applegate, J., Baltuck, M., . . . Dunham,  
 1079 K., & others, 1987. Tectonic denudation of the upper mantle along passive margins: a  
 1080 model based on drilling results (ODP leg 103, western Galicia margin, Spain).  
 1081 *Tectonophysics* 132, 335–342.  
 1082 Boirie, J.-M., 1981. Etude Sédimentologique des Poudingues de Mendibelza (Pyrénées  
 1083 Atlantiques). Université Paul Sabatier de Toulouse (Sciences), Toulouse.  
 1084 Boirie, J.-M., & Souquet, P., 1982. Les poudingues de Mendibelza: dépôts de cônes sous-  
 1085 marins du rift albien des Pyrénées. *Bull. Cent. Rech. Explor.-Prod. Elf-Aquitaine* 6,  
 1086 405–435.

- Bois, C., 1992. The evolution of the layered lower crust and the Moho through geological time in Western Europe: contribution of deep seismic reflection profiles. *Terra Nova* 4, 99–108.
- Bois, C., & Courtillot, V., 1988. Deep Seismic Profiling of the Crust and Evolution of the Lithosphere 69, 987–988.
- Bois, C., & ECORS Scientific team, 1990. Major geodynamic processes studied from the ECORS deep seismic profiles in France and adjacent areas. *Tectonophysics* 173, 397–410.
- Bois, C., Gabriel, O., Lefort, J.-P., Rolet, J., Brunet, M.-F., Masse, P., & Olivet, J.-L., 1997. Geologic contribution of the Bay of Biscay deep seismic survey: a summary of the main scientific results, a discussion of the open questions and suggestions for further investigation. *Mém Soc Géol Fr.* 193–309.
- Bois, C., & Gariel, O., 1994. Deep Seismic Investigation in the Parentis Basin (Southwestern France), in: Mascle, A. (Ed.), *Hydrocarbon and Petroleum Geology of France*. Springer Berlin Heidelberg, Berlin, Heidelberg, pp. 173–186. [https://doi.org/10.1007/978-3-642-78849-9\\_13](https://doi.org/10.1007/978-3-642-78849-9_13)
- Boulvais, P., 2016. Fluid generation in the Boucheville Basin as a consequence of the North Pyrenean metamorphism. *Comptes Rendus Geosci.* 348, 301–311. <https://doi.org/10.1016/j.crte.2015.06.013>
- Bouroullec, J., Delfaud, J., & Deloffre, R., 1979. Organisations sédimentaire et paléocologique de l'Aptien supérieur à faciès urgonien dans les Pyrénées occidentales et l'Aquitaine méridionale. *Geobios* 12, 25–43.
- Bouroullec, J., & Deloffre, R., 1970. Interprétation sédimentologique et paléogéographique par microfaciès du Crétacé inférieur basal d'Aquitaine Sud-Ouest. *Bull. Cent. Rech. Pau-SNPA* 4, 381–429.
- Bourrouilh, R., Richert, J.-P., & Zolnai, G., 1995. The North Pyrenean Aquitaine Basin, France: Evolution and Hydrocarbons. *AAPG Bull.* 79, 831–853.
- BRGM, Elf, Esso, & SNPA, 1974. *Géologie du Bassin d'aquitaine*. BRGM Editions, Paris.
- Brune, S., Heine, C., Pérez-Gussinyé, M., & Sobolev, S.V., 2014. Rift migration explains continental margin asymmetry and crustal hyper-extension. *Nat. Commun.* 5. <https://doi.org/10.1038/ncomms5014>
- Brune, S., Williams, S.E., Butterworth, N.P., & Müller, R.D., 2016. Abrupt plate accelerations shape rifted continental margins. *Nature* 536, 201–204. <https://doi.org/10.1038/nature18319>
- Brunet, M.-F., 1991. Subsidence et géodynamique du Bassin d'Aquitaine. Relations avec l'ouverture de l'Atlantique.
- Brunet, M. F., 1994, Subsidence in the Parentis Basin (Aquitaine, France): Implications of the Thermal Evolution, ed, in Mascle, A., *Hydrocarbon and Petroleum Geology of France: Special Publication of the European Association of Petroleum Geoscientists*, Volume 4, p.187–198.
- Burg, J.-P., Van Den Driessche, J., & Brun, J.-P., 1994. Syn- to post-thickening extension : mode and consequences. *Comptes Rendus Académie Sci. Sér. 2 Sci. Terre Planètes* 319, 1019–1032.
- Cámara, P., 2020. Inverted turtle salt anticlines in the Eastern Basque-Cantabrian basin, Spain. *Marine and Petroleum Geology.* 117. <https://doi.org/10.1016/j.marpetgeo.2020.104358>
- Canérot, J., 1988. Manifestations de l'halocinèse dans les chaînons béarnais (zone Nord-Pyrénéenne) au Crétacé inférieur. *Comptes Rendus Académie Sci. Sér. 2 Mécanique Phys. Chim. Sci. Univers Sci. Terre* 306, 1099–1102.

1136 Canérot, J., 1989. Rifting éocrétaé et halocinèse sur la marge ibérique des Pyrénées  
 1137 Occidentales (France). Conséquences structurales. Bull. Cent. Rech. Explor.-Prod. Elf-  
 1138 Aquitaine 13, 87–99.  
 1139 Canérot, J., 2008. Les Pyrénées: Histoire géologique. Atlantica.  
 1140 Canérot, J., Hudec, M.R., & Rockenbauch, K., 2005. Mesozoic diapirism in the Pyrenean  
 1141 orogen: Salt tectonics on a transform plate boundary. AAPG Bull. 89, 211–229.  
 1142 <https://doi.org/10.1306/09170404007>  
 1143 Canérot, J., & Lenoble, J.-L., 1993. Diapirisme crétaé sur la marge ibérique des Pyrénées  
 1144 occidentales; exemple du pic de Lauriolle; comparaisons avec l'Aquitaine, les  
 1145 Pyrénées centrales et orientales. Bull. Société Géologique Fr. 164, 719–726.  
 1146 Canérot, J., Majesté-Menjoulas, C., & Ternet, Y., 1999. Le cadre stratigraphique et  
 1147 géodynamique des altérites et des bauxites sur la marge ibérique des Pyrénées  
 1148 occidentales (France). Comptes Rendus Académie Sci.-Ser. IIA-Earth Planet. Sci. 328,  
 1149 451–456.  
 1150 Carballo, A., Fernandez, M., Torne, M., Jiménez-Munt, I., & Villaseñor, A., 2015. Thermal  
 1151 and petrophysical characterization of the lithospheric mantle along the northeastern  
 1152 Iberia geo-transect. Gondwana Res. 27, 1430–1445.  
 1153 <https://doi.org/10.1016/j.gr.2013.12.012>  
 1154 Casas, A., Kearey, P., Rivero, L., & Adam, C.R., 1997. Gravity anomaly map of the Pyrenean  
 1155 region and a comparison of the deep geological structure of the western and eastern  
 1156 Pyrenees. Earth Planet. Sci. Lett. 150, 65–78.  
 1157 Casas, A.M., Cortés, A.L., & Maestro, A., 2000. Intra-plate deformation and basin formation  
 1158 during the Tertiary at the Northern Iberian Plate: origin and evolution of the Almazán  
 1159 Basin. Tectonics 19, 258–289.  
 1160 Casas, A.M., Villalaín, J.J., Soto, R., Gil-Imaz, A., del Río, P., & Fernández, G., 2009.  
 1161 Multidisciplinary approach to an extensional syncline model for the Mesozoic  
 1162 Cameros Basin (N Spain). Tectonophysics 470, 3–20.  
 1163 <https://doi.org/10.1016/j.tecto.2008.04.020>  
 1164 Casas Sainz, A.M., 1993. Oblique tectonic inversion and basement thrusting in the Cameros  
 1165 Massif (Northern Spain). Geodin. Acta 6, 202–216.  
 1166 <https://doi.org/10.1080/09853111.1993.11105248>  
 1167 Casas-Sainz, A.M., & Gil-Imaz, A., 1998. Extensional subsidence, contractional folding and  
 1168 thrust inversion of the eastern Cameros basin, northern Spain. Geol. Rundsch. 86,  
 1169 802–818. <https://doi.org/10.1007/s005310050178>  
 1170 Casas-Sainz, A.M., & Simón-Gómez, J., 1992. Stress field and thrust kinematics: a model for  
 1171 the tectonic inversion of the cameros massif (Spain). J. Struct. Geol. 14, 521–530.  
 1172 [https://doi.org/10.1016/0191-8141\(92\)90154-O](https://doi.org/10.1016/0191-8141(92)90154-O)  
 1173 Casquet, C., Galindo, C., González-Casado, J.M., Alonso, A., Mas, R., Rodas, M., García, E.,  
 1174 & Barrenechea, J.F., 1992. El metamorfismo en la cuenca de los Cameros;  
 1175 geocronologia e implicaciones tectonicas. Geogaceta 11, 22–25.  
 1176 Castañares, L.M., & Robles, S., 2004. El vulcanismo del Albiense-Santoniense en la Cuenca  
 1177 Vasco-Cantábrica. Geol. Esp.  
 1178 Castañares, L.M., Robles, S., & Vicente Bravo, J.C., 1997. Distribución estratigráfica de los  
 1179 episodios volcánicos submarinos del Albiense-Santoniense en la Cuenca Vasca (sector  
 1180 Gernika-Plentzia, Bizkaia).  
 1181 Casteras, M., 1933. Recherches sur la structure du versant nord des Pyrénées centrales et  
 1182 orientales. Librairie Polytechnique, C. Béranger.  
 1183 Casteras, M., 1971. Carte géologique de la France à 1/50 000: feuille de Tardets–Sorholus,  
 1184 Orléans, France.

1185 Chelalou, R., Nalpas, T., Bousquet, R., Prevost, M., Lahfid, A., Poujol, M., Ringenbach, J.-  
 1186 C., & Ballard, J.-F., 2016. New sedimentological, structural and paleo-thermicity data  
 1187 in the Boucheville Basin (eastern North Pyrenean Zone, France). *Comptes Rendus*  
 1188 *Géoscience* 348, 312–321.  
 1189 Chevrot, S., Sylvander, M., Diaz, J., Martin, R., Mouthereau, F., Manatschal, G., . . . Ruiz,  
 1190 M., 2018. The non-cylindrical crustal architecture of the Pyrenees. *Sci. Rep.* 8, 9591.  
 1191 <https://doi.org/10.1038/s41598-018-27889-x>  
 1192 Choukroune, P., 1974. Structure et évolution tectonique de la zone nord-pyrénéenne: analyse  
 1193 de la déformation dans une portion de chaîne à schistosité sub-verticale.  
 1194 Choukroune, P., & ECORS Team, 1989. The ECORS Pyrenean deep seismic profile  
 1195 reflection data and the overall structure of an orogenic belt. *Tectonics* 8, 23–39.  
 1196 Choukroune, P., & Mattauer, M., 1978. Tectonique des plaques et Pyrenees; sur le  
 1197 fonctionnement de la faille transformante nord-pyreneenne; comparaisons avec des  
 1198 modeles actuels. *Bull. Société Géologique Fr.* 7, 689–700.  
 1199 Clerc, C., 2012. Evolution du domaine nord-pyrénéen au Crétacé: amincissement crustal  
 1200 extrême et thermicité élevée: un analogue pour les marges passives. Paris 6.  
 1201 Clerc, C., Boulvais, P., Lagabrielle, Y., & de Saint Blanquat, M., 2014. Ophicalcites from the  
 1202 northern Pyrenean belt: a field, petrographic and stable isotope study. *Int. J. Earth Sci.*  
 1203 103, 141–163. <https://doi.org/10.1007/s00531-013-0927-z>  
 1204 Clerc, C., Lahfid, A., Monié, P., Lagabrielle, Y., Chopin, C., . . . de St Blanquat, M., 2015.  
 1205 High-temperature metamorphism during extreme thinning of the continental crust: a  
 1206 reappraisal of the North Pyrenean passive paleomargin. *Solid Earth* 6, 643–668.  
 1207 Clerc, C., & Lagabrielle, Y., 2014. Thermal control on the modes of crustal thinning leading  
 1208 to mantle exhumation: Insights from the Cretaceous Pyrenean hot paleomargins.  
 1209 *Tectonics* 33, 1340–1359. <https://doi.org/10.1002/2013TC003471>  
 1210 Clerc, C., Lagabrielle, Y., Labaume, P., Ringenbach, J.-C., Vauchez, A., Nalpas, T., . . .  
 1211 Fourcade, S., 2016. Basement – Cover decoupling and progressive exhumation of  
 1212 metamorphic sediments at hot rifted margin. Insights from the Northeastern Pyrenean  
 1213 analog. *Tectonophysics* 686, 82–97. <https://doi.org/10.1016/j.tecto.2016.07.022>  
 1214 Cobbold, P.R., & Szatmari, P., 1991. Radial gravitational gliding on passive margins.  
 1215 *Tectonophysics* 188, 249–289.  
 1216 Cochelin, B., 2016. Champ de déformation du socle paléozoïque des Pyrénées. *Géosciences*  
 1217 *Environnement Toulouse (GET)*.  
 1218 Cochelin, B., Chardon, D., Denèle, Y., Gumiaux, C., & Le Bayon, B., 2017. Vertical strain  
 1219 partitioning in hot Variscan crust: Syn-convergence escape of the Pyrenees in the  
 1220 Iberian-Armorican syntax. *Bull. Société Géologique Fr.* 188, 39.  
 1221 Cochelin, B., Lemirre, B., Denèle, Y., Blanquat, M. de S., Lahfid, A., Duchêne, S., 2018a,  
 1222 Structural inheritance in the central Pyrenees: the variscan to Alpine  
 1223 tectonometamorphic evolution of the axial zone. *J. Geol. Soc.*, v. 175, 336–351,  
 1224 [doi:10.1144/jgs2017-066](https://doi.org/10.1144/jgs2017-066).  
 1225 Cochelin, B., Gumiaux, C., Chardon, D., Denèle, Y., Le Bayon, B., 2018b, Multi-scale  
 1226 strainfield analysis using geostatistics: Investigating the rheological behavior of the  
 1227 hot Variscan crust of the Pyrenees (Axial Zone). *J. Struct. Geol.*, v. 116, 114–130,  
 1228 [doi:10.1016/j.jsg.2018.07.024](https://doi.org/10.1016/j.jsg.2018.07.024)  
 1229 Combes, P.-J., Peybernès, B., & Leyreloup, A.F., 1998. Altérites et bauxites, témoins des  
 1230 marges européenne et ibérique des Pyrénées occidentales au Jurassique supérieur—  
 1231 Crétacé inférieur, à l’ouest de la vallée d’Ossau (Pyrénées-Atlantiques, France).  
 1232 *Comptes Rendus Académie Sci.-Ser. IIA-Earth Planet. Sci.* 327, 271–278.

Corre, B., 2017. La bordure nord de la plaque ibérique à l'Albo-Cénomanién: architecture d'une marge passive de type ductile (Chaînons Béarnais, Pyrénées Occidentales) (PhD Thesis). Rennes 1.

Corre, B., Lagabriele, Y., Labaume, P., Fourcade, S., Clerc, C., & Ballèvre, M., 2016. Deformation associated with mantle exhumation in a distal, hot passive margin environment: New constraints from the Sarailé Massif (Chaînons Béarnais, North-Pyrenean Zone). *Comptes Rendus Geosci.* 348, 279–289. <https://doi.org/10.1016/j.crte.2015.11.007>

Cuevas, J., & Tubia, J.M., 1999. The discovery of scapolite marbles in the Biscay Synclinorium (Basque-Cantabrian basin, Western Pyrenees): geodynamic implications. *Terra Nova* 11, 259–265. <https://doi.org/10.1046/j.1365-3121.1999.00255.x>

Curnelle, R., 1983. Evolution structuro-sédimentaire du Trias et de l'Infra-Lias d'Aquitaine. *Bull Cent Rech Explor Prod Elf-Aquitaine* 7, 69–99.

Curnelle, R., & Dubois, P., 1986. Evolution mesozoïque des grands bassins sédimentaires français; bassins de Paris, d'Aquitaine et du Sud-Est. *Bull. Soc. Geol. Fr. II*, 529–546. <https://doi.org/10.2113/gssgfbull.II.4.529>

Curnelle, R., Dubois, P., Seguin, J.C., Whitaker, D., Matthews, D.H., Roberts, D.G., . . . Kholief, M.M., 1982. The Mesozoic-Tertiary Evolution of the Aquitaine Basin [and Discussion]. *Philos. Trans. R. Soc. Math. Phys. Eng. Sci.* 305, 63–84. <https://doi.org/10.1098/rsta.1982.0026>

Daignières, M., Séguret, M., Specht, M., & Team, E., 1994. The Arzacq-western Pyrenees ECORS deep seismic profile, in: *Hydrocarbon and Petroleum Geology of France*. Springer, pp. 199–208.

Dañoebitia, J.J., Arguedas, M., Gallart, J., Banda, E., & Makris, J., 1992. Deep crustal configuration of the Valencia trough and its Iberian and Balearic borders from extensive refraction and wide-angle reflection seismic profiling. *Tectonophysics* 203, 37–55.

Dardel, R.A., & Rosset, R., 1971. Histoire géologique et structurale du bassin de Parentis et de son prolongement en mer. *Hist. Struct. Golfe Gasc.* 2.

Dauteuil, O., & Ricou, L.-E., 1989. Une circulation de fluides de haute-température à l'origine du métamorphisme crétacé nord-pyrénéen. *Geodin. Acta* 3, 237–249. <https://doi.org/10.1080/09853111.1989.11105190>

de Saint Blanquat, M., 1993. La faille normale ductile du massif du Saint Barthélémy. Evolution hercynienne des massifs nord-pyrénéens catazonaux considérée du point de vue de leur histoire thermique. *Geodin. Acta* 6, 59–77.

de Saint Blanquat, M., Bajolet, F., Grand'Homme, A., Proietti, A., Zanti, M., Boutin, A., . . . Labaume, P., 2016. Cretaceous mantle exhumation in the central Pyrenees: New constraints from the peridotites in eastern Ariège (North Pyrenean zone, France). *Comptes Rendus Geosci.* 348, 268–278. <https://doi.org/10.1016/j.crte.2015.12.003>

Debroas, E.J., 1978. Evolution de la fosse du flysch ardoisier de l'Albien supérieur au Senonien inférieur (zone interne métamorphique des Pyrénées navarro-languedociennes). *Bull. Société Géologique Fr.* 7, 639–648.

Debroas, E.-J., 1987. Modèle de bassin triangulaire à l'intersection de décrochements divergents pour le fossé albo-cénomanién de la Ballongue (zone nord-pyrénéenne, France). *Bull. Société Géologique Fr.* 3, 887–898. <https://doi.org/10.2113/gssgfbull.III.5.887>

Debroas, E.J., 1990. Le flysch noir albo-cénomanién témoin de la structuration albienne a senonienne de la Zone nord-pyrénéenne en Bigorre (Hautes-Pyrénées, France). *Bull. Soc. Geol. Fr. VI*, 273–285. <https://doi.org/10.2113/gssgfbull.VI.2.273>

1283 Debroas, E.J., Canérot, J., & Bilotte, M., 2010. Les brèches d'Urdach, témoins de  
1284 l'exhumation du manteau pyrénéen dans un escarpement de faille vraconnien-  
1285 cénomanien inférieur (Zone nord-pyrénéenne, Pyrénées-Atlantiques, France).  
1286 *Géologie Fr.* 2, 53–63.

1287 DeFelipe, I., Pedreira, D., Pulgar, J.A., Iriarte, E., & Mendia, M., 2017. Mantle exhumation  
1288 and metamorphism in the Basque-Cantabrian Basin (NSpain): Stable and clumped  
1289 isotope analysis in carbonates and comparison with ophicalcites in the North-Pyrenean  
1290 Zone (Urdach and Lherz). *Geochem. Geophys. Geosystems* 18, 631–652.  
1291 <https://doi.org/10.1002/2016GC006690>

1292 Del Río, P., Barbero, L., Mata, P., & Fanning, C.M., 2009. Timing of diagenesis and very  
1293 low-grade metamorphism in the eastern sector of the Sierra de Cameros (Iberian  
1294 Range, Spain): a U-Pb SHRIMP study on monazite: U-Pb dating of diagenetic and  
1295 low-grade monazite from the Iberian Range (Spain). *Terra Nova* 21, 438–445.  
1296 <https://doi.org/10.1111/j.1365-3121.2009.00900.x>

1297 Delfaud, J., 1969. Essai sur la géologie dynamique du domaine aquitano-pyrénéen durant le  
1298 Jurassique et le Crétacé inférieur. Université de Bordeaux.

1299 Delfaud, J., & Gautier, J., 1967. Evolution des milieux de dépôts au passage Jurassique–  
1300 Crétacé du forage de Lacq 104 (Aquitaine, France, Sud-Ouest). *Bull. Cent. Rech. Pau-*  
1301 *SNPA* 1, 77–89.

1302 Delfaud, J., & Henry, J., 1967. Evolution des bassins jurassiques dans la zone nord-  
1303 pyrénéenne occidentale. 64ème Congrès AFAS Bordx. 75–80.

1304 Delfaud, J., & Villanova, M., 1967. Evolution des bassins pendant le Crétacé inférieur dans  
1305 les Pyrénées occidentales et la bordure de l'Aquitaine. 64ème Congrès AFAS Bordx.  
1306 87–92.

1307 Demercian, S., Szatmari, P., & Cobbold, P.R., 1993. Style and pattern of salt diapirs due to  
1308 thin-skinned gravitational gliding, Campos and Santos basins, offshore Brazil.  
1309 *Tectonophysics* 228, 393–433.

1310 Dercourt, J., Zonenshain, L.P., Ricou, L.-E., Kazmin, V.G., Le Pichon, X., Knipper, A.L., . . .  
1311 Biju-Duval, B., 1986. Geological evolution of the tethys belt from the atlantic to the  
1312 pamirs since the LIAS. *Tectonophysics* 123, 241–315. [https://doi.org/10.1016/0040-](https://doi.org/10.1016/0040-1951(86)90199-X)  
1313 [1951\(86\)90199-X](https://doi.org/10.1016/0040-1951(86)90199-X)

1314 Désaglaux, P., & Brunet, M.-F., 1990. Tectonic subsidence of the Aquitaine basin since  
1315 Cretaceous times. *Bull. Société Géologique Fr.* 8, 295–306.

1316 Dielforder, A., Frasca, G., Brune, S & Ford, M., 2019. Formation of the Iberian-European  
1317 Convergent Plate Boundary Fault and Its Effect on Intraplate Deformation in Central  
1318 Europe. *Geochemistry Geophysics Geosystems*.  
1319 <https://doi.org/10.1029/2018GC007840>.

1320 Driscoll, N.W., Hogg, J.R., Christie-Blick, N., & Karner, G.D., 1995. Extensional tectonics in  
1321 the Jeanne d'Arc Basin, offshore Newfoundland: implications for the timing of break-  
1322 up between Grand Banks and Iberia. *Geol. Soc. Lond. Spec. Publ.* 90, 1–28.  
1323 <https://doi.org/10.1144/GSL.SP.1995.090.01.01>

1324 Ducoux, M., 2017. Structure, thermicité et évolution géodynamique de la Zone Interne  
1325 Métamorphique des Pyrénées. Institut des Sciences de la Terre d'Orléans (ISTO).

1326 Ducoux, M., Jolivet, L., Callot, J. -P., Aubourg, C., Masini, E., Lahfid, A., . . . Baudin, T.,  
1327 2019. The Nappe des Marbres unit of the Basque-Cantabrian Basin: the  
1328 tectono-thermal evolution of a fossil hyperextended rift basin. *Tectonics*  
1329 2018TC005348. <https://doi.org/10.1029/2018TC005348>

1330 Duée, G., Lagabriele, Y., Coutelle, A., & Fortané, A., 1984. Les lherzolites associées aux  
1331 Chaînons Béarnais (Pyrénées Occidentales): Mise à l'affleurement anté-dogger et



1332       resédimentation albo-cénomaniennne. Comptes-Rendus Séances Académie Sci. Sér. 2  
1333       Mécanique-Phys. Chim. Sci. Univers Sci. Terre 299, 1205–1210.

1334 Duretz, T., Asti, R., Lagabrielle, Y., Brun, J., Jourdon, A., Clerc, C., & Corre, B., 2019.  
1335 Numerical modelling of Cretaceous Pyrenean Rifting: The interaction between mantle  
1336 exhumation and syn-rift salt tectonics. Basin Res. bre.12389.  
1337 <https://doi.org/10.1111/bre.12389>

1338 Espurt, N., Angrand, P., Teixell, A., Labaume, P., Ford, M., de Saint Blanquat, M., &  
1339 Chevrot, S., 2019. Crustal-scale balanced cross-section and restorations of the Central  
1340 Pyrenean belt (Nestes-Cinca transect): Highlighting the structural control of Variscan  
1341 belt and Permian-Mesozoic rift systems on mountain building. Tectonophysics 764,  
1342 25–45.

1343 Ettheve, N., 2016. Le bassin de Valence à la frontière des domaines ibérique et méditerranéen:  
1344 Evolution tectonique et sédimentaire du Mésozoïque au Cénozoïque. Université de  
1345 Cergy Pontoise.

1346 Ettheve, N., Mohn, G., Frizon de Lamotte, D., Roca, E., Tugend, J., & Gómez-Romeu, J.,  
1347 2018. Extreme Mesozoic Crustal Thinning in the Eastern Iberia Margin: The Example  
1348 of the Columbrets Basin (Valencia Trough). Tectonics 37, 636–662.

1349 Fabriès, J., Lorand, J.-P., & Bodinier, J.-L., 1998. Petrogenetic evolution of orogenic  
1350 lherzolite massifs in the central and western Pyrenees. Tectonophysics 292, 145–167.

1351 Fabriès, J., Lorand, J.-P., Bodinier, J.-L., & Dupuy, C., 1991. Evolution of the Upper Mantle  
1352 beneath the Pyrenees: Evidence from Orogenic Spinel Lherzolite Massifs. J. Petrol.  
1353 Special\_Volume, 55–76. [https://doi.org/10.1093/petrology/Special\\_Volume.2.55](https://doi.org/10.1093/petrology/Special_Volume.2.55)

1354 Fernandez, M., Foucher, J.P., & Jurado, M.J., 1995. Evidence for the multi-stage formation of  
1355 the south-western Valencia Trough. Mar. Pet. Geol. 12, 101–109.  
1356 [https://doi.org/10.1016/0264-8172\(95\)90390-6](https://doi.org/10.1016/0264-8172(95)90390-6)

1357 Ferrer, O., Jackson, M.P.A., Roca, E., & Rubinat, M., 2012. Evolution of salt structures  
1358 during extension and inversion of the Offshore Parentis Basin (Eastern Bay of Biscay).  
1359 Geol. Soc. Lond. Spec. Publ. 363, 361–380. <https://doi.org/10.1144/SP363.16>

1360 Ferrer, O., Roca, E., Benjumea, B., Muñoz, J.A., Ellouz, N., & MARCONI Team, 2008. The  
1361 deep seismic reflection MARCONI-3 profile: Role of extensional Mesozoic structure  
1362 during the Pyrenean contractional deformation at the eastern part of the Bay of Biscay.  
1363 Mar. Pet. Geol. 25, 714–730. <https://doi.org/10.1016/j.marpetgeo.2008.06.002>

1364 Ferrer, O., Roca, E., Jackson, M.P.A., & Muñoz, J.A., 2009. Effects of Pyrenean contraction  
1365 on salt structures of the offshore Parentis Basin (Bay of Biscay). Trab. Geol. 29.

1366 Fixari, G., 1984. Stratigraphie, faciès et dynamique tecto-sédimentaire du flysch albien  
1367 (flysch noir et poudingues de mendibelza) dans la région de Mauléon-Tardets  
1368 (Pyrénées Atlantiques). Université Paul Sabatier de Toulouse (Sciences).

1369 Fort, X., Brun, J.-P., & Chauvel, F., 2004a. Salt tectonics on the Angolan margin,  
1370 synsedimentary deformation processes. AAPG Bull. 88, 1523–1544.

1371 Fort, X., Brun, J.P., & Chauvel, F., 2004b. Contraction induced by block rotation above salt  
1372 (Angolan margin). Mar. Pet. Geol. 21, 1281–1294.

1373 Fortané, A., Duée, G., Lagabrielle, Y., & Coutelle, A., 1986. Lherzolites and the western  
1374 “Chaînons Béarnais” (French Pyrenees): Structural and paleogeographical pattern.  
1375 Tectonophysics 129, 81–98. [https://doi.org/10.1016/0040-1951\(86\)90247-7](https://doi.org/10.1016/0040-1951(86)90247-7)

1376 Frizon de Lamotte, D., Raulin, C., Mouchot, N., Wrobel-Daveau, J.-C., Blanpied, C., &  
1377 Ringenbach, J.-C., 2011. The southernmost margin of the Tethys realm during the  
1378 Mesozoic and Cenozoic: Initial geometry and timing of the inversion processes:  
1379 TETHYS SOUTHERNMOST MARGIN. Tectonics 30, n/a-n/a.  
1380 <https://doi.org/10.1029/2010TC002691>

- Froitzheim, N., & Manatschal, G., 1996. Kinematics of Jurassic rifting, mantle exhumation, and passive-margin formation in the Austroalpine and Penninic nappes (eastern Switzerland). *Geol. Soc. Am. Bull.* 108, 1120–1133. [https://doi.org/10.1130/0016-7606\(1996\)108<1120:KOJRME>2.3.CO;2](https://doi.org/10.1130/0016-7606(1996)108<1120:KOJRME>2.3.CO;2)
- Gallart, J., Rojas, H., Diaz, J., & Dañobeitia, J.J., 1990. Features of deep crustal structure and the onshore-offshore transition at the Iberian flank of the Valencia Trough (Western Mediterranean). *J. Geodyn.* 12, 233–252.
- Gallart, J., Vidal, N., & Danobeitia, J., 1994. Lateral variations in the deep crustal structure at the Iberian margin of the Valencia trough imaged from seismic reflection methods. *Tectonophysics* 232, 59–75. [https://doi.org/10.1016/0040-1951\(94\)90076-0](https://doi.org/10.1016/0040-1951(94)90076-0)
- García Mondéjar, J., Agirrezabala, L., M., Aranburu, A., Fernandez-Mendiola, P., A., Gomèz-Pérèz, I., Lopez-Horgue, M., & Rosales, I., 1996. Aptian—Albian tectonic pattern of the Basque—Cantabrian Basin (Northern Spain). *Geol. J.* 31, 13–45.
- García-Lasanta, C., Casas-Sainz, A., Villalaín, J.J., Oliva-Urcia, B., Mochales, T., & Speranza, F., 2017. Remagnetizations used to unravel large-scale fold kinematics: A case study in the Cameros Basin (Northern Spain): Unfolding in Basin Inversion. *Tectonics* 36, 714–729. <https://doi.org/10.1002/2016TC004459>
- García-Senz, J., Pedrera, A., Ayala, C., Ruiz-Constán, A., Robador Moreno, A., Rodríguez-Fernández, R., 2019, Inversion of the North-Iberian hyperextended margin: the role of exhumed mantle indentation during continental collision. *Geological Society, London, Special Publications*, 490, doi: <https://doi.org/10.1144/SP490-2019-112>.
- Gaullier, V., Brun, J.P., Gueñin, G., & Lecanu, H., 1993. Raft tectonics: the effects of residual topography below a salt décollement. *Tectonophysics* 228, 363–381.
- Golberg, J.M., Guiraud, M., Maluski, H., & Séguret, M., 1988. Caractères pétrologiques et âge du métamorphisme en contexte distensif du bassin sur décrochement de Soria (Crétacé inférieur, Nord Espagne). *Comptes Rendus Académie Sci. Sér. 2 Mécanique Phys. Chim. Sci. Univers Sci. Terre* 307, 521–527.
- Golberg, J.M., & Leyreloup, A.F., 1990. High temperature-low pressure Cretaceous metamorphism related to crustal thinning (Eastern North Pyrenean Zone, France). *Contrib. Mineral. Petrol.* 104, 194–207. <https://doi.org/10.1007/BF00306443>
- Golberg, J.-M., & Maluski, H., 1988. Données nouvelles et mise au point sur l'âge du métamorphisme pyrénéen. *Comptes Rendus Académie Sci. Sér. 2 Mécanique Phys. Chim. Sci. Univers Sci. Terre* 306, 429–435.
- Golberg, J.M., Maluski, H., & Leyreloup, A.F., 1986. Petrological and age relationship between emplacement of magmatic breccia, alkaline magmatism, and static metamorphism in the North Pyrenean Zone. *Tectonophysics* 129, 275–290. [https://doi.org/10.1016/0040-1951\(86\)90256-8](https://doi.org/10.1016/0040-1951(86)90256-8)
- Gomez-Ortiz, D., Agarwal, B.N.P., Tejero, R., & Ruiz, J., 2011. Crustal structure from gravity signatures in the Iberian Peninsula. *Geol. Soc. Am. Bull.* 123, 1247–1257. <https://doi.org/10.1130/B30224.1>
- Gómez-Romeu, J., Masini, E., Tugend, J., Ducoux, M., & Kusznir, N., 2019. Role of rift structural inheritance in orogeny highlighted by the Western Pyrenees case-study. *Tectonophysics* 766, 131–150. <https://doi.org/10.1016/j.tecto.2019.05.022>
- Gottis, M., 1972. Construction d'un modèle géodynamique pyrénéen. *Comptes Rendus Académie Sci.* 275, 2099.
- Gong, Z., C. G. Langereis, and T. A. T. Mullender, 2008, The rotation of Iberia during the Aptian and the opening of the Bay of Biscay: *Earth and Planetary Science Letters*, v. 273, no. 1–2, p. 80–93, doi:10.1016/j.epsl.2008.06.016.

- Grandjean, G., 1994. Etude des structures crustales dans une portion de chaîne et de leur relation avec les bassins sédimentaires. Application aux Pyrénées occidentales. *Bull Cent Rech Explor Prod Elf Aquitaine* 18, 391–420.
- Guimerà, J., Alonso, Á., & Mas, J.R., 1995. Inversion of an extensional-ramp basin by a newly formed thrust: the Cameros basin (N. Spain). *Geol. Soc. Lond. Spec. Publ.* 88, 433–453. <https://doi.org/10.1144/GSL.SP.1995.088.01.23>
- Guiraud, M., & Séguret, M., 1985. A releasing solitary overstep model for the Late Jurassic–Early Cretaceous (Wealdian) Soria strike-slip basin (northern Spain). *AAPG Bull.*
- Hart, N.R., Stockli, D.F., Lavier, L.L., & Hayman, N.W., 2017. Thermal evolution of a hyperextended rift basin, Mauléon Basin, western Pyrenees: Thermal evolution of hyperextended rift. *Tectonics*. <https://doi.org/10.1002/2016TC004365>
- Henry, J., Zolnai, G., Le Pochat, G., & Mondeilh, C., 1987. Carte géologique de la France au 1/50 000: feuille d'Orthez, Orléans, France.
- Huismans, R.S., & Beaumont, C., 2003. Symmetric and asymmetric lithospheric extension: Relative effects of frictional-plastic and viscous strain softening. *J. Geophys. Res. Solid Earth* 108. <https://doi.org/10.1029/2002JB002026>
- Huismans, R.S., & Beaumont, C., 2008. Complex rifted continental margins explained by dynamical models of depth-dependent lithospheric extension. *Geology* 36, 163. <https://doi.org/10.1130/G24231A.1>
- Huismans, R.S., & Beaumont, C., 2011. Depth-dependent extension, two-stage breakup and cratonic underplating at rifted margins. *Nature* 473, 74–78. <https://doi.org/10.1038/nature09988>
- Huismans, R.S., & Beaumont, C., 2014. Rifted continental margins: The case for depth-dependent extension. *Earth Planet. Sci. Lett.* 407, 148–162. <https://doi.org/10.1016/j.epsl.2014.09.032>
- Incerpi, N., Manatschal, G., Martire, L., Bernasconi, S. M., Gerdes, A., Bertok, C., 2020. Characteristics and timing of hydrothermal fluid circulation in the fossil Pyrenean hyperextended rift system: new constraints from the Chaînons Béarnais (W Pyrenees). *International Journal of Earth Sciences*. <https://doi.org/10.1007/s00531-020-01852-6>
- Issautier, B., Saspiturry, N., Serrano, O., 2020. Structural inheritance and salt tectonics controlling pseudosymmetric rift formation during Early Cretaceous hyperextension of the Arzacq and Tartas Basins (southwest France). *Marine and Petroleum Geology*. [10.1016/j.marpetgeo.2020.104395](https://doi.org/10.1016/j.marpetgeo.2020.104395)
- Jackson, M. P., & Hudec, M. R. (2005). Stratigraphic record of translation down ramps in a passive-margin salt detachment. *Journal of Structural Geology*, 27(5), 889–911. <https://doi.org/10.1016/j.jsg.2005.01.010>
- James, V., 1998. La plate-forme carbonatée ouest-pyrénéenne au jurassique moyen et supérieur stratigraphie séquentielle, stades d'évolution, relations avec la subsurface en aquitaine méridionale.
- James, V., & Canérot, J., 1999. Diapirisme et structuration post-triasique des Pyrénées occidentales et de l'Aquitaine méridionale (France). *Eclogae Geol. Helvetiae* 92, 63–72.
- Jammes, S., 2009. Processus d'amincissement crustal en contexte transtensif : l'exemple du Golfe de Gascogne et des Pyrénées basques. PhD thesis, Strasbourg University.
- Jammes, S., Manatschal, G., Lavier, L., & Masini, E., 2009. Tectono-sedimentary evolution related to extreme crustal thinning ahead of a propagating ocean: Example of the western Pyrenees. *Tectonics* 28. <https://doi.org/10.1029/2008TC002406>
- Jammes, S., Tiberi, C., & Manatschal, G., 2010a. 3D architecture of a complex transcurrent rift system: The example of the Bay of Biscay–Western Pyrenees. *Tectonophysics* 489, 210–226. <https://doi.org/10.1016/j.tecto.2010.04.023>

1479 Jammes, S., Lavier, L., & Manatschal, G., 2010b. Extreme crustal thinning in the Bay of  
 1480 Biscay and the Western Pyrenees: From observations to modeling. *Geochem.*  
 1481 *Geophys. Geosystems* 11. <https://doi.org/10.1029/2010GC003218>  
 1482 Jammes, S., Manatschal, G., & Lavier, L., 2010c. Interaction between prerift salt and  
 1483 detachment faulting in hyperextended rift systems: The example of the Parentis and  
 1484 Mauléon basins (Bay of Biscay and western Pyrenees). *AAPG Bull.* 94, 957–975.  
 1485 <https://doi.org/10.1306/12090909116>  
 1486 Jiménez-Munt, I., Fernández, M., Vergés, J., Afonso, J.C., Garcia-Castellanos, D., & Fulla,  
 1487 J., 2010. Lithospheric structure of the Gorringe Bank: Insights into its origin and  
 1488 tectonic evolution: GORRINGE BANK STRUCTURE AND EVOLUTION. *Tectonics* 29, n/a-n/a. <https://doi.org/10.1029/2009TC002458>  
 1489 Labaume, P., & Teixell, A., 2020. Evolution of salt structures of the Pyrenean rift (Chaînons  
 1490 Béarnais, France): From hyper-extension to tectonic inversion. *Tectonophysics*.  
 1491 <https://doi.org/10.1016/j.tecto.2020.228451>.  
 1492 Lagabrielle, Y., & Bodinier, J.-L., 2008. Submarine reworking of exhumed sub-continental  
 1493 mantle rocks: field evidence from the Lherz peridotites, French Pyrenees: Cretaceous  
 1494 exhumation of pyrenean mantle. *Terra Nova* 20, 11–21.  
 1495 <https://doi.org/10.1111/j.1365-3121.2007.00781.x>  
 1496 Lagabrielle, Y., Labaume, P., & de Saint Blanquat, M., 2010. Mantle exhumation, crustal  
 1497 denudation, and gravity tectonics during Cretaceous rifting in the Pyrenean realm (SW  
 1498 Europe): Insights from the geological setting of the Iherzolite bodies. *Tectonics* 29.  
 1499 <https://doi.org/10.1029/2009TC002588>  
 1500 Lagabrielle, Y., Clerc, C., Vauchez, A., Lahfid, A., Labaume, P., Azambre, B., Fourcade, S.,  
 1501 & Dautria, J.-M., 2016. Very high geothermal gradient during mantle exhumation  
 1502 recorded in mylonitic marbles and carbonate breccias from a Mesozoic Pyrenean  
 1503 palaeomargin (Lherz area, North Pyrenean Zone, France). *Comptes Rendus Geosci.*  
 1504 348, 290–300. <https://doi.org/10.1016/j.crte.2015.11.004>  
 1505 Lagabrielle, Y., Asti, R., Fourcade, S., Corre, B., Poujol, M., Uzel, J., . . . Maury, R., 2019a.  
 1506 Mantle exhumation at magma-poor passive continental margins. Part I. 3D  
 1507 architecture and metasomatic evolution of a fossil exhumed mantle domain (Urdach  
 1508 Iherzolite, north-western Pyrenees, France). *BSGF - Earth Sci. Bull.* 190, 8.  
 1509 <https://doi.org/10.1016/j.earscirev.2019.103071>.  
 1510 Lagabrielle, Y., Asti, R., Duretz, T., Clerc, C., Fourcade, S., Teixell, A., . . . Saspiturry, N.,  
 1511 2020. A review of cretaceous smooth-slopes extensional basins along the Iberia-  
 1512 Eurasia plate boundary: How pre-rift salt controls the modes of continental rifting and  
 1513 mantle exhumation. *Earth-Science Reviews*. 201.  
 1514 <https://doi.org/10.1051/bsgf/2019007>  
 1515 Lamare, P., 1936. Recherches géologiques dans les Pyrénées basques d'Espagne. Société  
 1516 géologique de France.  
 1517 Lavier, L.L., & Manatschal, G., 2006. A mechanism to thin the continental lithosphere at  
 1518 magma-poor margins. *Nature* 440, 324–328. <https://doi.org/10.1038/nature04608>  
 1519 Le Pochat, G., Bolthenhagen, C., Lenguin, M., Lorsignol, S., & Thibault, C., 1976. Carte  
 1520 géologique de France au 1/50 000: Mauléon-licharre, Orléans, France.  
 1521 Lefort, J.-P., & Agarwal, B.N., 1999. Of what is the centre of the Ibero-Armorican arc  
 1522 composed? *Tectonophysics* 302, 71–81. [https://doi.org/10.1016/S0040-1951\(98\)00275-3](https://doi.org/10.1016/S0040-1951(98)00275-3)  
 1523 Lemoine, M., Tricart, P., & Boillot, G., 1987. Ultramafic and gabbroic ocean floor of the  
 1524 Ligurian Tethys (Alps, Corsica, Apennines): In search of a genetic imodel. *Geology*  
 1525 15, 622–625. [https://doi.org/10.1130/0091-7613\(1987\)15<622:UAGOFO>2.0.CO;2](https://doi.org/10.1130/0091-7613(1987)15<622:UAGOFO>2.0.CO;2)  
 1526  
 1527

1528 Lenoble, J.-L., 1992. Les plates-formes carbonatées ouest-pyrénéennes du dogger à l'Albien,  
1529 stratigraphie séquentielle et évolution géodynamique. Université Paul Sabatier de  
1530 Toulouse (Sciences).

1531 Lescoutre, R., 2019. Formation and reactivation of the Pyrenean-Cantabrian rift system :  
1532 inheritance, segmentation and thermal evolution. Strasbourg.

1533 Lescoutre, R., Tugend, J., Brune, S., Masini, E., & Manatschal, G., 2019. Thermal Evolution  
1534 of Asymmetric Hyperextended Magma-Poor Rift Systems: Results From Numerical  
1535 Modeling and Pyrenean Field Observations. *Geochem. Geophys. Geosystems*  
1536 2019GC008600. <https://doi.org/10.1029/2019GC008600>

1537 Liro, L.M., & Coen, R., 1995. Salt deformation history and postsalt structural trends, offshore  
1538 southern Gabon, West Africa.

1539 Lucas, C., 1985. Le grès rouge du versant nord des Pyrénées: essai sur la géodynamique de  
1540 dépôts continentaux du permien et du trias.

1541 Lundin, E.R., 1992. Thin-skinned extensional tectonics on a salt detachment, northern  
1542 Kwanza Basin, Angola. *Mar. Pet. Geol.* 9, 405–411.

1543 Manatschal, G., 2004. New models for evolution of magma-poor rifted margins based on a  
1544 review of data and concepts from West Iberia and the Alps. *Int. J. Earth Sci.* 93.  
1545 <https://doi.org/10.1007/s00531-004-0394-7>

1546 Manatschal, G., Engström, A., Desmurs, L., Schaltegger, U., Cosca, M., Müntener, O., &  
1547 Bernoulli, D., 2006. What is the tectono-metamorphic evolution of continental break-  
1548 up: The example of the Tasna Ocean–Continent Transition. *J. Struct. Geol.* 28, 1849–  
1549 1869. <https://doi.org/10.1016/j.jsg.2006.07.014>

1550 Manatschal, G., & Nievergelt, P., 1997. A continent-ocean transition recorded in the Err and  
1551 Platta nappes (Eastern Switzerland). *Eclogae Geol. Helvetiae* 90, 3–28.

1552 Marillier, F., Tomassino, A., Patriat, P., & Pinet, B., 1988. Deep structure of the Aquitaine  
1553 shelf: constraints from expanding spread profiles on the ECORS Bay of Biscay  
1554 transect. *Mar. Pet. Geol.* 5, 65–74.

1555 Martínez-Torres, L.M., 1989. El manto de los mármoles (Pirineo occidental): geología  
1556 estructural y evolución geodinámica (PhD Thesis). Universidad del País Vasco-Euskal  
1557 Herriko Unibertsitatea.

1558 Mas, J.R., Alonso, A., & Guimerà, J., 1993. Evolución tectonosedimentaria de una cuenca  
1559 extensional intraplaca: la cuenca finijurásica–eocretácica de Los Cameros (La Rioja–  
1560 Soria). *Rev. Soc. Geológica Esp.* 6, 129–144.

1561 Mas, R., Benito, M.I., Arribas, J., Alonso, A., Arribas, M.E., Lohmann, K.C., . . . Suárez, P.,  
1562 2011. Evolution of an intra-plate rift basin: the latest Jurassic-early Cretaceous  
1563 Cameros basin (Northwest Iberian ranges, North Spain). *Geo-Guías* 8, 117–154.

1564 Masini, E., Manatschal, G., Mohn, G., Ghienne, J.-F., & Lafont, F., 2011. The tectono-  
1565 sedimentary evolution of a supra-detachment rift basin at a deep-water magma-poor  
1566 rifted margin: the example of the Samedan Basin preserved in the Err nappe in SE  
1567 Switzerland: Tectono-sedimentary evolution of a supra-detachment rift basin. *Basin*  
1568 *Res.* 23, 652–677. <https://doi.org/10.1111/j.1365-2117.2011.00509.x>

1569 Masini, E., Manatschal, G., Tugend, J., Mohn, G., & Flament, J.-M., 2014. The tectono-  
1570 sedimentary evolution of a hyper-extended rift basin: the example of the Arzacq–  
1571 Mauléon rift system (Western Pyrenees, SW France). *Int. J. Earth Sci.* 103, 1569–  
1572 1596. <https://doi.org/10.1007/s00531-014-1023-8>

1573 Mata, M.P., Casas, A.M., Canals, A., Gil, A., & Pocovi, A., 2001. Thermal history during  
1574 Mesozoic extension and Tertiary uplift in the Cameros Basin, northern Spain. *Basin*  
1575 *Res.* 13, 91–111.

1576 Mathieu, C., 1986. Histoire géologique du sous-bassin de Parentis. *Bull. Cent. Rech. Explor.*  
1577 *Elf-Aquitaine* 10, 22–47.

1578 Mattauer, M., 1968. Les traits structuraux essentiels de la chaîne Pyrénéenne. *Rev. Géologie*  
 1579 *Dyn. Géographie Phys.* 10, 3–11.  
 1580 Mauriaud, P., 1987. La tectonique salifère d'Aquitaine. Le bassin d'Aquitaine. *Rev. Pétrole*  
 1581 *Tech.* 335, 38–41.  
 1582 Mediavilla, F., 1987. La tectonique salifère d'Aquitaine. Le Bassin de Parentis. *Rev. Pétrole*  
 1583 *Tech.* 335, 35–37.  
 1584 Mendia, M.S., & Ibarguchi, J.I.G., 1991. High-grade metamorphic rocks and peridotites along  
 1585 the Leiza Fault (Western Pyrenees, Spain). *Geol. Rundsch.* 80, 93–107.  
 1586 Mohn, G., Karner, G.D., Manatschal, G., & Johnson, C.A., 2015. Structural and stratigraphic  
 1587 evolution of the Iberia–Newfoundland hyper-extended rifted margin: a quantitative  
 1588 modelling approach. *Geol. Soc. Lond. Spec. Publ.* 413, 53–89.  
 1589 <https://doi.org/10.1144/SP413.9>  
 1590 Monchoux, P., 1970. Les lherzolites pyrénéennes: contribution à l'étude de leur minéralogie,  
 1591 de leur genèse et de leurs transformations. Université Paul Sabatier de Toulouse  
 1592 (Sciences).  
 1593 Montadert, L., de Charpal, O., Roberts, D., Guennoc, P., & Sibuet, J.-C., 1979. Northeast  
 1594 Atlantic passive continental margins: Rifting and subsidence processes, in: Talwani,  
 1595 M., Hay, W., Ryan, W.B.F. (Eds.), Maurice Ewing Series. American Geophysical  
 1596 Union, Washington, D. C., pp. 154–186. <https://doi.org/10.1029/ME003p0154>  
 1597 Montadert, L., & Winnock, E., 1971. L'histoire structurale du Golf de Gascogne. *Technip*.  
 1598 Montigny, R., Azambre, B., Rossy, M., & Thuizat, R., 1986. K-Ar Study of cretaceous  
 1599 magmatism and metamorphism in the Pyrenees: Age and length of rotation of the  
 1600 Iberian Peninsula. *Tectonophysics, The Geological Evolution of the Pyrenees* 129,  
 1601 257–273. [https://doi.org/10.1016/0040-1951\(86\)90255-6](https://doi.org/10.1016/0040-1951(86)90255-6)  
 1602 Nebot, M., & Guimerà, J.J., 2016. Structure of an inverted basin from subsurface and field  
 1603 data: the Late Jurassic-Early Cretaceous Maestrat Basin (Iberian Chain). *Geol. Acta*  
 1604 14, 0155–177.  
 1605 Nirrengarten, M., Manatschal, G., Tugend, J., Kusznir, N., Sauter, D., 2017. Kinematic  
 1606 evolution of the southern North Atlantic: implications for the formation of hyper-  
 1607 extended rift systems: Kinematic of hyper-extended rift systems. *Tectonics*. 37.  
 1608 [10.1002/2017TC004495](https://doi.org/10.1002/2017TC004495)  
 1609 Olivier, P., Gleizes, G., & Paquette, J.L., 2004. Gneiss domes and granite emplacement in an  
 1610 obliquely convergent regime: New interpretation of the Variscan Agly Massif (Eastern  
 1611 Pyrenees, France). *Spec. Pap.-Geol. Soc. Am.* 229–242.  
 1612 Omodeo-Salé, S., Guimerà, J., Mas, R., & Arribas, J., 2014. Tectono-stratigraphic evolution  
 1613 of an inverted extensional basin: the Cameros Basin (north of Spain). *Int. J. Earth Sci.*  
 1614 103, 1597–1620. <https://doi.org/10.1007/s00531-014-1026-5>  
 1615 Omodeo-Salé, S., Salas, R., Guimerà, J., Ondrak, R., Mas, R., Arribas, J., Suárez-Ruiz, I., &  
 1616 Martínez, L., 2017. Subsidence and thermal history of an inverted Late Jurassic-Early  
 1617 Cretaceous extensional basin (Cameros, North-central Spain) affected by very low- to  
 1618 low-grade metamorphism. *Basin Res.* 29, 156–174. <https://doi.org/10.1111/bre.12142>  
 1619 Ortí, F., 1974. El Keuper del levante español. *Estud. Geológicos* 30, 7–46.  
 1620 Ortí, F., Pérez-López, A., & Salvany, J.M., 2017. Triassic evaporites of Iberia:  
 1621 Sedimentological and palaeogeographical implications for the western Neotethys  
 1622 evolution during the Middle Triassic–Earliest Jurassic. *Palaeogeogr. Palaeoclimatol.*  
 1623 *Palaeoecol.* 471, 157–180. <https://doi.org/10.1016/j.palaeo.2017.01.025>  
 1624 Osmundsen, P.T., & Ebbing, J., 2008. Styles of extension offshore mid-Norway and  
 1625 implications for mechanisms of crustal thinning at passive margins: STYLES OF  
 1626 EXTENSION OFFSHORE NORWAY. *Tectonics* 27, n/a-n/a.  
 1627 <https://doi.org/10.1029/2007TC002242>

- Osmundsen, P.T., & Péron-Pinvidic, G., 2018. Crustal-Scale Fault Interaction at Rifted Margins and the Formation of Domain-Bounding Breakaway Complexes: Insights From Offshore Norway. *Tectonics* 37, 935–964. <https://doi.org/10.1002/2017TC004792>
- Osmundsen, P.T., Sommaruga, A., Skilbrei, J.R., & Olesen, O., 2002. Deep structure of the Mid Norway rifted margin. *Nor. J. Geol. Geol. Foren.* 82.
- Pedreira, D., Pulgar, J.A., Gallart, J., & Torné, M., 2007. Three-dimensional gravity and magnetic modeling of crustal indentation and wedging in the western Pyrenees-Cantabrian Mountains. *J. Geophys. Res.* 112. <https://doi.org/10.1029/2007JB005021>
- Pedreira, A., García-Senz, J., Ayala, C., Ruiz-Constán, A., Rodríguez-Fernández, L.R., Robador, A., & González Menéndez, L., 2017. Reconstruction of the exhumed mantle across the North Iberian Margin by crustal-scale 3-D gravity inversion and geological cross section. *Tectonics* 36, 3155–3177.
- Pedreira, A., García-Senz, J., Peropadre, C., Robador, A., Lopez Mir, B., Diaz Alvarado, J., & Rodríguez-Fernández, L.R., 2020. The Getxo crustal-scale cross-section: testing tectonic models in the Bay of Biscay-Pyrenean rift system. *Earth-Sciences Review*, doi: 10.1016/j.earscirev.2020.103429.
- Pereira, R., Alves, T.M., 2012, Tectono-stratigraphic signature of multiphased rifting on divergent margins (deep-offshore Southwest Iberia, North Atlantic). *Tectonics*. 31. doi:10.1029/2011TC003001
- Pérez-Gussinyé, M., 2013. A tectonic model for hyperextension at magma-poor rifted margins: an example from the West Iberia–Newfoundland conjugate margins. *Geol. Soc. Lond. Spec. Publ.* 369, 403–427. <https://doi.org/10.1144/SP369.19>
- Péron-Pinvidic, G., Manatschal, G., Masini, E., Sutra, E., Flament, J.M., Hauptert, I., & Unternehr, P., 2015. Unravelling the along-strike variability of the Angola–Gabon rifted margin: a mapping approach. *Geol. Soc. Lond. Spec. Publ.* 438, 49–76. <https://doi.org/10.1144/SP438.1>
- Péron-Pinvidic, G., Manatschal, G., Minshull, T.A., & Sawyer, D.S., 2007. Tectonosedimentary evolution of the deep Iberia–Newfoundland margins: Evidence for a complex breakup history. *Tectonics* 26, 1–19. <https://doi.org/10.1029/2006TC001970>
- Peybernès, B., 1976. Le Jurassique et le Crétacé inférieur des Pyrénées franco-espagnoles entre la Garonne et la Méditerranée. Toulouse.
- Peybernès, B., 1979. L’Urgonien des Pyrénées, Essai de synthèse. *Geobios* 12, 79–87.
- Peybernès, B., 1982. Création puis évolution de la marge nord-ibérique des Pyrénées au Crétacé inférieur. *Cuad. Geol. Ibérica* 8, 987–1004.
- Peybernès, B., & Combes, P.-J., 1994. Stratigraphie séquentielle du Crétacé basal (intervalle Berriasien-Hauterivien) des Pyrénées centrales et orientales franco-espagnoles. *Cretac. Res.* 15, 535–546. <https://doi.org/10.1006/cres.1994.1032>
- Pichel, L. M., Peel, F., Jackson, C. A.-L., & Huuse, M. (2018). Geometry and kinematics of salt-detached ramp syncline basins. *Journal of Structural Geology*, 115, 208–230. <https://doi.org/10.1016/j.jsg.2018.07.016>
- Pichel, L. M., Finch, E., & Gawthorpe, R. L. (2019). The Impact of Pre-Salt Rift Topography on Salt Tectonics: A Discrete-Element Modeling Approach. *Tectonics*, 38(4), 1466–1488.
- Pinet, B., Montadert, L., Curnelle, R., Cazes, M., Marillier, F., Rolet, J., . . . Brunet, M.F., 1987a. Crustal thinning on the Aquitaine shelf, Bay of Biscay, from deep seismic data. *Nature* 325, 513.

- Pinet, Bertrand, Montadert, L., & ECORS Scientific Party, 1987b. Deep seismic reflection and refraction profiling along the Aquitaine shelf (Bay of Biscay). *Geophys. J. Int.* 89, 305–312. <https://doi.org/10.1111/j.1365-246X.1987.tb04423.x>
- Platt, N.H., 1986. Sedimentology and Tectonics of the Western Cameros Basin, Province of Burgos, Northern Spain (PhD Thesis). University of Oxford.
- Platt, N.H., 1989. Continental sedimentation in an evolving rift basin: the Lower Cretaceous of the western Cameros Basin (northern Spain). *Sediment. Geol.* 64, 91–109. [https://doi.org/10.1016/0037-0738\(89\)90086-9](https://doi.org/10.1016/0037-0738(89)90086-9)
- Platt, N.H., 1990. Basin evolution and fault reactivation in the western Cameros Basin, Northern Spain. *J. Geol. Soc.* 147, 165–175. <https://doi.org/10.1144/gsjgs.147.1.0165>
- Quijada, I.E., Suárez González, P., Isabel, B.M., Mas, J.R., & Alonso, Á., 2010. Un ejemplo de llanura fluvio-deltaica influenciada por las mareas: el yacimiento de icnitas de Serrantes (Grupo Oncala, Berriasiense, Cuenca de Cameros, N. de España). *Geogaceta* 15–18.
- Rat, J., Mouthereau, F., Brichau, S., Crémades, A., Bernet, M., Balvay, M., . . . Gautheron, C., 2019. Tectonothermal Evolution of the Cameros Basin: Implications for Tectonics of North Iberia. *Tectonics* 38, 440–469. <https://doi.org/10.1029/2018TC005294>
- Rat, P., 1988. The Basque-Cantabrian Basin between the Iberian and European plates, some facts but still many problems. *Rev Soc Geol Esp.* 327–348.
- Rat, P., Amiot, M., Feuillée, P., Floquet, M., Mathey, B., Pascal, A., . . . Lamolda, M., others, 1983. Vue sur le Cretacé basco-cantabrique et nord-ibérique. *Une Marge Son Arriere-Pays Ses Environ. Sedimentaires Memoires Geol. Univ. Dijon* 9, 191.
- Ravier, J., 1957. Le métamorphisme des terrains secondaires des Pyrénées. Université, Faculté des Sciences.
- Razin, P., 1989, Evolution tecto-sédimentaire alpine des Pyrénées basques à l'ouest de la transformante de Pamplona, Province du Labourd. PhD thesis, University of Bordeaux 3, France, 464 p.
- Reston, T.J., 2009. The structure, evolution and symmetry of the magma-poor rifted margins of the North and Central Atlantic: A synthesis. *Tectonophysics* 468, 6–27. <https://doi.org/10.1016/j.tecto.2008.09.002>
- Reston, T.J., Krawczyk, C.M., & Hoffmann, H.-J., 1995. Detachment tectonics during Atlantic rifting: analysis and interpretation of the S reflection, the west Galicia margin. *Geol. Soc. Lond. Spec. Publ.* 90, 93–109. <https://doi.org/10.1144/GSL.SP.1995.090.01.05>
- Ribes, C., Ghienne, J.-F., Manatschal, G., Decarlis, A., Karner, G.D., Figueredo, P.H., & Johnson, C.A., 2019. Long-lived mega fault-scarps and related breccias at distal rifted margins: Insights from present-day and fossil analogues. *J. Geol. Soc.* jgs2018-181. <https://doi.org/10.1144/jgs2018-181>
- Roca, E., 1996. La cubeta mesozoica de las Columbrets: aportaciones al conocimiento de la estructura del surco de Valencia. *Geogaceta* 20, 1711–1714.
- Roma, M., Ferrer, O., Roca, E., Pla, O., Escosa, F.O., & Butillé, M., 2018. Formation and inversion of salt-detached ramp-syncline basins. Results from analog modeling and application to the Columbrets Basin (Western Mediterranean). *Tectonophysics* 745, 214–228. <https://doi.org/10.1016/j.tecto.2018.08.012>
- Rossi, P., Cocherie, A., Fanning, C.M., & Ternet, Y., 2003. Datation U-Pb sur zircons des dolérites tholéiitiques pyrénéennes (ophites) à la limite Trias–Jurassique et relations avec les tufs volcaniques dits « infra-liasiques » nord-pyrénéens. *Comptes Rendus Geosci.* 335, 1071–1080. <https://doi.org/10.1016/j.crte.2003.09.011>



1724 Rouby, D., Raillard, S., Guillocheau, F., Bouroullec, R., & Nalpas, T., 2002. Kinematics of a  
 1725 growth fault/raft system on the West African margin using 3-D restoration. *J. Struct.*  
 1726 *Geol.* 24, 783–796.  
 1727 Roux, J.-C., 1983. Recherches stratigraphiques et sédimentologiques sur les flyschs crétacés  
 1728 pyrénéens au sud d'Oloron (Pyrénées Atlantiques). Université Paul Sabatier de  
 1729 Toulouse (Sciences).  
 1730 Ruiz, M., 2007. Caracterització estructural i sismotectònica de la litosfera en el domini  
 1731 Pirenaico-Cantàbric a partir de mètodes de sísmica activa i passiva. Universitat de  
 1732 Barcelona.  
 1733 Sàbat, F., Roca, E., Muñoz, J.A., Vergès, J., Santanach, P., & Masana, E., 1997. Role of  
 1734 extension and compression in the evolution of the eastern margin of Iberia: The ESCI-  
 1735 València trough seismic profile. *Rev. Soc. Geològica Esp.* 8, 431–448.  
 1736 Salas, R., Guimerà, J., Mas, R., Martín-Closas, C., Meléndez, A., & Alonso, A., 2001.  
 1737 Evolution of the Mesozoic central Iberian Rift System and its Cainozoic inversion  
 1738 (Iberian chain). *Peri-Tethys Mem.* 6, 145–185.  
 1739 Saspiturry, N., Cochelin, B., Razin, P., Leleu, S., Lemirre, B., Bouscary, C., . . . Allanic, C.,  
 1740 2019a. Tectono-sedimentary evolution of a rift system controlled by Permian post-  
 1741 orogenic extension and metamorphic core complex formation (Bidarray Basin and  
 1742 Ursuya dome, Western Pyrenees). *Tectonophysics* 768, 228180.  
 1743 <https://doi.org/10.1016/j.tecto.2019.228180>  
 1744 Saspiturry, N., Razin, P., Baudin, T., Serrano, O., Issautier, B., Lasseur, E., . . . Leleu, S.,  
 1745 2019b. Symmetry vs. asymmetry of a hyper-thinned rift: Example of the Mauléon  
 1746 Basin (Western Pyrenees, France). *Mar. Pet. Geol.* 104, 86–105.  
 1747 <https://doi.org/10.1016/j.marpetgeo.2019.03.031>  
 1748 Saspiturry, N., Razin, P., Allanic, C., Issautier, B., Baudin, T., Lasseur, E., . . . Leleu, S.,  
 1749 2020a, Closure of a hyperextended system in an orogenic lithospheric pop-up,  
 1750 Western Pyrenees: The role of mantle buttressing and rift structural inheritance: *Terra*  
 1751 *Nova.* 10.1111/ter.12457.  
 1752 Saspiturry, N., Lahfid, A., Baudin, T., Guillou-Frottier, G., Razin, P., Issautier, B., Le Bayon,  
 1753 B., Serrano, O., Lagabrielle, Y., Corre, B., 2020b. Paleogeothermal Gradients across  
 1754 an Inverted Hyperextended Rift System: Example of the Mauléon Fossil Rift (Western  
 1755 Pyrenees). *Tectonics.* 10.1029/2020TC006206  
 1756 Saspiturry, N., 2019. Evolution sédimentaire, structurale et thermique d'un rift hyper-aminci :  
 1757 de l'héritage post-hercynien à l'inversion alpine, Exemple du bassin de Mauléon  
 1758 (Pyrénées). PhD thesis, Bordeaux University, 444p.  
 1759 Schettino, A., & Turco, E., 2011. Tectonic history of the western Tethys since the Late  
 1760 Triassic. *Geol. Soc. Am. Bull.* 123, 89–105. <https://doi.org/10.1130/B30064.1>  
 1761 Serrano, O., Delmas, J., Hanot, F., Vially, R., Herbin, J.-P., Houel, P., & Tourlière, B., 2006.  
 1762 Le bassin d'Aquitaine: valorisation des données sismiques, cartographie structurale et  
 1763 potentiel pétrolier. Bureau de Recherche Géologique et minière.  
 1764 Soares, D.M., Alves, T.M., Terrinha, P., 2012. The breakup sequence and associated  
 1765 lithospheric breakup surface: their significance in the context of rifted continental  
 1766 margins (West Iberia and Newfoundland margins, North Atlantic). *Earth Planet*  
 1767 *Sci.Lett.* 355–356, 311–326. <https://doi.org/10.1016/j.epsl.2012.08.036>.  
 1768 Soares, D.M., 2014. Sedimentological and stratigraphical aspects of the syn- to post-rift  
 1769 transition on fully separated conjugate margins. PhD thesis, Cardiff University. 305p.  
 1770 Soto, J.I., Flinch, F., & Tari, G., 2017. Permo-Triassic Salt Provinces of Europe, North Africa  
 1771 and the Atlantic Margins: Tectonics and Hydrocarbon Potential, in: In Soto et Al.,  
 1772 Eds, Permo-Triassic Salt Provinces of Europe, North Africa and the Atlantic Margins.  
 1773 Tectonics and Hydrocarbon Potential. Elsevier.

1774 Souquet, P., 1967. Le Crétacé supérieur Sud-Pyrénéen, en Catalogne, Aragon et Navarre. E.  
1775 Privat.

1776 Souquet, P., Debroas, E.-J., Boirie, J.-M., Pons, P., Fixari, G., Roux, J.-C., . . . Manivit, H.,  
1777 others, 1985. Le groupe du Flysch noir (albo-cénomanién) dans les Pyrénées. Bull  
1778 Cent Rech Exlpo-Prod Elf-Aquitaine Pau 9, 183–252.

1779 Suárez González, P., Quijada, I.E., Mas, J.R., & Benito, M.I., 2010. Nuevas aportaciones  
1780 sobre la influencia marina y la edad de los carbonatos de la Fm Leza en el sector de  
1781 Préjano (SE de La Rioja). Cretácico Inferior, Cuenca de Cameros. Geogaceta 7–10.

1782 Teixell, A., Labaume, P., Ayarza, P., Espurt, N., de Saint Blanquat, M., & Lagabrielle, Y.,  
1783 2018. Crustal structure and evolution of the Pyrenean-Cantabrian belt: A review and  
1784 new interpretations from recent concepts and data. Tectonophysics 724, 146–170.  
1785 <https://doi.org/10.1016/j.tecto.2018.01.009>

1786 Teixell, A., Labaume, P., & Lagabrielle, Y., 2016. The crustal evolution of the west-central  
1787 Pyrenees revisited: Inferences from a new kinematic scenario. Comptes Rendus  
1788 Geosci. 348, 257–267. <https://doi.org/10.1016/j.crte.2015.10.010>

1789 Ternet, Y., Majesté-Menjoulas, C., Canérot, J., Baudin, T., Cocherie, A., Guerrot, C., &  
1790 Rossi, P., 2004. Carte géologique de la France au 1/50 000: Laruns-Somport, Orléans,  
1791 France.

1792 Thiébaud, J., Durand-Wackenheim, C., Debeaux, M., & Souquet, P., 1992. Métamorphisme  
1793 des évaporites triasiques du versant nord des Pyrénées centrales et Occidentales. Bull.  
1794 Société Hist. Nat. Toulouse 128, 77–84.

1795 Thinon, I., 1999. Structure profonde de la marge Nord Gascogne et du Bassin armoricain.  
1796 Université de Bretagne occidentale-Brest.

1797 Thinon, I., Fidalgo-González, L., Réhault, J. P. and Olivet, J. L., 2001, Pyrenean deformations  
1798 in the Bay of Biscay: Comptes Rendus de l'Académie des Sciences, Série IIa, v.332,  
1799 p.561–568.

1800 Thinon, I., Matias, L., Réhault, J.P., Hirn, A., Fidalgo-González, L., & Avedik, F., 2003.  
1801 Deep structure of the Armorican Basin (Bay of Biscay): a review of Norgasis seismic  
1802 reflection and refraction data. J. Geol. Soc. 160, 99–116. [https://doi.org/10.1144/0016-](https://doi.org/10.1144/0016-764901-103)  
1803 764901-103

1804 Tomassimo, A., & Marillier, F., 1997. Processing and interpretation in the tau-p domain of the  
1805 ECORS Bay of Biscay expanding spread profiles. Mém. Société Géologique Fr. 171,  
1806 31–43.

1807 Torné, M., Banda, E., & Fernandez, M., 1996. The Valencia Trough: Geological and  
1808 geophysical constraints on the basin formation model., in: In P. A. Ziegler, & F.  
1809 Horvath (Eds.), Structure and Prospects of Alpine Basins and Forelands, Mem. Nat  
1810 Hist. Mus. pp. 103–128.

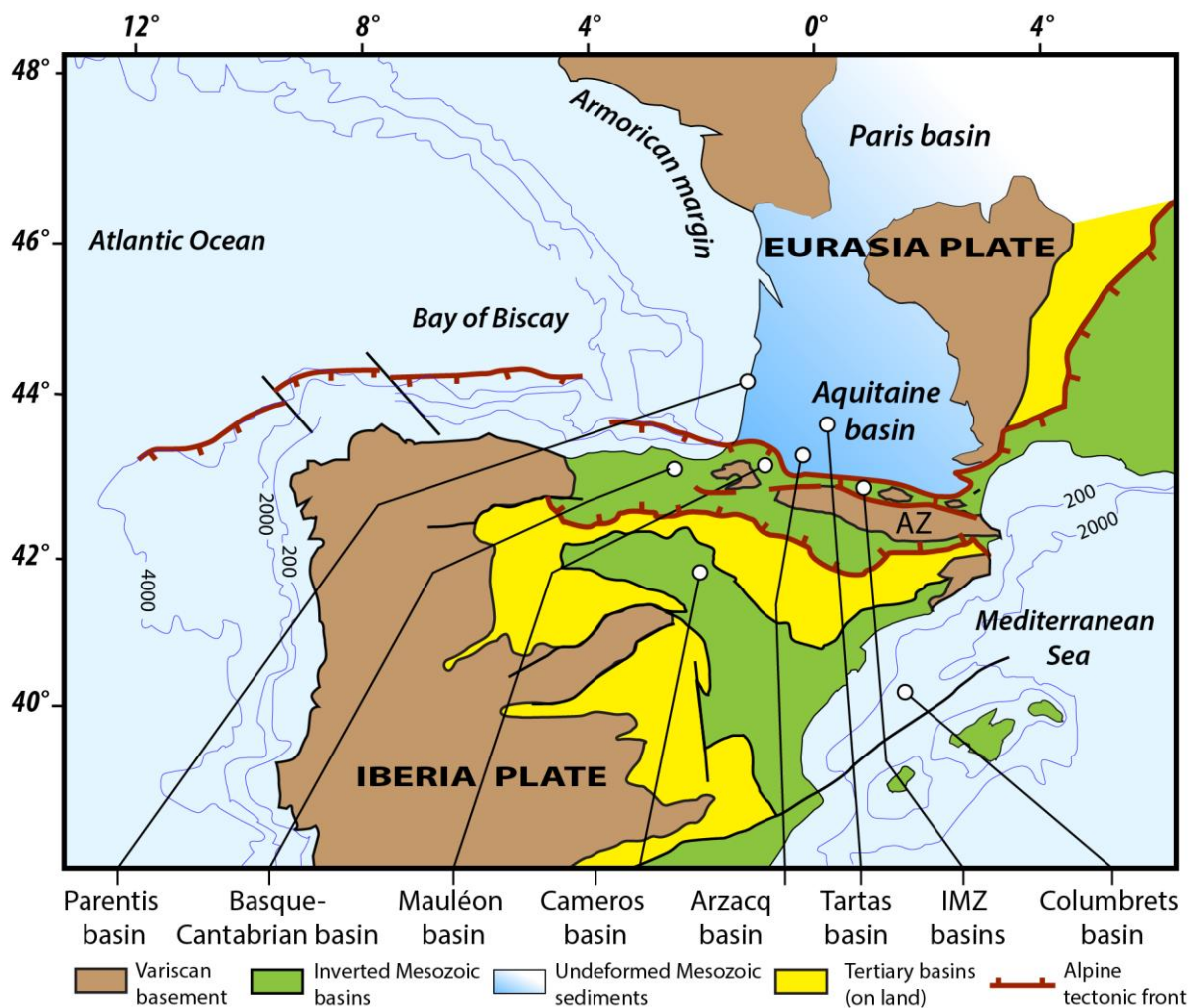
1811 Torné, M., Pascal, G., Buhl, P., Watts, A.B., & Mauffret, A., 1992. Crustal and velocity  
1812 structure of the Valencia trough (western Mediterranean), Part I. A combined  
1813 refraction/ wide-angle reflection and near-vertical reflection study. Tectonophysics  
1814 203, 1–20. [https://doi.org/10.1016/0040-1951\(92\)90212-O](https://doi.org/10.1016/0040-1951(92)90212-O)

1815 Tugend, J., Manatschal, G., Kusznir, N.J., & Masini, E., 2015. Characterizing and identifying  
1816 structural domains at rifted continental margins: application to the Bay of Biscay  
1817 margins and its Western Pyrenean fossil remnants. Geol. Soc. Lond. Spec. Publ. 413,  
1818 171–203. <https://doi.org/10.1144/SP413.3>

1819 Tugend, J., Manatschal, G., Kusznir, N.J., Masini, E., Mohn, G., & Thinon, I., 2014.  
1820 Formation and deformation of hyperextended rift systems: Insights from rift domain  
1821 mapping in the Bay of Biscay-Pyrenees. Tectonics 33, 1239–1276.  
1822 <https://doi.org/10.1002/2014TC003529>

- Vacher, P., & Souriau, A., 2001. A three-dimensional model of the Pyrenean deep structure based on gravity modelling, seismic images and petrological constraints. *Geophys. J. Int.* 145, 460–470. <https://doi.org/10.1046/j.0956-540x.2001.01393.x>
- Vacherat, A., Mouthereau, F., Pik, R., Bernet, M., Gautheron, C., Masini, E., . . . Lahfid, A., 2014. Thermal imprint of rift-related processes in orogens as recorded in the Pyrenees. *Earth Planet. Sci. Lett.* 408, 296–306. <https://doi.org/10.1016/j.epsl.2014.10.014>
- Valladares, I., 1980. Evolución de facies en el Jurasico calcareo del sector sur-occidental de la provincia de Burgos. *Stud. Geol. Salamanticensia* 16, 37–57.
- Vargas, H., Gaspar-Escribano, J.M., López-Gómez, J., Van Wees, J.-D., Cloetingh, S., de La Horra, R., & Arche, A., 2009. A comparison of the Iberian and Ebro Basins during the Permian and Triassic, eastern Spain: A quantitative subsidence modelling approach. *Tectonophysics* 474, 160–183. <https://doi.org/10.1016/j.tecto.2008.06.005>
- Vaucher, A., Clerc, C., Bestani, L., Lagabriele, Y., Chauvet, A., Lahfid, A., & Mainprice, D., 2013. Preorogenic exhumation of the North Pyrenean Agly massif (Eastern Pyrenees-France). *Tectonics* 32, 95–106. <https://doi.org/10.1002/tect.20015>
- Vergés, J., & García-Senz, J., 2001. Mesozoic evolution and Cenozoic inversion of the Pyrenean rift. *Mém. Muséum Natl. Hist. Nat.* 186, 187–212.
- Vidal, N., Gallart, J., & Dañobeitia, J.J., 1997. Contribution of the ESCI-Valencia Trough wide-angle data to a crustal transect in the NE Iberian margin. *Rev. - Soc. Geológica Esp.* 417–429.
- Vielzeuf, D., & Kornprobst, J., 1984. Crustal splitting and the emplacement of Pyrenean lherzolites and granulites. *Earth Planet. Sci. Lett.* 67, 87–96. [https://doi.org/10.1016/0012-821X\(84\)90041-4](https://doi.org/10.1016/0012-821X(84)90041-4)
- Wang, Y., Chevrot, S., Monteiller, V., Komatitsch, D., Mouthereau, F., Manatschal, G., . . . Martin, R., 2016. The deep roots of the western Pyrenees revealed by full waveform inversion of teleseismic P waves. *Geology* 44, 475–478. <https://doi.org/10.1130/G37812.1>
- Whitmarsh, R.B., Manatschal, G., & Minshull, T.A., 2001. Evolution of magma-poor continental margins from rifting to seafloor spreading. *Nature* 413, 150–154. <https://doi.org/10.1038/35093085>
- Wilson, R. C. L., G. Manatschal, and S. Wise (2001), Rifting along non-volcanic passive margins: Stratigraphic and seismic evidence from the Mesozoic successions of the Alps and western Iberia, in *Nonvolcanic Continental Margins: A Comparison of Evidence From Land and Sea*, edited by R. C. L. Wilson et al., *Geol. Soc. Spec. Publ.*, 187, 29 – 452.
- Zeyen, H., & Fernández, M., 1994. Integrated lithospheric modeling combining thermal, gravity, and local isostasy analysis: Application to the NE Spanish Geotranssect. *J. Geophys. Res. Solid Earth* 99, 18089–18102. <https://doi.org/10.1029/94JB00898>
- Ziegler, P.A., 1982. Triassic rifts and facies patterns in Western and Central Europe. *Geol. Rundsch.* 71, 747–772. <https://doi.org/10.1007/BF01821101>

1864 **Figure.1**



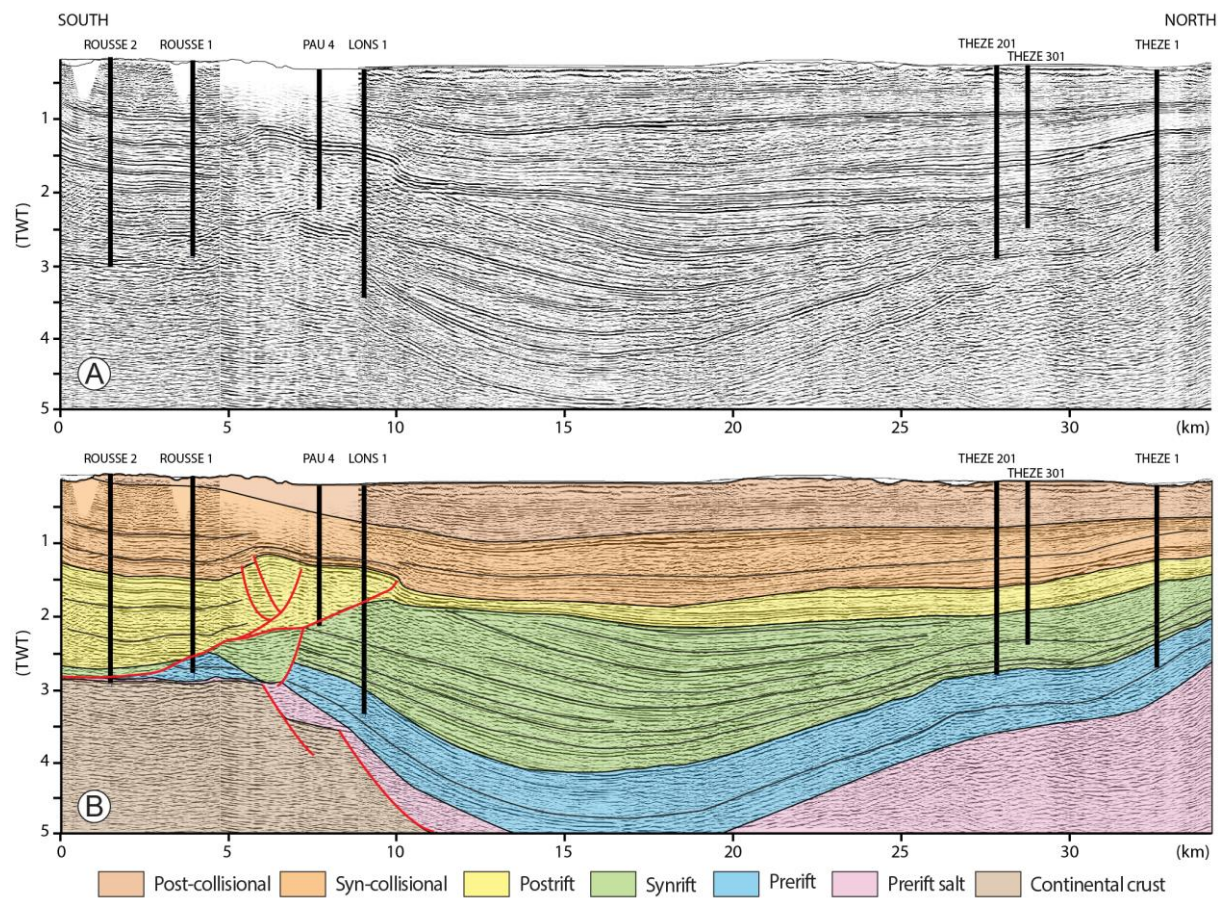
1865

1866

1867

1868

**FIGURE 1** Simplified structural map of the Cantabrian-Pyrenean orogenic system and adjoining Iberia showing deformed and undeformed domains in the Eurasia plate and the locations of basins in this study (modified from Lagabrielle et al., 2020).



1870

1871 **FIGURE 2** Interpretation of a South-North seismic reflection profile across the Arzacq basin:  
1872 (A) Rousse-Thèze seismic reflection profile, calibrated using, from south to north, the  
1873 Rousse-2, Rousse-1, Pau-4, Lons-1, Thèze 201, Thèze 301 and Thèze 1 boreholes (Issautier et  
1874 al., 2020). (B) Interpreted section (modified from Issautier et al., 2020). The syn-rift sequence  
1875 is characterized by a maximum time thickness of around 2.5 TWT seconds corresponding to a  
1876 thickness of nearly 2000–3000 m. The depocenter of the syn-rift sequence in the Arzacq basin  
1877 migrates south from its position, indicating a northward salt-controlled cover gliding during  
1878 the rifting stage. The Arzacq syn-rift basin is characterized by a slight asymmetry of its  
1879 depocenter.



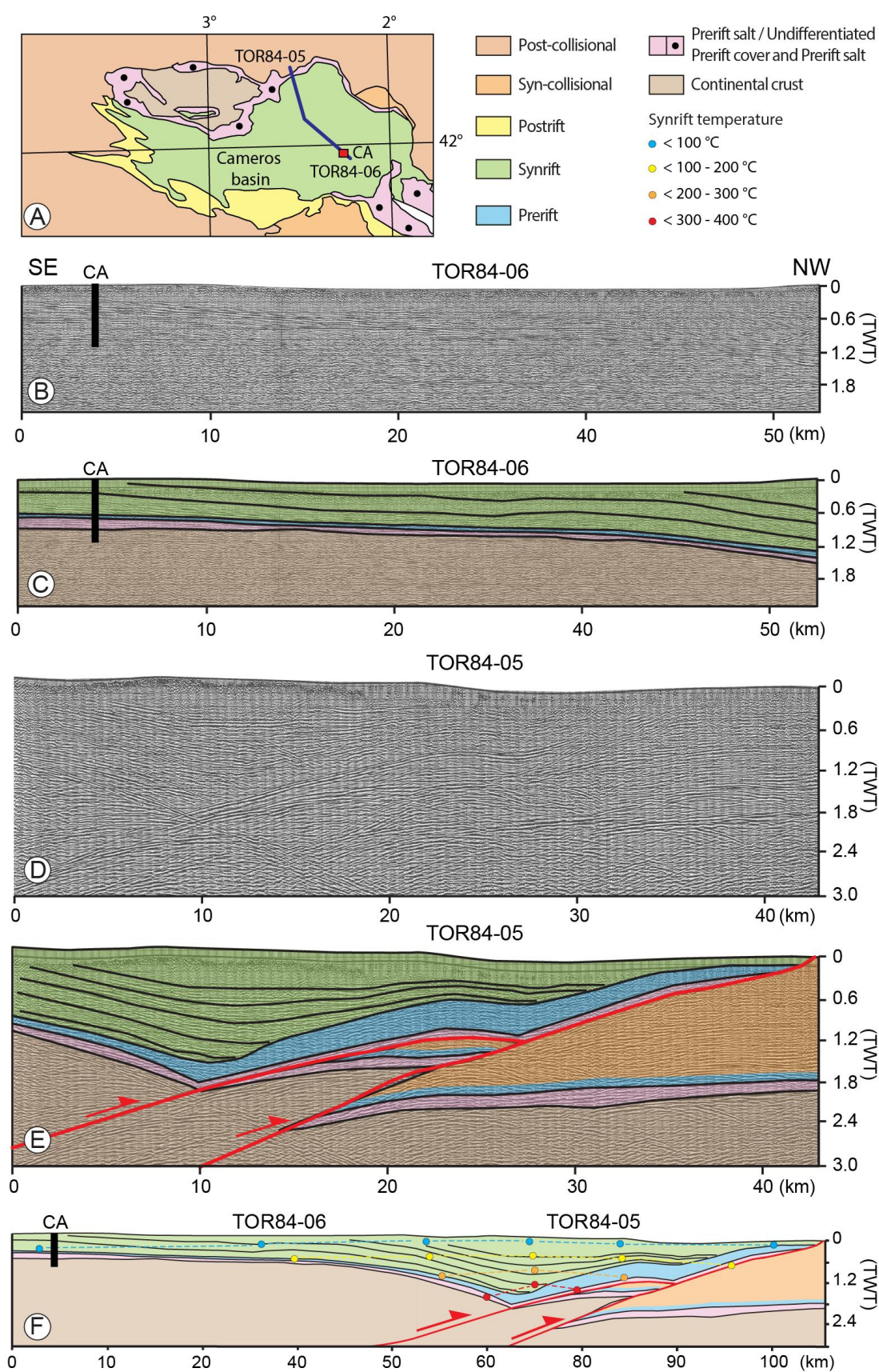


**FIGURE 3** (A) Geological map of the Cameros basin (modified from Omodeo-Salé et al., 2014); (B-C) Interpretation of the SE-NW TOR84-06 seismic reflection profiles across the Cameros basin, location on Figure 3A (Omodeo-Salé et al., 2014), CA: Castelfrio 1 borehole; (D-E) Interpretation of the SE-NW TOR84-05 seismic reflection profiles across the Cameros basin, location on Figure 3A (Omodeo-Salé et al., 2014). (F) Line-drawing of the TOR84-05 and TOR84-06 seismic reflection profiles. The syn-rift sequence displays an onlap geometry on the marine Jurassic substrate towards the north. The depocenter of the syn-rift sequence in the Cameros basin migrates north from its position, indicating southward salt-controlled cover gliding during the rifting stage rooting at depth on a crustal structure. The Cameros syn-rift basin is characterised by a slight asymmetry of its depocenter. The syn-rift sequence is characterised by a maximum time thickness of around 1.5 TWT seconds corresponding to a thickness of nearly 1500–2000 m. Available syn-rift paleotemperatures from Rat et al. (2019) indicate that the base of the syn-rift basin reached temperatures of around 300–400 °C.

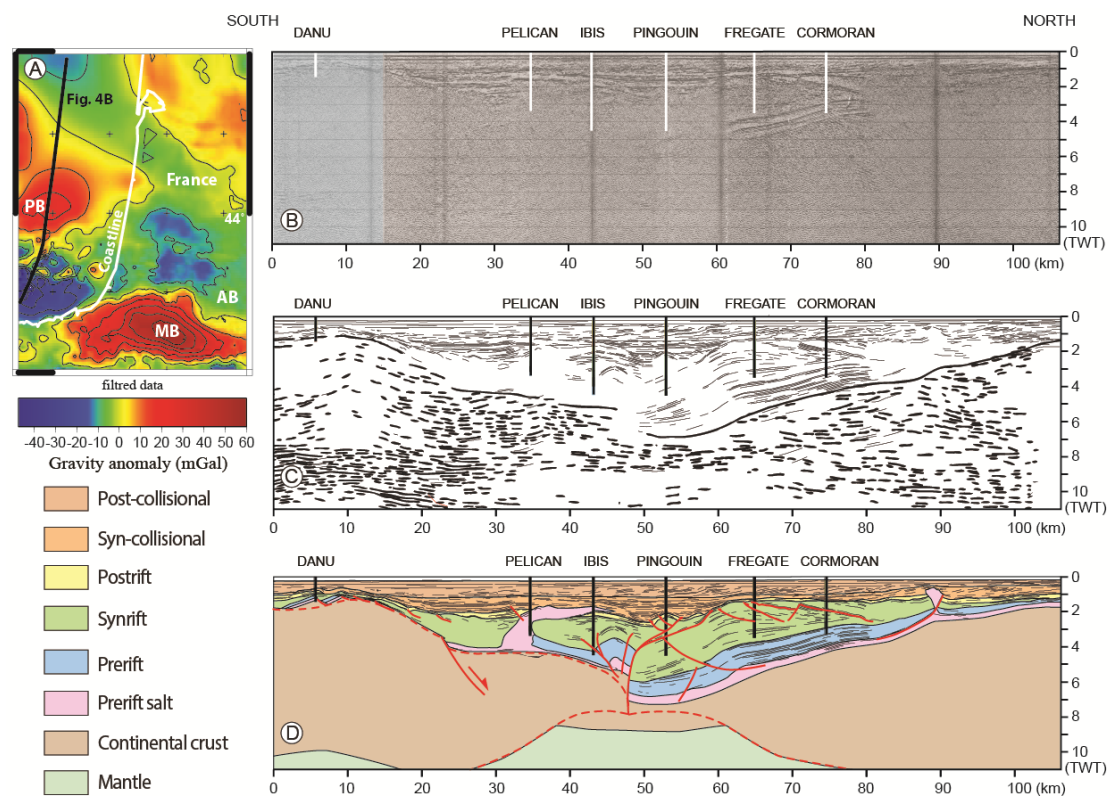
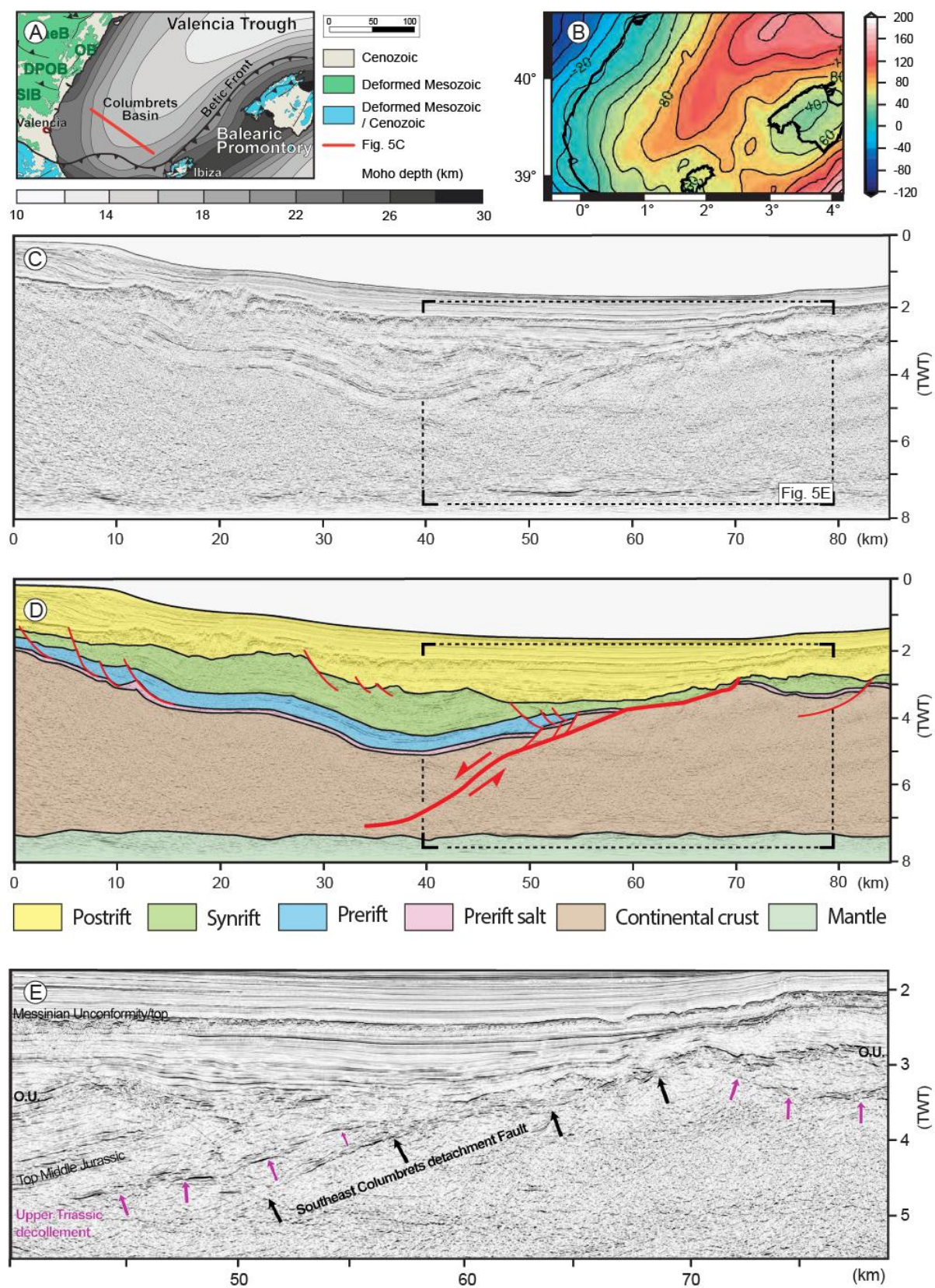


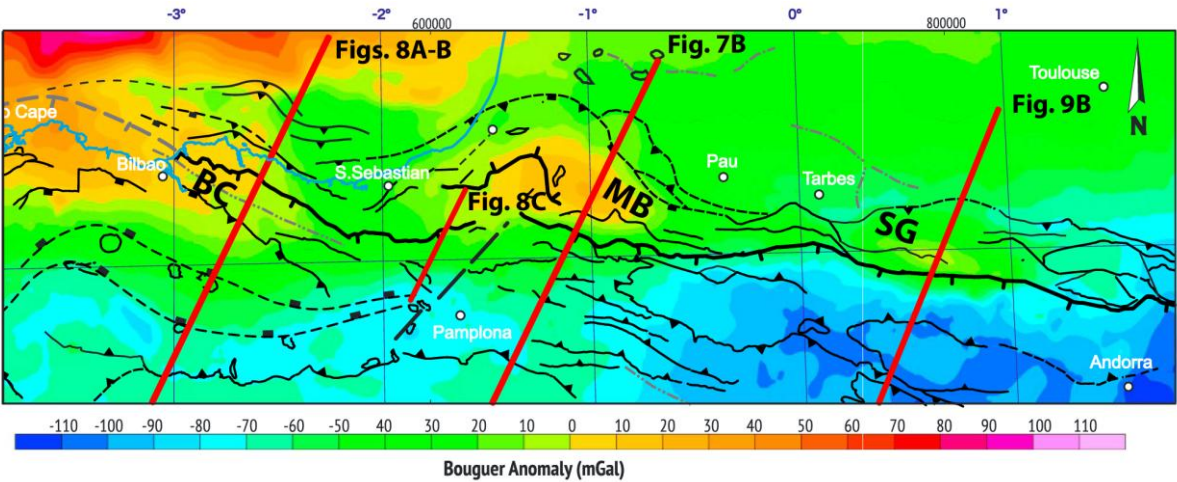
**FIGURE 4** Parentis basin architecture. (A) Filtered Bouguer gravity anomaly map (Jammes, 2009); PB: Parentis basin Bouguer Anomaly; MB: Mauléon basin Bouguer Anomaly; AB: Arzacq basin. (B) Bay of Biscay ECORS profile, calibrated using, from south to north, the Danu, Pelican, Ibis, Pingouin, Fregate and Cormoran boreholes (in Jammes, 2009). (C) Line drawing of the sedimentary structures and deep crustal structures of the Bay of Biscay ECORS profile (in Jammes, 2009). (D) Interpreted Bay of Biscay ECORS profile (modified from Jammes, 2019). The depocenter of the syn-rift sequence in the Parentis basin migrates south from its position indicating northward salt-controlled cover gliding during the rifting stage, interpreted by Jammes (2009) and Tugend et al. (2014) as a northward-deepening décollement rooting at depth on a crustal detachment fault. The Parentis syn-rift basin is characterized by a mildly asymmetry of its depocenter. The syn-rift sequence is characterised by a maximum time thickness of around 4 TWT seconds corresponding to a thickness of nearly 3000–4500 m.





1912 **FIGURE 5** (A) Geological and structural map of the Columbrets basin showing the Moho  
1913 depth varying from 10 to 30 km depth (modified from Etheve et al., 2018). (B) Map of the  
1914 Bouguer anomaly (modified from et al., 2015). (C) NW-SE SGV01-113 seismic reflection  
1915 profile; location on Figure 5A (Etheve et al., 2018). (D) Interpreted SGV01-113 seismic  
1916 reflection profile (modified from Etheve et al., 2018). The syn-rift sequence is characterised  
1917 by a maximum time thickness of around 1.5 TWT seconds corresponding to a thickness of  
1918 nearly 1500–2000 m; however, its true thickness was greater as the top of this sequence is  
1919 affected by a major Tertiary erosional unconformity. The depocenter of the syn-rift sequence  
1920 in the Columbrets basin migrates south from its position, indicating northward salt-controlled  
1921 cover gliding during the rifting stage interpreted by Etheve et al. (2018) as a northward-  
1922 deepening salt décollement rooting at depth on a ductile crustal detachment fault. (E) Detail of  
1923 the southern part of the SGV01-113 seismic reflection profile showing the northward-  
1924 deepening ductile crustal detachment fault (Etheve et al., 2018).

1925 **Figure.6**



1926

1927 **FIGURE 6** Bouguer anomaly map from the Basque-Cantabrian basin to the Central Pyrenees

1928 (Pedrera et al., 2017). BC, Basque-Cantabrian Bouguer anomaly; MB, Mauléon basin

1929 Bouguer anomaly; SG, Saint-Gaudens Bouguer anomaly.

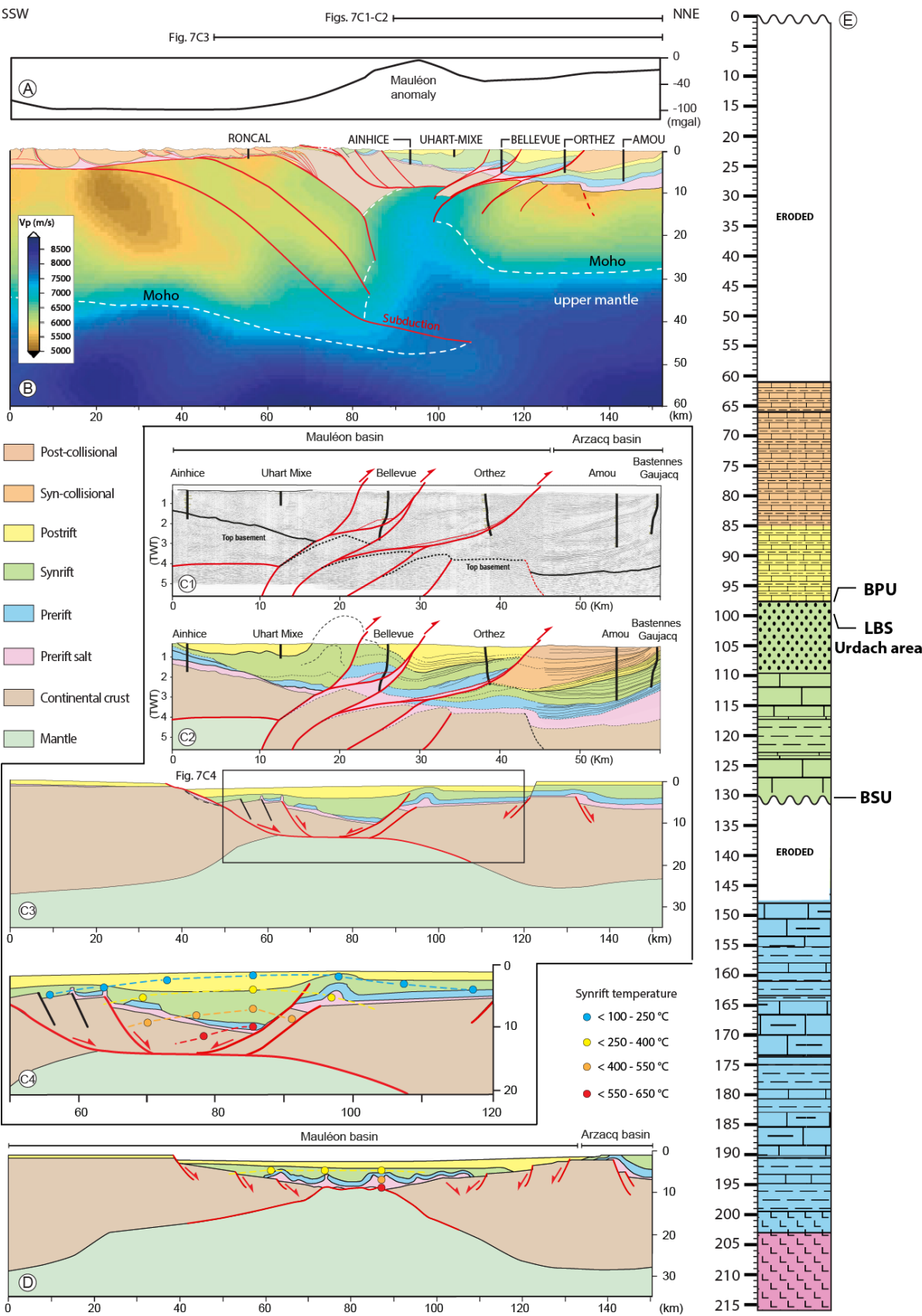


**FIGURE 7** Mauléon basin overall architecture. (A) Bouguer anomaly (Casas et al., 1997). (B) Mauléon basin lithospheric section (see location on Figure 6). The lowermost part corresponds to the Wang et al. (2016) Vp model showing the presence at shallow depth of continental lithospheric mantle. The uppermost part is materialized by the Saspiturry et al. (2020a) crustal-scale balanced cross-section calibrated using (from south to north) the Ronca, Ainhice, Uhart-Mixe, Bellevue, Orthez, Amou and Bastennes Gaujacq boreholes. (C1, C2) Geological section through the present-day Mauléon basin based on interpreted seismic lines and field data (modified from Saspiturry et al., 2019a). The Mauléon basin is exposed within a pop-up structure formed during N-S Pyrenean compression. (C3) Palinspastic restoration, to Santonian time, of the Saspiturry et al. (2020a) crustal-scale balanced cross-section. (C4) Detail of the palinspastic restoration of the Saspiturry et al. (2020a) crustal-scale balanced cross-section, with RSCM syn-rift paleotemperature of Saspiturry (2019). (D) Palinspastic restoration, to Santonian time, of the Teixell et al. (2016) crustal-scale balanced cross-section, with RSCM syn-rift paleotemperature of Corre (2017). (E) Stratigraphic chart showing the position of the key markers of the Mauléon basin. BSU, basal syn-rift unconformity; LBS, lithospheric breakup surface; BPU, basal post-rift unconformity.



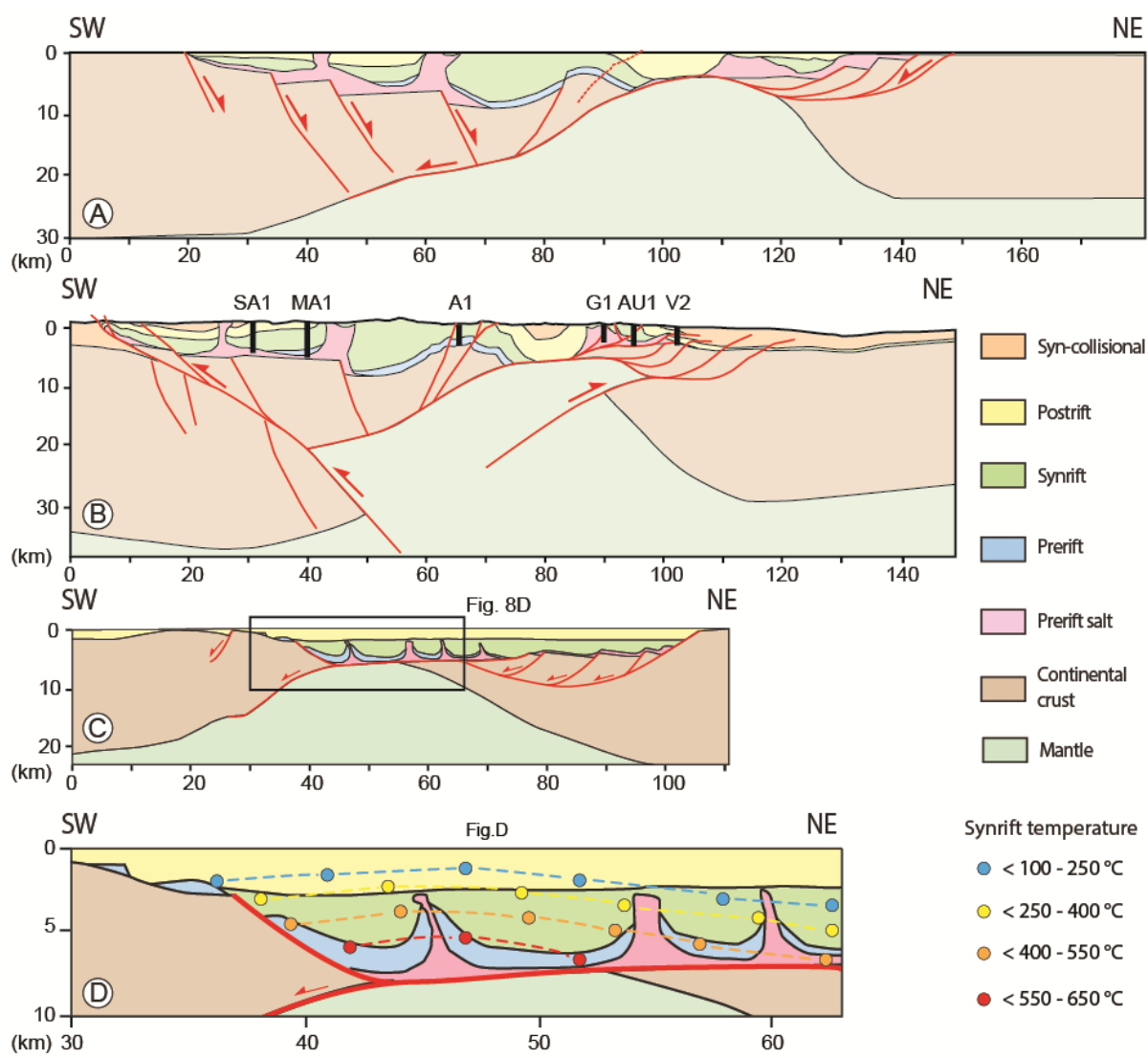
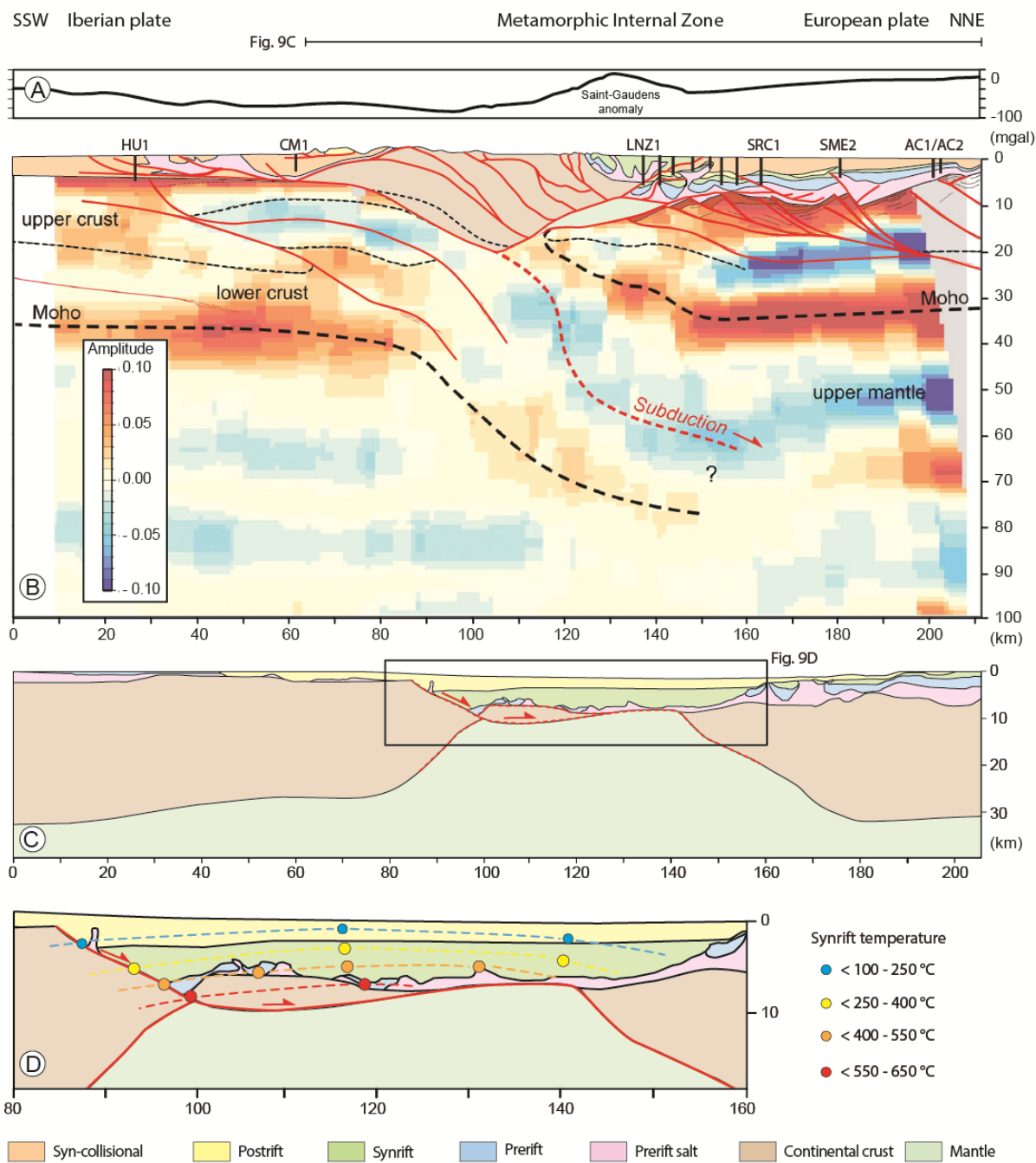


**FIGURE 8** (A) Basque-Cantabrian basin palinspastic restoration, to Santonian time, of the Pedrera et al. (2017) crustal-scale balanced cross-section (see location on Fig. 6). (B) Basque-Cantabrian basin crustal-scale balanced cross-section (Pedrera et al., 2017), calibrated using (from south to north) the San Antonio 1 (SA-1), Marinda 1 (MA-1), Arratia 1 (A1), Gernika 1 (G1), Aulesti 1 (AU1) and Vizcaya C2 (V2) boreholes. (C) Schematic restoration of the eastern part of the Basque-Cantabrian basin in the “Nappe des Marbres” (Ducoux et al., 2019). (D) Detail of (C) with the RSCM syn-rift paleotemperatures measured by Ducoux et al. (2019).

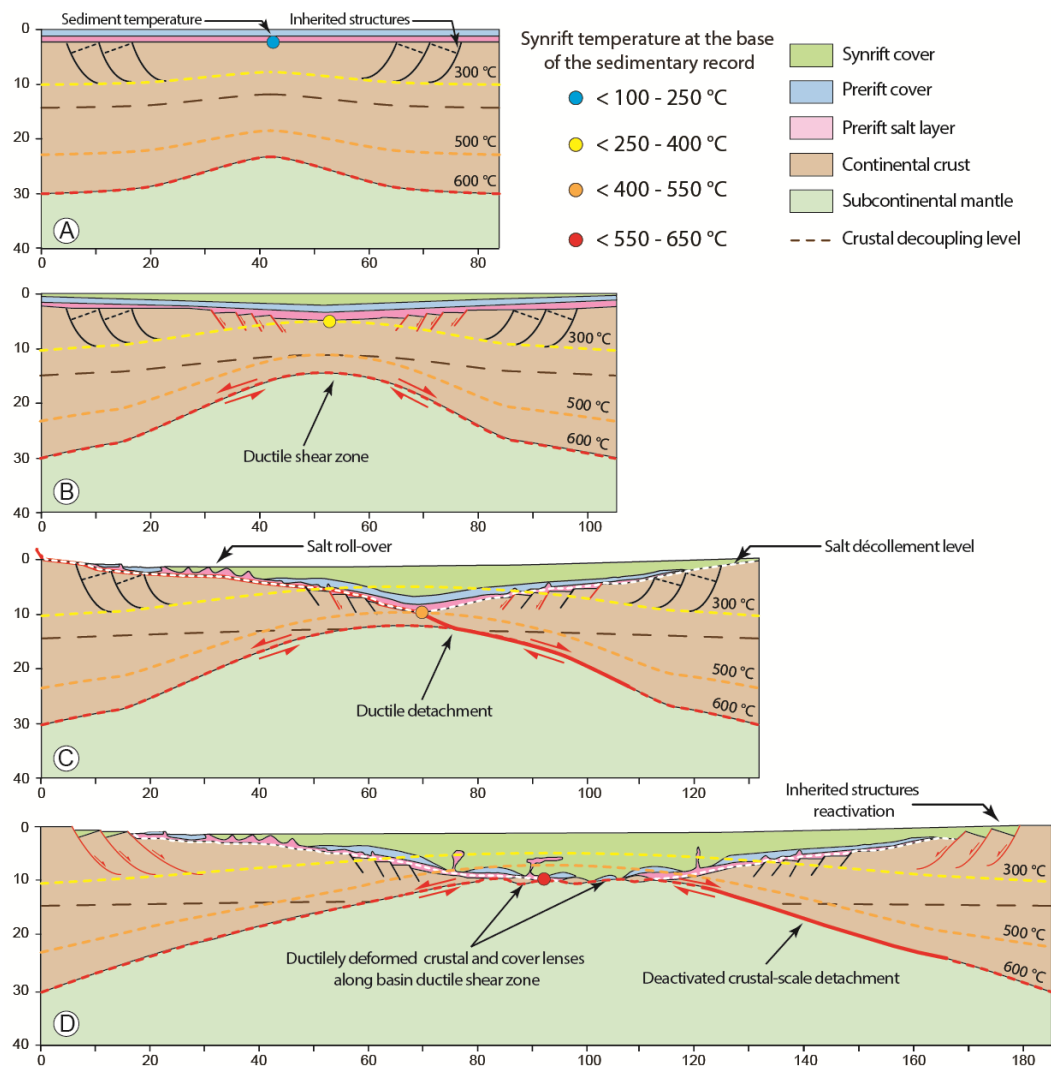


1959

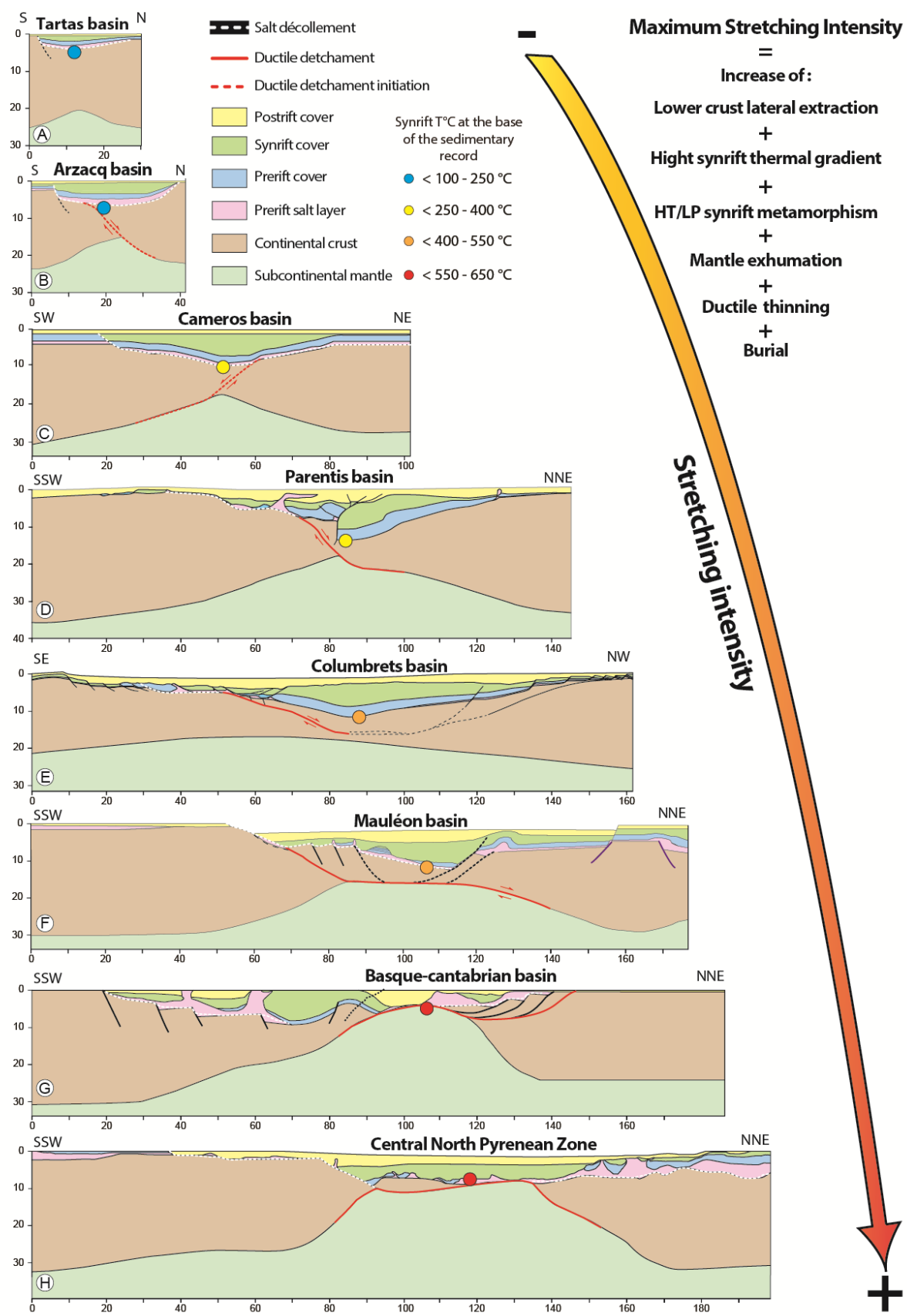
1960 **FIGURE 9** Metamorphic Internal Zone overall architecture. (A) Bouguer anomaly (in Espurt  
1961 et al., 2019). (B) Metamorphic Internal Zone basin lithospheric section (see location on Figure  
1962 6). The lowermost part corresponds to the stack profile of receiver functions for the OROGEN  
1963 West profile across the Central Pyrenean belt (in Espurt et al., 2019) showing the presence at

1964 shallow depth of continental lithospheric mantle. The uppermost part is based on the Espurt et  
1965 al. (2019) crustal-scale balanced cross-section calibrated using (from south to north) the  
1966 Huesca 1 (HU-1), Campanue-1 (CM-1), Lannemezan 1 (LNZ1), Sariaç 1 (SRC-1), Saint  
1967 Médard 2 (SME-2), Auch 1 (AC-1) and Auch 2 (AC-2) boreholes. (C) Palinspastic  
1968 restoration, to Santonian time, of the Espurt et al. (2019) crustal-scale balanced cross-section.  
1969 (D) Detail of the palinspastic restoration of the Espurt et al. (2019) crustal-scale balanced  
1970 cross-section, with RSCM syn-rift paleotemperatures.





1973 **FIGURE 10** Conceptual model of the evolution of a smooth-slope type basin. (A) Inherited  
 1974 thin lithosphere. (B) Pure shear dominated thinning: formation of a symmetric basin  
 1975 characterized by shallow-water sediments. (C) Simple shear dominated thinning: basinward  
 1976 gliding of the pre-rift sedimentary cover along a major detachment connecting towards the  
 1977 surface with the Late Triassic salt décollement, leading to an asymmetrical basin shape. (D)  
 1978 Breakup stage resulting in the formation of a pseudo-symmetric basin undergoing brittle  
 1979 deformation on the proximal margins and ductile deformation in the basin core. No vertical  
 1980 exaggeration. Coloured dashed lines represent crustal isotherms; coloured circles indicate  
 1981 maximum sediment temperatures during HT/LP metamorphism.



1984 **FIGURE 11** Smooth-slope type basins classified according to the degree of continental crust  
1985 extension: (A) Tartas sub-basin (Issautier et al., 2020); (B) Arzacq sub-basin (Issautier et al.,  
1986 2020); (C) Cameros basin (modified after Casas-Sainz & Gil-Imaz, 1998); (D) Parentis basin  
1987 (Tugend et al., 2014); (E) Columbrets basin (Etheve et al., 2018); (F) Mauléon basin  
1988 (Saspiturry et al., 2019a); (G) Basque-Cantabrian basin (Pedrera et al., 2017); (H) Central  
1989 North Pyrenean Zone basins (Espurt et al., 2019); locations in Figure 1. No vertical  
1990 exaggeration. The large arrow indicates the degree of extension and the rise in peak  
1991 metamorphic temperatures throughout the basin evolutionary sequence. Coloured circles  
1992 indicate maximum sediment temperatures during HT/LP metamorphism.

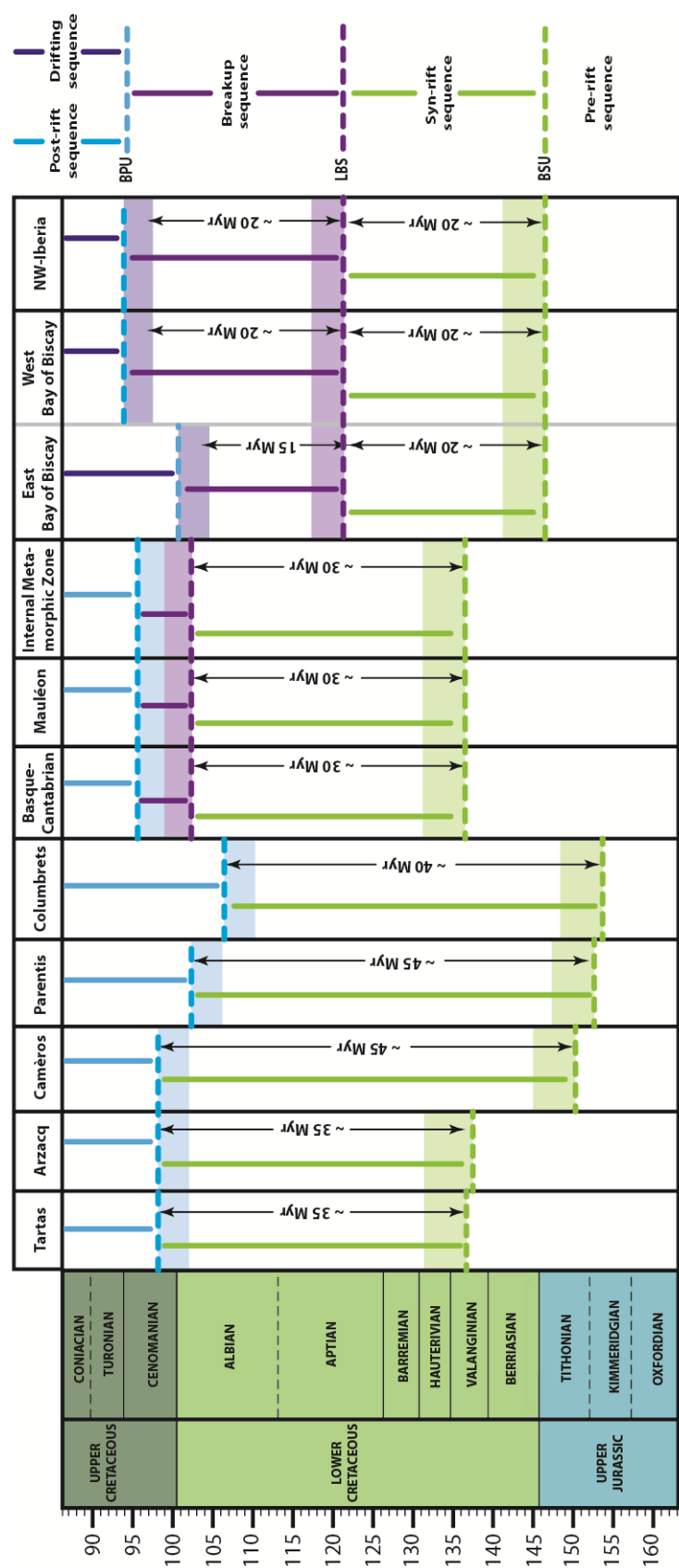
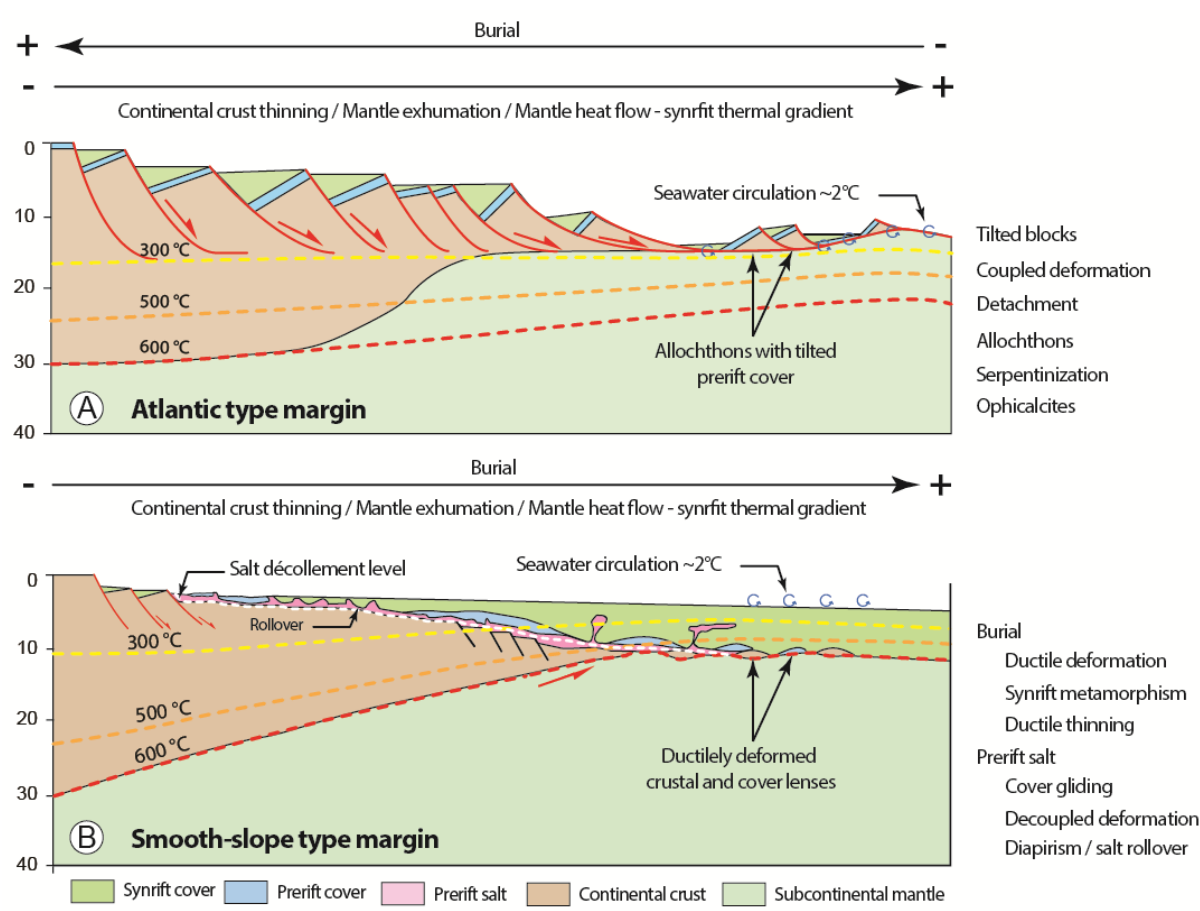


**FIGURE 12** Chronological chart showing the timing of the syn-rift, late syn-rift, breakup (mantle exhumation), post-rift and oceanic spreading events of the reviewed basins, the West Iberia basins and the Bay of Biscay margins. References used to define the timing of the different events: Tartas and Arzacq basins (Désaglaux & Brunet, 1990; Brunet, 1991; Serrano et al., 2006; Issautier et al., 2020), Camèros basin (Platt, 1990; Mas et al., 1993; Casas-Sainz & Gil-Imaz, 1998; Salas et al., 2001; Omodeo-Salé et al., 2014, 2017), Parentis basin (Brunet, 1994; Ferrer et al., 2008; Jammes et al., 2009; Tugend et al., 2015), Columbrets basin (Salas et al., 2001; Nebot & Guimerà, 2016; Etheve, 2016; Etheve et al., 2018; Roma et al., 2018), Basque-Cantabrian basin (Azambre & Rossy, 1976; Rat et al., 1983; Rat, 1988; García Mondéjar et al., 1996; Castañares et al., 1997; Castañares & Robles, 2004; Pedrera et al., 2017; Ducoux et al., 2019), Mauléon basin (Boirie, 1981; Fixari, 1984; Souquet et al., 1985; Jammes et al., 2009; Debroas et al., 2010; Masini et al., 2014; Teixell et al., 2016; Saspiturry et al., 2019a; Labaume and Teixell, 2020), Internal Metamorphic Zone basin (Lagabrielle & Bodinier, 2008; Lagabrielle et al., 2010, 2019; Clerc & Lagabrielle, 2014; Clerc et al., 2014, 2015; de Saint Blanquat et al., 2016; Teixell et al., 2018; Espurt et al., 2019), Northwest-Iberia margin (Soares et al., 2012; Pereira & Alves, 2012, Alves & Cunha, 2018; Alves et al., 2020), and Bay of Biscay margins (Montardet et al., 1979; Brunet 1994; Thinon, 1999; Thinon et al., 2001, 2003; Gong et al., 2008; Tugend et al., 2015). BSU, basal syn-rift unconformity; LBS, lithospheric breakup surface; BPU, basal post-rift unconformity. Coloured shaded areas represent time uncertainty of the BSU, LBS and BPU unconformities.

2015 **Figure.13**



2016

2017 **FIGURE 13** Schematic diagrams showing (A) Atlantic-type margin architecture (section

2018 modified from Péron-Pinvidic et al., 2015) and (B) smooth-slope type margin architecture.

2019 Coloured dashed lines represent crustal isotherms; coloured circles indicate maximum

2020 sediment temperatures during HT/LP metamorphism.